Photoresist Derived Carbon as a Substratum For Neuron Cell Culture

A Major Qualifying Project Report

Submitted to the Faculty of the

WORCESTER POLYTECHNIC INSTITUTE

In partial fulfillment of the requirements
for a Bachelor of Science Degree
in the field of Chemical Engineering

By:

_____
Richard P. Pampuro

Date: May 5, 2008

Approvals:

_____
Assistant Professor Susan Zhou, Advisor of Record

Acknowledgements

I would like to thank Professor Susan Zhou for her tireless guidance and support. Also, I would like to thank Professor Jianhua Zhou and Tie Zou from the University of Massachusetts Medical School for their help and advice with cell culture and assays. Moreover, Dr. Jaingdong Deng of Harvard University must be thanked for his assistance in the Oxygen Plasma application process and the use of his laboratory. Linxiao Chen and Stephanie Miskell deserve thanks for their temporary assistance with experiments, as well as David Munger for his untiring collaboration with substrate fabrication and characterization. Additionally, I would like to thank Oljora Rezhdo, Matthew Perrone and Chunwei Kuo for their help with cell morphology studies. The assistance of each of these individuals has enabled this project to exist in its current form.

Abstract

Photoresist derived carbon films offer a unique set of properties that may prove useful as substratum for neuron cell growth. At this early stage in realizing the material's potential as a platform for neuron culture, it is necessary to examine surface properties and neuronal cell behavior. Surfaces are characterized by means relevant for studying cell-surface response, including electrochemistry and surface energy. Comparing gene expression levels, adhesion and morphology of PC12 cells grown on photoresist derived carbon to that of alternative materials elucidates cell-surface interactions in context of known surface properties. Results show that photoresist derived carbon is a viable alternative to current materials, offering the advantages of modification and electrical properties.

Table of Contents

Table of Figures

Table of Tables

1. Introduction

For centuries, neurological damage from trauma and neurodegenerative disorders has long remained a largely untreatable condition. Recent advances have enabled unprecedented new progress and understanding in the field of neuroregenerative medicine. Chief among these advances is the development of microelectromechanical systems (MEMS), which have seen application in areas ranging from microchip design to drug delivery platforms. In parallel, advances in neurobiology and neurochemistry have elucidated the behavior of individual neuron cells *in vitro* and *in vivo*.

Research driven largely by the semiconductor industry has given birth to a dizzying array of MEMS fabrication techniques. Most notably, photolithography has proven to be an extremely versatile and low cost option for manufacture of MEMS. Using silicon wafers coated in photoreactive material, it is possible to create a deliberate pattern of material on the wafer with a resolution as small as 1 µm. Recent advances have seen the application of MEMS techniques to the creation of micropatterned biocompatible materials. Procedures to fabricate photoresist derived carbon substrates have the capacity to create micropatterned biocompatible materials with unique chemical and electrical properties.

Until recently, neuronal cell response to even the most basic environmental conditions was not understood. Laboratory studies have shed light on the process of neuronal differentiation and the individual neuron's response to environmental cues. These advances, though only crude *in vitro* models of *in vivo* processes, have provided insight regarding the *in vivo* process of neuron growth. Photoresist derived carbon holds promise as a means to further characterize these behaviors. In addition to being biocompatible, the material has the capacity to be easily modified chemically and its electrical properties offers great potential for the study of neuron cells.

Photoresist derived carbon films are produced from the pyrolysis of photoresist films. The resulting carbon film is biocompatible, easily modified and electrically conductive—a rather unique set of properties for MEMS materials. The range of applications for this novel material has yet to be fully explored and thus it is necessary to first characterize the material's properties and begin to demonstrate capabilities for cell growth. Initial findings have demonstrated that photoresist derived carbon is a viable substrate for nerve cell growth and differentiation.

This project seeks to further the understanding of photoresist-derived carbon films' potential application in biological systems. In addition to developing procedures to fabricate and characterize thin carbon films, these preliminary studies have sought to gauge cellular response to the surface's unique properties. Fabrication procedures included development of a method to coat thick layers from a thin-layer photoresist and a pyrolysis procedure to suit the photoresist precursor's unique properties. Films were characterized for mass and thickness loss, as well as evaluating the film's electrochemical properties with the use of cyclic voltammetry. Cell culture procedures were adapted from previous work and genetic assays were devised in an effort to gauge different levels of cell differentiation on the surface. Additionally, adhesion assays assessed some aspects of cell-surface response.

2. Background

2.1. Neural Tissue

Neural tissue is organized into two broad groups: the central nervous system (CNS) and the peripheral nervous system (PNS). The CNS consists of the brain and spinal cord. The CNS is responsible for interpreting sensory input and dictating motor responses. It works with the PNS to receive afferent signals from sensory systems and transmit efferent signals. Afferent signals are transmitted by sensory receptors in the PNS to the CNS, while efferent signals are control signals from the CNS to muscles and glands (Marieb & Hoehn, 2007).

The most obvious component of the CNS is the brain. Though only 2% of total body weight, the human brain demands nearly 20% of body oxygen consumption and 25% of body glucose consumption. The extremely high glucose demand is due largely to the fact that most of the brain is capable of metabolizing only glucose. Because of the brain's sensitivity, it is isolated from the rest of the body by the blood-brain barrier. The barrier consists of a series of small gaps between endothelial cells that have very high concentrations of transmembrane proteins and are called tight junctions (Marieb & Hoehn, 2007).

The human brain is divided into four major regions by location and function: the cerebral hemispheres, diencephalon, brainstem and cerebellum. The Cerebral hemispheres constitute about 83% of total brain mass and are composed largely of folds of tissue. For the most part, the cerebral hemispheres are responsible for higher functions including consciousness, language, voluntary motor control and sensory perception among many other important roles. The diencephalon is composed of the thalamus and hypothalamus. With afferent impulses from all of the senses connecting to at least one neuron in the thalamus, the structure serves as a sort of switching station between the brain and the rest of the body, The hypothalamus is essential to overall homeostasis, regulating, among other systems, the autonomic nervous system, body temperature, food intake/water balance and sleep-wake cycles. The brain stem functions to carry out automatic behavior and is a major pathway for conduits between higher and lower neural centers. The final major brain region is the cerebellum, which is responsible largely for coordination and transmission of signals from the higher brain to the body. All activity in the cerebellum is subconscious (Marieb & Hoehn, 2007).

2.1.1. The Neuron

The basic unit of any neurological structure is the nerve cell. Nerve cells or neurons are structured in a manner that permits for signal transmission. Neurons possess a unique set of features aside from their obvious structural properties including being unable to divide, outliving most other cells and having very high metabolic rates. Once differentiated, neuron cells are unable to divide further and carry out the bulk of their lifetime with little structural change. Some hippocampal regions, however, are able to form new cells with the help of undifferentiated stem cells, assisting in memory formation. Since neurons cannot divide, they must live for a very long time without losing any functional capacity. Additionally, neurons operate with a very high metabolic rate, demanding a constant supply of glucose compared to

most other cell types. The elevated glucose consumption rates are due in large part to high metabolic demands of signal propagation (Marieb & Hoehn, 2007).

Each neuron is separated into two basic parts: the cell body and neurites or processes. The cell body contains the nucleus, a very well developed Golgi Apparatus and a number of other organelles. The Golgi Apparatus in the neuron cell body is very well developed so that the cell may transport key molecules along the length of the cell's processes. Neurites extend from the cell body as long, narrow and often branching structures that are analogous to wires. Indeed, the analogy to a wire is even more poignant when observing that neurites are structured to carry signals. Neurites are divided into two different categories based on their function and structure: dendrites and axons. Dendrites are responsible for receiving signals from adjacent neurons, while axons initiate and transmit signals (Marieb & Hoehn, 2007).

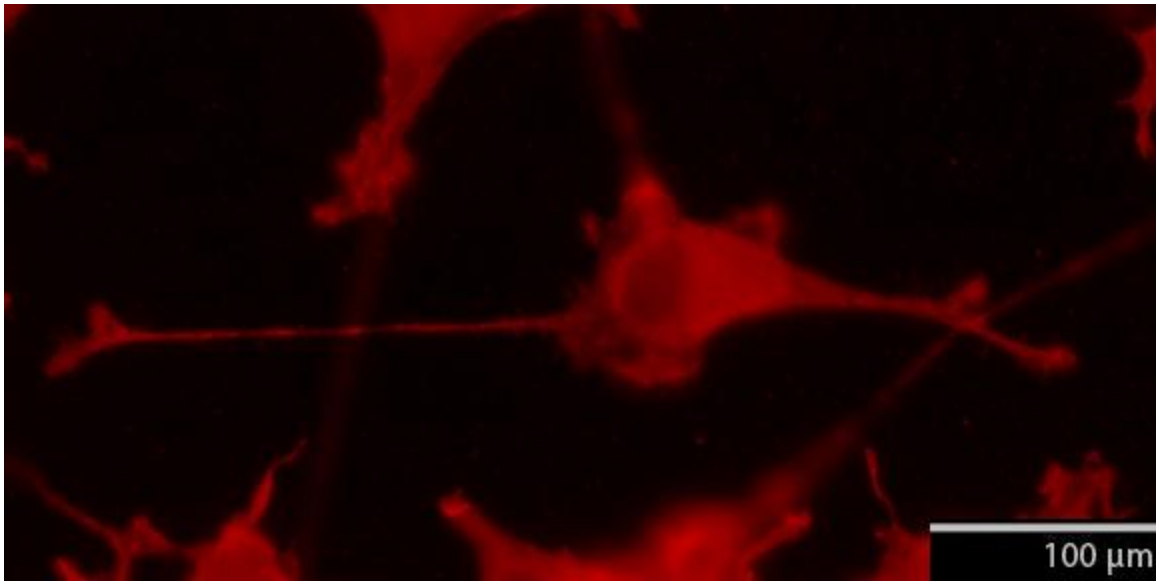

Figure 2.1.1.1: Micrograph of a neuron cell.
Notice the Axon emerging from the right of the cell body, while a dendrite grows from the left of the cell body. This particular cell appears to be a bipolar neurite, with an axon and a dendrite each emerging from opposite ends of the cell. The far right is the terminus of the axon, which appears to branch into telodendria.

Neurons may be classified by neurite structure. There are three basic groups of neurons: unipolar, bipolar and multipolar. Unipolar neurons have only one neurite emerging from the cell body, extending from dendrite to axon. Bipolar cells have two neurites, one axon and one dendrite emerging from the cell body. Multipolar cells have more than two neurites emerging from the cell body. Though each of the classifications specify a limited number of neurites emerging from the cell body itself, it is important to remember that neurites almost always are branching and connect to a multitude of adjacent cells (Bear, Connors, & Paradiso, 2007). Unipolar and bipolar cells are typically found in sensory organs and the PNS respectively. Constituting the bulk of the CNS, multipolar neurons are by far the most common

neuron type (Marieb & Hoehn, 2007). Differentiated PC-12 cells used in this study form multipolar neurons (Greene, 1976).

Dendrites are the signal receiving end of a cell. They branch extensively, creating a very large surface area to receive signals from other cells. Along the length of a dendrite, small structures called dendritic spines form, branching outward. The shape of the spines is said to be intended to isolate certain processes from the remainder of the cell (Marieb & Hoehn, 2007). Discovery of mRNA and protein synthesis in these small, isolated regions of the neuron is believed to be linked to memory formation. Additionally, dendrite structure is useful in cell classification. Two broad cell classes are distinguished by the shape of the dendrite formations. Stellate cells are star shaped, with dendrites emerging from all directions, while pyramidal cells have the bulk of their dendrites emerging from the cell body along a single axis or perpendicular to that axis (Bear, Connors, & Paradiso, 2007). Differentiated PC-12 cells used in this study tend to form stellate structures (Greene, 1976).

2.1.2. The Axon

The axon is connected to the cell body by a cone shaped area called the axon hillock and extends for a very long distance, often representing the majority of the cell's length. Each neuron has only one axon, but the axon often has several branches or collaterals. The terminal end of the axon branches extensively to maximize contact with neighboring cells. In certain cells, these terminal branches or telodendria easily number in excess of ten thousand. At the terminus of the telodendria, the axon connects to neighboring cells via a round structure called an axon terminal or synaptic knob. The terminus of the axon often has organelles present, namely mitochondria. Virtually any organelle can be found at any point along the axon, save ribosomes, Golgi Apparatus and, of course, a nucleus (Marieb & Hoehn, 2007). Refer to Figure 2.1.1.1 for an image of a nerve cell.

Principally, the axon functions to initiate and transmit nerve impulses. Signals are transmitted along the length of the axon or conduction region, toward the secretory region at the terminus. Neurotransmitters are released upon the signal's reaching a synaptic knob, perpetuating the signal to a neighboring neuron (Bear, Connors, & Paradiso, 2007). The axon's length is supported by a multitude of structural proteins. Microtubules stabilized by Tao proteins and tubulin along the axon's length. Indeed, upregulation of Tao genes is associated with axon growth (Drubin, Feinstein, Shooter, & Kirschner, 1985). Since the axon is quite long, there are challenges associated with getting important chemicals throughout the structure's length. Neurons do have a rather well developed Golgi Apparatus, but mere diffusion is not sufficient to carry vesicles to the synaptic knobs. Thus, active transport within the cell is necessary. Kinesin complexes are used to guide vesicles from the Golgi Apparatus along microtubules to other sections of the cell. Transport away from the cell body is referred to as anterograde transport, while transport toward the cell body is called retrograde transport and relies on dynein to transport vesicles. A different protein is needed for transport in each direction because microtubules are directionally aligned and each protein is designed for transport in only one direction along a microtubule (Bear, Connors, & Paradiso, 2007).

2.1.3. Neuron Signaling

Signal initiation and transmission in neurons is performed along the length of the axon with the help of gated ion channels. Naturally, the inside of the cell has a slight negative charge of around -70 mV, which is referred to as the resting membrane potential. The voltage difference between the interior and exterior of the cell is maintained by ion gradients created by protein channels. A great deal of a nerve cell's metabolic demand is dedicated to operation of channels to create ion gradients. As signals are transmitted along the length of an axon, an action potential changes the local charge inside the neuron. By rapidly allowing sodium ions to enter the cell, the membrane potential increases very rapidly. The rapidly changing potential opens voltage gated potassium channels, releasing sodium into the extracellular space and rapidly lowering the local charge gradient. Upon returning to a lower potential, the potassium gates close and the cell gradually restores resting membrane potential over the following 2.0 ms to 2.5 ms. The end result is a rapid and severe cycling of cell membrane potential that transmits signals at a rate as fast as one hundred meters per second (Marieb & Hoehn, 2007).

Transmission of signals along neurons is referred to as an all or none phenomena, where the signal is either transmitted or not, but always with the same intensity. This observation reveals a parallel to human designed digital signaling, where mere on and off signals carry data. The rate of firing, that is the rate of signal initiation, determines the signal being transmitted. Typical approaches to measuring neuron signaling involve inserting a probe into the cell and measuring voltage changes during signal transmission. Most commonly, this is done with the use of a very thin glass pipette containing a conductive salt solution. In addition to being able to observe action potentials, it is possible to create them. By using a small glass pipette containing a solution with a positive charge, it is possible to depolarize the cell and create an action potential. Non penetrating techniques for detecting action potentials also exist, relying on changes in voltage on the cell's outer surface.

More recent advances in neuron cell monitoring include electrode arrays upon which cells are grown and monitored. These multi-electrode arrays are often manufactured with MEMS techniques and permit the analysis of a neuronal network *in situ*. An electrode array fabricated by Berdondini et al. (2005) demonstrated the capacity to monitor *in vitro* neuronal network activity. The team reported successful observation of signal propagation with neuronal rat cardiomyocytes, with most data errors apparently due to poor cell-electrode contact. Photoresist derived carbon surfaces hold promise as a substitute for the gold electrodes used in this experiment as higher adhesion surfaces that may perhaps be more easily patterned (Berdondini, van der Wal, Guenat, de Rooij, Koudelka-Hep, & Seitz, 2005). Other attempts to create neuronal network activity sensing devices have focused on the use of neuron cells as biosensors. A very intricate and complicated network sensing device was made by Gross et al. in 1995 with the intent of demonstrating network responses to pharmacological agents. Photoresist derived carbon holds promise as a means to fabricate such a sensing network with less work and greater cell-electrode contact at an even higher resolution than previous devices.

2.2. Substrate Fabrication

Fabrication of thin carbon films involves the pyrolysis of photoresist layers. A photoresist is a photoreactive polymer that changes solubility in a particular media after exposure to radiation. Among other desirable qualities, these materials are inexpensive, easy to work with and may be used in microfabrication. In being able to be micropatterned, materials made from resist precursors may also be made in patterns. Pyrolysis involves the heating of a material in an inert atmosphere. When this technique is applied to organic chemicals, the result is a carbon based material that behaves very similarly to graphite or glassy carbon.

2.2.1. Photolithography

First developed for applications in semiconductor manufacture, photolithography is a low cost and easy way to build micrometer scale structures. The process begins by selecting a substrate upon which the material will be fabricated. Typically, a wafer of polished silicon crystal is used as a substrate to support the microfabrication. When making microchips, a semiconductor (normally SiO_2) is placed on the wafer, which is then coated in photoresist. For the purposes of this project, the silicon wafer is merely coated with photoresist and its semiconductor properties are not relevant.

A photoresist is a light reactive polymer. Upon exposure to a specific frequency of ultraviolet (UV) light, the solubility of the polymer in the exposed area changes. In the case of a positive photoresist, the exposure forms cross links between aromatic rings within the polymer and increases stability in the exposed area. By contrast, negative photoresists are composed of aliphatic polymers that typically include a number of epoxide groups. UV exposure of negative photoresists decreases solubility within the exposed area by breaking epoxide cross links.

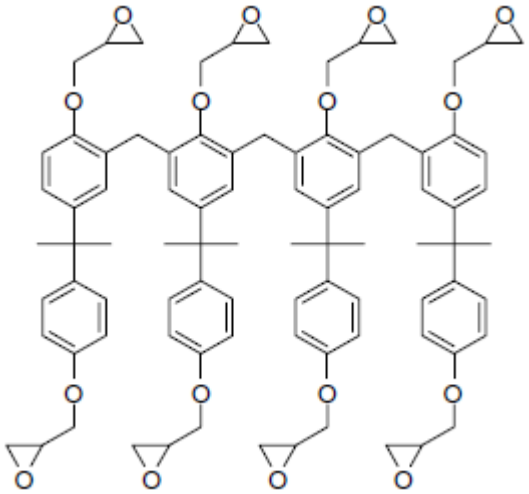

Figure 2.2.1.1: A SU-8 Monomer.
The epoxide groups cross link between chains when the photo-acid-generator is exposed to UV light and creates protons to catalyze this reaction (del Campo & Greiner, 2007).

There are two photoresists used in this project. The first is SU-8, a negative epoxy type near UV photoresist that is commonly used in high aspect ratio MEMS devices. SU-8 is a commonly used photoresist in MEMS applications for its low cost, ability to be easily patterned and capacity to make high aspect ratio structures. Monomers of SU-8 consist of eight highly reactive epoxide groups that cross link very readily in the presence of an acid. Also in the supplied solution is a photoacid generator which, upon exposure to UV light, creates a strong acid in low concentrations. The acid catalyzes cross-linking of the photoresist, stabilizing regions that are exposed to light. Copolymers of SU-8 and photoacid generating complexes constitute the functional part of the photoresist, while a solvent (gamma-butyrolactone) makes spin coating this polymer possible (del Campo & Greiner, 2007).

The photoresist used for the bulk of this investigation is S1813. As a positive photoresist, S1813 has a structure based largely on polymers of aromatic rings. It has a low viscosity and is able to form very thin and very uniform layers when spin cast. It is very soluble in acetone, and stable in deionized water. S1814 has been observed to adhere poorly to a substrate when subjected to force after soft bake, exposure and developing. It is capable of being pyrolyzed, and produces a thin carbon film as would be expected (Shipley, 2005).

2.2.2. Micropatterning

The capacity to pattern a substrate with high precision on a small scale is one tool that may be used in creating deliberately guided neurite growth. Photolithography offers a very good approach to patterning with its ease of use, high potential volume and level of detail. Often, patterned photoresist materials are used as precursors to other substrates. For example, micropatterned photoresist may be used with replica molding to make microfabricated polymer structures, with chemical masking techniques to create patterned small molecules or proteins or it may be modified to create microscale structures with a unique set of properties.

Other approaches to studying neurite growth have used replica molding to create polymer surfaces with desired surfaces. Replica molding is done by creating a negative relief of the desired shapes with photolithography and pressing that mold against a soft polymer. Baking or curing the polymer leaves a permanent imprint of the desired shape with a high degree of accuracy. This technique has been applied to neuron cultures with success (Li & Folch, 2005). This process, though capable of creating a very accurate mold, is rather labor intensive and lacks the desired electrical properties that are achieved with photoresist derived carbon.

Replica molding is commonly used to create small scale structures of biocompatible polymers—PDMS most notably. PDMS has been long used in medical implants for its high degree of biocompatibility (Belanger & Marois, 2001; Folch & & Toner, 2000). It is a common choice for its ability to be fabricated with hundred nanometer resolutions while supporting cell growth and permitting easy observation of cells (Uttayarat, Toworfe, Dietrich, Lelkes, & Composto, 2005; Karuri, Liliensiek, Teixeira, Abrams, Nealey, & Murphy, 2004). Yet, despite its favorable qualities, PDMS (like the vast majority of polymer substrates) is unable to provide the exact chemical and electrical properties of carbon. In particular, surface modifications of carbon may utilize long established graphite based techniques for immobilizing

molecules on surfaces, where PDMS demands slightly more elaborate techniques (Gomez, Lu, Chen, & Schmidt, 2007; Hu, Ni, Montana, Haddon, & Parpura, 2004).

Using photoresist structures to mask underlying silicon substrates allows selective modification of the silicon surface. In microelectronics manufacture, this technique is used to etch grooves in the silicon, but by exploiting silane chemistry it is possible to immobilize nearly any molecule on the silicon surface. Subsequent stripping of the photoresist leaves an area of functional groups attached to the silicon surface in the shape of where the photoresist was not previously adhered. Notably, this technique has been used to create patterns of proteins (Kleinfeld, Kahler, & Hockberger, 1988).

Modification of a photoresist layer can yield a material with the physical dimensions of the photoresist layer but with a new set of properties. For example, reactive oxygen plasma etching and pyrolysis create drastically different material properties but maintain photoresist shape. Reactive oxygen plasma etching exposes the material to an oxygen plasma, etching away surface features and leaving a number of functional oxygen groups on the exposed surface (carboxyl groups, alcohols and carboxylic acids most notably). Pyrolyzing a photoresist material leaves a carbon structure in the photoresist's place. This study utilizes this technique to produce substrates for neuron growth (Walther, et al., 2007).

2.2.3. Pyrolysis

One of the first thorough studies of the pyrolysis of patterned photoresist as a means to create carbon films or microstructures was conducted by AM Lyons, LP Hale and CW Wilkins Jr. at AT&T Laboratories in 1985. Rather than etch a conductive or semi-conductive layer covered by photoresist, the group sought to directly modify common materials to create desired properties. The team reported the ability to create insulating, semiconductive and semimetalic structures while maintaining the quality of the pattern (Lyons, Hale, & Wilkins, 1985).

Pyrolysis is a process that involves heating a sample in an inert atmosphere. In most cases, the atmosphere used is a vacuum, forming gas or nitrogen. Experiments by Madou et al. illustrate the affect of atmosphere selection on material loss during the pyrolysis process. Findings indicate that a vacuum is best at preventing film thickness reduction, and that nitrogen is better than forming gas (Ranganathan, McCreery, Majji, & Madou, 2000). Maintaining a high vacuum demands special equipment considerations for the pyrolysis furnace and forming gas reacts with the carbon film at temperatures in excess of 800C (Lyons, Hale, & Wilkins, 1985). Nitrogen is thus a reasonable compromise between performance availability and material considerations for this study.

Heating a photoresist to high temperatures forms cross links in polymer chains. X-ray photoelectron spectroscopy (XPS) spectra of pyrolyzed positive photoresist shows a clear shift from C-O bonds to C=O (or C-O-C) bonds with increases in temperature (Kostecki, Schnyder, Alliata, Song, Kinoshita, & Kotz, 2001). Additional results by Ranganathan et al. demonstrated a lowering of oxygen to carbon ratio with increasing pyrolysis temperature. An increase in O/C ratio was observed after letting samples rest in air for several days. Forming gas has demonstrated the ability to create the lowest O/C ratios, indicating the purest carbon film because the hydrogen acts as an oxygen scavenger, but at the cost of a great deal

more surface loss (Ranganathan, McCreery, Majji, & Madou, 2000). Experiments have demonstrated that O/C ratios level out to about 0.05 at temperature above 1000C. This tends to indicate that little benefit may be gained by pyrolyzing to temperatures in excess of 1000C.

Analysis has demonstrated that the film left after pyrolysis of photoresist is largely made of carbon. The declining O/C ratio demonstrates an increase in purity of the carbonized residue with an increase in pyrolysis temperature. Electrochemical studies have compared pyrolyzed photoresist to a polished glass carbon standard. Ranganathan et al. demonstrated ΔE_P values that are up to within 17% of those for the glass carbon standard (Ranganathan, McCreery, Majji, & Madou, 2000). Though glassy carbon is completely non-amorphous, the electrochemical studies are not sufficient to draw conclusions regarding the film's structure (Harris, 2005).

Raman spectroscopy has also demonstrated parallels between pyrolyzed photoresist and a glassy carbon standard. Raman shift observations at 1360 cm^{-1} and 1582 cm^{-1} demonstrates a shift from sp^2 hybridized carbon to sp^3 hybridized carbon with increases in temperature. The structural changes demonstrated by XPS and Raman spectroscopy coordinate very well with electrochemical observations (Ranganathan, McCreery, Majji, & Madou, 2000). The surface of a spin cast photoresist layer is virtually uniform prior to the pyrolysis process. The pyrolysis process appears to not drastically change the surface topography. One particular procedure produced a surface with a 15 angstrom peak to peak variation and a root mean square roughness of 3.3 angstroms (Teixidor, et al., 2008).

2.3. Cell Culturing

2.3.1. Nerve Cells

While the physical properties of photoresist-derived carbon films are well understood, the material's application to biological systems has not seen as much research. One prior study has demonstrated biocompatibility of photoresist-derived carbon. It was demonstrated that SK-N-MC, SY5Y and P-19 cells adhere quite well to this substrate. These cultures demonstrated that cells will divide on the surface. The SK-N-MC cells in particular grew very well, exhibiting overlapping growth after four days. Each of the three cell types is known to have good adhesion properties and to divide well in suitable conditions. The team turned then to PC-12 cells, to place greater scrutiny on the substrate's suitability for cell growth (Zhou, Gupta, Zou, & Zhou, 2007).

PC-12 cells are cells from clonal line of rat pheochromocytoma that respond to nerve growth factor (NGF). The cell line, started by L Greene and A Tischler in 1978, is a clonal line of noradrenergic cells from a rat adrenal gland. This cell line is most often used to simulate neurite growth and is useful in modeling neuronal repair. Upon exposure to NGF, the cells stop dividing and within just a few days neurites begin to grow. Prolonged exposure (in excess of two weeks) to NGF results in cells that have neurites reaching up to 1 mm in length. When exposure is discontinued, the neurite growth drops of sharply and within one day neurites are degraded and cell division resumes within one more day. Unfortunately, PC-12 cells do not adhere well to non-functionalized traditional substrates. When using

glass or plastic to grow PC-12 cells, coating the surface with poly-lysine (PL) polymers greatly enhances the cellular adhesion and neurite length (Greene, 1976).

Since PC-12 cells adhere poorly to surfaces, any means to enhance surface adhesion is helpful when culturing these cells. Zhou et al. demonstrated that PC-12 cells adhere to and are capable of differentiation on photoresist-derived carbon surfaces. Moreover, it was demonstrated that neurite growth rate is greater on carbon than PL coated glass. These findings demonstrate not only biocompatibility of photoresist-derived carbon, but also a novel approach to the poor adhesion of PC-12 cells to surfaces (Zhou, Gupta, Zou, & Zhou, 2007).

2.3.2. Cellular Response to Microtopography

Arrangement of micropatterned surfaces may be used to create a specific cellular response on a surface. Recent studies have worked to quantify cellular response on patterned substrates. One such study in 2004 by Karuri et al. examined adhesive properties on varying surface topographies. By applying sheer stress to the cells, it is possible to gauge adhesive properties on that surface. Substrates were fabricated with a series of grooves with pitches ranging between 400 nm and 4000 nm. The ridge and groove sizes are approximately half the pitch each. Using a fluid flow system, sheer stress was applied by flowing growth media perpendicular to the surface parallel to the direction of the grooves. Known concentrations of corneal epithelial cells were seeded on the substrate and incubated for 24 hours. After exposure to sheer stress, the cells were counted to determine adhesion. The team found that after an 80 Pa sheer stress the cells responded very differently to different surfaces. 400 nm pitch surfaces saw the best adhesion, with about 67% retention, while 4000 nm pitch surfaces had about 42% retention. The 4000 nm pitch surfaces did manage to perform better than a planar surface by almost 6%. It was noted that adhesion before flow was similar for most pitch sizes, with 1600 nm pitch and planar surfaces outperforming the rest by about 8%. Generally, cells adhered better after sheer stress on smaller pitch surfaces (Karuri, Liliensiek, Teixeira, Abrams, Nealey, & Murphy, 2004).

Surface topography has also been demonstrated to dictate cellular proliferation rates as well. Using a surface similar to that used by Karuri et al. in 2004, Liliensiek et al. studied response of corneal epithelial and corneal fibroblasts to varying surface parameters. Grooved surfaces with pitches between 400 nm and 4000 nm served as the substrates for cell growth. After seeding a known concentration of cells onto substrate samples, the cells were incubated for five days and then the cell numbers were counted. The team noted that corneal epithelial cells responded to surface topography with lower rates of proliferation. The 400 nm pitch surfaces saw a 45% increase in cell number, compared to the 163% of the 4000nm pitch surface. By contrast, the corneal fibroblasts did not demonstrate a significant response to the micropatterning until 14 days after plating, when it was noticed that 400 nm pitch surfaces had a 31% change in proliferation compared to the 178% change in the 4000 nm pitch surface. In both cases, the results on the 4000 nm pitch surface are not significantly different than the planar control. Trends indicated that smaller topographies correlate directly to lower proliferation (Liliensiek, Campbell, Nealey, & Murphy, 2006).

Height of topographic features also plays an important role in cellular response. In 2003, Dalby et al. used a polystyrene and poly n-butyl methacrylate substrate with 10 nm and 50 nm tall features to assess cytoskeleton structure in fibroblasts. Cells on 10 nm islands tended to form cytoskeletons that appear similar to those in cells on planar surfaces, while cells on 50 nm islands are noticeably deformed. It was also noticed that the cells tended to adhere better to the 10 nm islands after 180 minutes, with adhesion on the 50 nm surface being poor by contrast (Dalby, Riehle, Johnstone, Affrossman, & Curtis, 2003). An earlier study demonstrated similar results with 13 nm islands (Dalby, Yarwood, Riehle, Johnstone, Affrossman, & Curtis, 2002).

Further insight regarding feature depth has been gained through the use of grooved surfaces with varying depths. A 2005 study by Uttayarat et al. demonstrated changes in morphology that correlate with topography. Using grooves with depths ranging from 200 nm to 5000 nm, cell surface alignment and proliferation extent were measured. Additionally, florescent microscopy was used to examine arrangement of focal adhesions and actin arrangements. The team reported that cells grown on deeper topographies, 1000 nm and 5000 nm, the cells tended to align with the direction of the grooves more so than those at shallower topographies. The 1000 nm deep ridges saw 90% of cells aligning with the groove direction in the first hour after seeding. Additionally, higher cell densities were observed on substrates with deeper grooves. Fluorescent microscopy demonstrated that focal adhesions were formed on the top of ridges and partway down the sides. In the case of shallower depths, focal adhesions form on the floor of a groove, which appears to confirm results from islands of varying heights. Additionally, it was noticed that actin filaments do not align with the substrate, forming a rather tangled arrangement (Uttayarat, Toworfe, Dietrich, Lelkes, & Composto, 2005). This tends to suggest that micropatterned surfaces are able to affect changes in adhesion by dictating arrangement of focal adhesions.

2.3.3. Cellular Response to Surface Chemistry

Surface chemistry plays an important role in cellular response. Traditional approaches to encouraging cellular adhesion typically involve coating surfaces with positively charged molecules. It has long been established that coating surfaces with poly-lysine (PL) drastically improves adhesion of neuronal cells (Yavin & Yavin, 1974). While many other chemical cues have been demonstrated to encourage adhesion, PL is often used because it is easy to use, effective and relatively inexpensive. Novel materials may also encourage cellular adhesion. Among other new materials, self arranging surfaces and carbon nanotubes offer promise in this area.

Recent studies have looked at chemical cues on surfaces not merely as a way of encouraging adhesion, but also as a means to encourage close bonding to surfaces. Having a cell as close to a surface as possible is important when building electrical sensors that rely on close contact to measure very small changes in voltage. Immobilizing a number of common adhesion molecules including PL, aminopropyltriethoxy silane (APTES), Laminin, RGDC adhesion peptide, and cysteine terminated recombinant proteins Cys-axonin-1 and Cys-NgCAM. The last three of which were immobilized using APTES's available amino group. Using fluorescent interference contrast microscopy, it is possible to

measure distance between the solid substrate and the cell. The team noted that a smaller adhesion molecule did not necessarily correlate with a closer adhesion, as PL resulted in a larger distance than RGDC, Cys-axonin-1 and Cys-NG-CAM. It was observed that Cys-axonin-1 resulted in the closest adhesion, with about 37 nm, followed closely by APTES at 39 nm. Laminin had the longest adhesion by far, at 91 nm, but also had the greatest level of neurite growth with 90% of cells developing neurites. By contrast, APTES, despite its good adhesion properties, saw only a 20% neurite differentiation rate (Sorribas & Padeste, Photolithographic generation of protein micropatterns for neuron culture applications, 2002).

Distance between substrate and cell as determined by adhesion molecules may not correlate directly to strength of adhesion. Smaller adhesion promoters like PL and APTES seem to promote adhesion with their positively charged functional group. In cases of non-specific adhesion promoters, distance between the cell membrane and substrate are determined largely by the thickness of the glycoalyx (Sorribas & Padeste, Photolithographic generation of protein micropatterns for neuron culture applications, 2002). The correlation between positively charged functional groups and cellular adhesion was demonstrated some time earlier in 1988. It was noticed that adhesion promoters with more positively charged functional groups per molecule tended to promote more cell growth on substrates. Surface coats of diethylenetriamine propane outperformed ethylenediamine propane with outperformed aminopropane when culturing nerve cells on silicon and quartz substrates (Kleinfeld, Kahler, & Hockberger, 1988). Large protein complexes used to encourage adhesion bind to specific receptors on the cell's exterior. The distances between substrate and cell membrane is determined by the size of the adhesion promoter and the target receptors on the cell surface, which may extend up to 20 nm into the extracellular space. That is unless the promoter-receptor complex is shorter than the glycoalyx, in which case the glycoalyx determines binding distances. Indeed, the fact that Sorribas et al. reported no adhesion closer than 35 nm confirms the assertion that the glycoalyx ultimately determines cell to substrate distances. Given the close performance of most adhesion promoters, it is important then to choose an adhesion promoter based on the desired neurite growth performance (Sorribas, Braun, Leder, Sonderegger, & Tiefenauer, 2001).

In addition to adhesion response, surfaces may be chemically functionalized to induce morphological changes. As noted previously, findings by Sorribas et al. (2001) demonstrated varying levels of neurite differentiation with the use of different adhesion promoters. Immobilization of growth factors or certain proteins on surfaces provides a way to encourage specific morphological changes in cultures. Kleinfeld et al. (1988) demonstrated ways to immobilize molecules with functional amino groups on surfaces patterned with photolithography. Treating a silicon oxide surface coated in photoresist with alkyl-trichlorosilanes prior to wet stripping leaves a layer of alkyl-trichlorosilanes bonded strongly only to the oxide layer after stripping. Using wet stripping to remove the photoresist leaves an area of silicon oxide that is able to bind functionalized silane molecules, amino-trihydroxysilane for example. The result is a deliberately patterned area of substrate with functional groups available to cells (Kleinfeld, Kahler, & Hockberger, 1988). Later studies would use techniques virtually identical to methods used by Kleinfeld et al. to immobilize proteins using silanes. Most proteins will not bond directly to the functional amine group, so it is treated with sGMBS, permitting proteins with a terminal cystine to

attach easily. Alternately, silanes with a mercapto group may be attached to proteins which have had their N-terminus treated with sMBS. Either method results in a covalently immobilized protein on a patterned surface (Sorribas & Padeste, Photolithographic generation of protein micropatterns for neuron culture applications, 2002).

Surface energy has been demonstrated to have a profound effect on cell-surface interactions. A 2006 paper by Kennedy et al. demonstrated a relationship between surface energy and cell migration and proliferation. A surface of graded surface energies was coated in fibronectin and mouse fibroblasts cells were grown on the surface. It was observed that cells on hydrophobic regions had a higher rate of proliferation and a higher density per unit area. Coating the surface in fibronectin and the choice of fibroblast cells (which adhere via a fibronectin mediated mechanism) prior to seeding cells permits this study to be used draw conclusions only about fibronectin-mediated cell adhesion and proliferation (Kennedy et al., 2005).

2.3.4. Neurite Guidance

One key aspect of the use of MEMS structures as substrates for neuron growth is the ability to control surface geometry and chemistry with a high degree of spatial accuracy. Among other advantages, this ability to precisely fabricate materials has proved useful in studying cellular response to surface properties. In particular, neurite outgrowth in the context of particular surface features is a large area of study. Recent studies have looked at neurite response to surface chemistry, topographic features and the integration of the two.

Early studies with neuron response to surface immobilized molecules focused on using adhesion promoting peptides to encourage specific neuron adhesion. A 1988 study by Kleinfeld, Kahler and Hockberger used photodefined patterns of immobilized ethylenediamine propane (EDA-P) to control cell adhesion. It was observed that cells adhered almost exclusively to regions coated in the adhesion promoting molecules. Additionally, neurite outgrowth was confined to adhesion promoting regions, demonstrating a propensity to guide neurite outgrowth by varying surface adhesive properties (Kleinfeld, Kahler, & Hockberger, 1988).

Immobilizing NGF in a three dimensional matrix or on a two dimensional surface has elucidated cellular response to chemical cues. A 2003 study by Kapur and Shiochet sought to examine cellular response to gradients of NGF. In a hydrogel matrix, a gradient of varying NGF concentration was established and immobilized. Culturing PC12 cells in the matrix, it was observed that at gradients of 357 ng/mL/mm the cells tend to favor the direction of the gradient. Further experiments demonstrated the fact that it is the gradient that encourages the neurite growth, rather than the NGF presence in the media. No preference was observed for lower gradients (the closest being 137 ng/mL/mm). Neurites growing in the direction of the gradient were guided at an average angle of 8.2 degrees in reference to the direction of the gradient. It is important to note that these results were observed at very high concentrations of NGF, with the final gradient ranging between 1e5 and 3e5 ng/mL in a roughly linear pattern with respect to displacement (Kapur & Shoichet, 2004).

Microfabricated surfaces may be created with topographic features that attempt to model cell substratum properties. Such surfaces may be used to study cellular response to three dimensional topographical cues. Notably, such studies have demonstrated cell alignment, axon guidance and neurite response to topographical cues. Neuron cells grown on surfaces with grooves that are of similar scale to processes tend to align themselves in the direction of the grooves. Additionally, processes tend not to respond to topographical features that are much smaller than the process. This behavior seems to be best explained as a function of the ratio between the size of the neurite growth cone and the dimensions of the grooves (Johnansson, Carlberg, Danielson, Montelius, & Kanje, 2006).

Studies using three dimensional constraints on two dimensional topography have further elucidated the role of growth cone-surface interactions in neurite outgrowth. A 2007 study by Francisco et al. demonstrated that the number of "collisions" a neurite has with a wall drastically reduces further outgrowth potential. This was most strongly shown in investigating axon growth through corners of varying degrees and widths and by totally confined cells. In both cases, neurites were not observed to continue outgrowth after a few collisions with the confining wall. The team expected the neurites to grow to fill the chamber or perhaps grow with a limited length, not to stop growing completely (Francisco, Yellen, Halverson, Friedman, & Gallo, 2007).

2.4 Surface Characterization

Characterizing surface properties may offer insight regarding cell-surface response. As discussed in Section 2.3, minute variations in surface features may have drastic consequences for cell adhesion, morphology or even survival. Of particular interest to cell-surface interactions is the surface's chemical properties. Cyclic voltammetry is used to assess electrochemical properties of the surface. By comparing a sample to a known standard, it is possible to draw conclusions about the surface's electrochemical properties. Surface energy is a measure of surface's chemical behavior. By measuring the contact angle of a droplet on the surface, one may see how the surface interacts with the fluid and assess the surface's bulk polarity properties.

2.3.1. Cyclic Voltammetry

Carbon films are characterized to ensure that the chemical and physical properties are indeed as desired. Additionally, a survey of film features is necessary to understand the cell's response to the surface. Of particular interest is the substrate's chemical properties, which may have drastic effects on cell adhesion and gene expression. One common technique to evaluate a surface's chemical properties is cyclic voltammetry (CV), an electrochemical technique that surveys a material's response to changes in voltage while exposed to a standard ion solution.

Cyclic voltammetry is a technique that examines changes in current that result from changes in potential influencing a surface. A solution is subjected to a potential that increases and then decreases (or decreases and then increases depending on the scan profile) and the resulting current is measured. Peaks in current are observed when an ion in solution becomes a solid on the electrode surface or a solid on the surface is ionized into solution. This technique is commonly used to detect metals in

solution, as each metal will become a solid at different potentials and different metals can thus be discerned easily.

2.3.1. Surface Energy

Placing a droplet on a flat surface and observing the contact angle lends insight regarding the surface's interaction with the droplet. A flatter contact angle indicates greater wettability and domination of surface-liquid interfacial interactions over the gas-liquid interactions. For example, a flat droplet of water on a surface indicates that the surface has the capacity to form hydrogen bonds with the fluid, where a round droplet with a greater contact angle corresponds to a reduced surface affinity for the droplet.

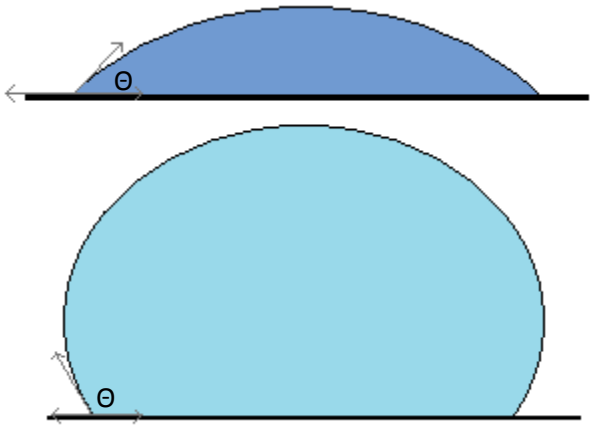

Figure 2.3.1.1: Drawing of droplet-surface interaction illustrating differences in surface energy.
Droplet contact angle is marked by a "Θ" on the inside of the angle measured. The surface with less energy is displayed at bottom, with a much larger contact angle than the high energy surface at top. The droplet's shape is determined by the ratio between the fluid's surface tension at the fluid-gas interface (the diagonal force vector in grey) and the fluid-surface interaction (solid-liquid surface tension illustrated by the horizontal grey vector pointing inward toward the droplet) and the solid-gas surface tension (the horizontal vector pointing outward away the droplet).

A lower surface energy results in domination of surface tension forces at the fluid-gas interface and a rounder droplet with a higher contact angle is formed. The strength of the solid-liquid interfacial stress is directly proportional to the cosine of the contact angle, that is to the horizontal component of the diagonal vector. A higher energy surface has a greater solid-liquid interaction force than liquid-gas interaction (surface tension), the result is a lower contact angle and greater wettability. By contrast, the low energy surface sees domination of liquid-gas interaction (surface tension) and the droplet is more spherical with a larger contact angle.

3. Materials and Methods

3.1. Photoresist Derived Carbon Film Fabrication

Fabrication of thin carbon films is broken into two major parts: preparing the photoresist film and pyrolyzing the photoresist film into a carbon film. The photoresist film is prepared by spin coating a thin layer positive photoresist, S1813 (Shipley) using a novel procedure to achieve the necessary film thickness to overcome surface loss during the pyrolysis procedure. The pyrolysis procedure is developed in an effort to reduce time and inert gas and energy use while maintaining a quality product. For a detailed and illustrated guide to procedures, refer to Appendix D and Appendix E for a detailed explanation of clean room preparation and the spin coating procedure. Additionally, a detailed guide to pyrolyzing photoresist films to produce thin carbon films may be found in Appendix F.

3.1.1. Preparation of S1813 photoresist film

In a clean room, polished silicon wafers are cleaned in preparation for spin coating. The wafers are first left to soak in acetone for 4 minutes in a large Petri dish. Over the course of the soaking period, the dish is agitated or the wafer moved to ensure that any material dislodged from the surface is washed away. Next, the wafer is sonicated in a bath of methanol for 4 minutes. Upon completion of the ultrasonic methanol bath, the wafer is put in a Petri dish being filled and overflowing with a constant stream of deionized water. After 4 minutes in the water bath, the wafer is sprayed dry with nitrogen, ensuring that there are no droplets on the polished side of the wafer. A 1 minute bake in an oven at 110°C is then used to dry any remaining water. The wafer is removed and left to cool on a clean surface for 2 minutes.

Now clean, the wafer is ready to be spin coated. The wafer is positioned and centered on the spin coater's vacuum holder and spun for 10 seconds at 4000 rpm to ensure that it is centered and to remove any remaining water. To apply the photoresist, approximately 2ml of S1813 photoresist is pipetted into the center of the wafer using two pasture pipettes in parallel. The high viscosity of the photoresist does not allow the use of a single pipette because the time to fill and empty the pipette is too long and the photoresist begins to harden before it is all placed on the wafer. Once the photoresist is applied, the wafer is spun using one of two spin profiles.

The first consists of spinning the wafer at 3000 rpm for 90 seconds, yielding a very uniform but thin coating. The second spin profile is a spin at 500 rpm for 45 seconds, followed promptly by a 45 second spin at 1000 rpm. The 500 rpm spin helps to ensure there is an even coating of photoresist in the center and mid portions, while the 1000 rpm spin removes residue that collects at the wafer's outer edge due to surface tension of the liquid photoresist and further ensures that the photoresist forms a uniform layer.

After spin coating, the wafer is removed and placed into the 110°C furnace for 3 minutes for a soft bake. Having baked for 3 minutes, the wafer is left to cool at room temperature and is ready for another spin coat or pyrolysis. The first spin procedure is often coated four times to ensure a thick layer is produced,

while the second procedure demands only two coats to create a sufficiently thick layer. Precautions are taken during transport of the coated wafer to minimize exposure to oxygen and light, with the wafer being transported in an air tight case covered in tin foil. Additionally, the wafers are stored in a dark drawer to minimize light exposure.

3.1.2. Pyrolysis

The pyrolysis process was varied depending on the type of photoresist used. Unique chemical properties of each photoresist demanded a slightly different approach to the pyrolysis process. For example, the annealing temperature of SU-8 is around 300°C, thus requiring a brief rest at this temperature to encourage extensive cross-linking prior to carbonization (del Campo & Greiner, 2007). By contrast, S1813 did not need this rest and the temperature rates seem to be determined more by thermal expansion concerns.

Regardless of the photoresist used, the steps leading up to the pyrolysis are the same. The 100mm circular silicon wafers are cut into 22mm by 22mm chips by scoring the uncoated side with a diamond tipped pen and then breaking the wafer along a straight edge. The pieces are loaded onto a sled made of stainless steel (for 900°C maximum temperature), a silicon wafer or silica (for procedures up to 1000°C). The sled is then placed in a three inch diameter fused quartz tube and centered in the tube. Next, the tube's open end is sealed with a bolt on cap with a gas line attached. The tube is then placed into the split tube furnace and the open space between the quartz tube and the furnace are insulated with christobalite blocks. Pure N2 is then flowed through the now sealed quartz cylinder at 100 cm3 sccm for 10 min to ensure an inert atmosphere.

The furnace is turned on and programmed to the desired parameters. From room temperature to 300°C, the furnace is heated at 2°C/min. When using SU8, the temperature is then sustained at 300°C for one hour. After the 1 hour rest, the temperature is increased at a rate of 10°C/min to 900°C. When using S1813, the rest period is omitted from the procedure and the sample is heated at 10°C/min to 1000°C immediately after reaching 300°C at 2°C/min from room temperature. Samples may be left to sit at 1000°C for one hour, at which point the furnace was turned off and the samples are left to cool to room temperature in the still flowing N_2 atmosphere. Once the samples are cooled to room temperature, the gas is turned off and the samples are removed. See Table 3.2.1 for details of pyrolysis procedures. Oxygen plasma samples were prepared using O_2 plasma treatment at 150 mTorr and fifty watts for thirty seconds. Samples treated with oxygen plasma etching were prepared with pyrolysis method 16.

Table 3.2.1: Substrate Preparation Methods

Method	Heat rate 1	Rest 1	Heat rate 2	T_{max}	Rest 2	Photoresist
1	10°C/min	none	N/A	1000°C	60 min	SU-8
2	3°C/min	none	N/A	600°C	60 min	SU-8
3	2°C/min	40 min at 300°C	10°C/min	900°C	60 min	SU-8
4	2°C/min	40 min at 300°C	10°C/min	900°C	60 min	S1813
5	2°C/min	40 min at 300°C	10°C/min	1000°C	60 min	S1813

6	2°C/min	0 min at 300°C	10°C/min	1000°C	60 min	S1813
7	2°C/min	60 min at 300°C	10°C/min	1000°C	60 min	SU-8
8	2°C/min	60 min at 300°C	10°C/min	800°C	60 min	SU-8
9	2°C/min	60 min at 300°C	5°C/min	800°C	60 min	SU-8
10	2°C/min	60 min at 300°C	5°C/min	700°C	60 min	SU-8
11	2°C/min	60 min at 300°C	N/A	1000°C	60 min	SU-8
12	2°C/min	none	N/A	1000°C	60 min	SU-8
13*	2°C/min	none	N/A	800°C	300 min	SU-8
14*	2°C/min	none	N/A	800°C	60 min	SU-8
15*	2°C/min	none	N/A	800°C	0 min	SU-8
16	2°C/min	0 min at 300°C	10°C/min	1000°C	0 min	S1813
17	2°C/min	0 min at 300°C	8°C/min	1000°C	0 min	S1813

* indicates a 2°C/min cooling rate.

3.2. Cell Preparation

Cells used for neuron modeling experiments are from the PC12 rat pheochromocytoma clonal cell line. When not in use, cells are stored frozen at -80°C and are thawed for seeding plates. Cells are grown on 100mm plastic petri dishes in 10ml high glucose DMEM bovine serum in an incubator at 38°C and 5% CO_2. The PC12 cells have very high metabolic demands and are very sensitive to changes in environment and thus their media is changed daily or every other day to promote steady growth. After at least 4 days of growing on the large culture plates, cells are ready to be seeded onto sample plates. To seed cells on other plates, the medium is removed from the plates and the cells are washed 3 times with PBS. Next, 1ml 0.25% trypson is added and the plate is let sit in the 38°C incubator for 5 minutes. Upon removal, 9 ml media are added and the plate is washed thoroughly with the media to ensure that no cells remain attached to the plate. Cells concentration was determined by counting cell numbers on a hemocytometer. With the cell concentration in the Petri dish, it is possible to seed the desired number of cells onto the smaller dishes.

3.3. Neurite Differentiation Genetic Assay

Cells are prepared for this experiment as discussed in "Cell Preparation." For genetic assays, cells are seeded at concentrations between 1.0×10^6 cells/ml and 1.2×10^6 cells/ml. Cells, once seeded, are permitted to sit for 1 day to adhere before media are removed and replaced with NGF (if appropriate for the sample) media. NGF is added at a 1:1000 ratio, as in all other experiments. Media is changed every other day, with DMEM high glucose (Invitrogen) being used. After six days, cell concentration is determined using the same methods as for the adhesion assay. mRNA is extracted using the Guanidinium thiocyanate-phenol-chloroform extraction procedure utilizing a TRIzol Reagent (Invitrogen) following the manufacturer's instructions. Extracted mRNA concentration is measured with a UV-Vis spectrometer and 1 µg total mRNA is used as a template to make first strand cDNA.

First-strand cDNA is reverse transcribed from 1 μg of total RNA using a Promega RT/PCR kit, all conducted according to manufacturer's recommended procedures. Selected primers are used in accordance with Promega's recommended procedures. Primers chosen include Tau, a structural protein that stabilizes actin filaments, beta-actin, a structural protein that plays a key role in extra-cellular matrix structure and glyceraldehydes-3-phosphate dehydrogenase (GAPDH), a cytosolic enzyme that participates in glycolysis to act as a housekeeping gene.

3.4. Cellular Adhesion Assay

Cellular adhesion assays were devised as a means to potentially correlate discrepancies observed in genetic assay 2 with cell adhesion. The easily performed assay selected is to trypsinize cells and count those that are removed. This procedure will only remove cells that are not adhered strongly. More specifically, this assay is a measure of removable cells and may say very little about the total number of cells or cell density per unit area on the substrate.

3.4.1 Cell Adhesion Assay Method 1

This experiment was conducted on a silicon wafer coated with four layers of S1813 each spun at 4000 rpm for 90 seconds. Pyrolysis was conducted using method 6, as may be seen in Table 3.2.1. Four 22mm by 22mm carbon samples were used in addition to four 22mm by 22mm bare (unmodified) silicon squares and 30mm diameter bare glass samples. Each substrate was placed into a sterile 35mm Petri dish. All samples were washed with DI water and sterilized with overnight exposure to ultraviolet light. Two of each type of substrate were soaked in a 50mg/ml poly-lysine (PL) (30,000-70,000 molecular weight, Sigma-Aldrich) for four hours before being washed 3 times with PBS. The resulting sample set consisted of two 22mm by 22mm blank carbon substrates, two 22mm by 22mm carbon substrates coated in PL, two blank 22mm by 22mm blank silicon substrates and two 22 mm by 22mm silicon substrates coated in PL and two bare glass substrates and two PL coated glass substrates.

Substrates were washed 3 times each with PBS before seeding cells. Cells were first prepared using the procedure discussed in section 3.3. The concentration of cells in the seed plate was determined to be 2.2×10^6 cells/ml. From the 6ml total volume on the seed dish, 0.48 ml of the cell solution was added to each of the target Petri dishes. An additional 1.52 ml of high glucose DMEM serum media was added to each sample dish, to ensure that the volume of fluid was able to completely cover the substrates and resulting in a final seeded cell count of 10.56×10^5 cells at a concentration of 5.28×10^5 cells/ml. The Petri dishes were gently agitated to ensure good mixing of cells in the dishes. The cells were then placed in an incubator kept at 38 degrees Celsius.

The cells were left for 24 hours in the incubator to ensure that all the cells that could adhere had a chance to do so. Low adhesion rates of PC12 cells justify the long period granted for cells to adhere. The liquid media were carefully aspirated off and new media were prepared. NGF was diluted 1:1000 in 12 ml high glucose non-serum media. 2 ml of the mixture was added to one dish from each category (one carbon without PL, one carbon with PL, one silicon without PL, one silicon with PL, one glass without PL and one glass with poly-lysine). To each of the remaining dishes 2 ml of high glucose DMEM

non serum media were added. Non-serum media was used in an effort to halt proliferation among cells not treated with NGF to parallel the haltering of proliferation observed in cells treated with NGF. Great care was taken when introducing new medium to the dish so as to not dislodge any cells that had adhered to the substrate.

After two days the media in each of the dishes was aspirated off carefully and replaced with the same NGF or non-NGF non-serum media. Two days after the media were changed, the cells were counted. To count the cells, the cells were first separated from the substrate by adding 0.5 ml of 0.25% trypsin solution and being placed in a 38^{o} C incubator for 5 minutes. Upon retrieval from the incubator, 0.5 ml of non-serum media was added to each dish, and each substrate was washed very thoroughly with the solution in the dish in an effort to dislodge any remaining cells. A very small sample (about 10 µl) was removed and a drop was placed on a hemocytometer. Using a microscope, cell numbers in three squares on the hemocytometer were counted to find a cell concentration in each dish. Between counting cell numbers the hemocytometer was cleaned and sterilized.

3.4.2. Cell Adhesion Assay Method 2

Shortcomings in findings from Trial 1 (failure of assay on silicon and low cell seeding concentration most notably) prompted slight revisions to be made to the procedure. In addition to cells being seeded in a higher concentration, 3 ml of solution was used rather than 2 ml in an effort to ensure that the substrates would be completely covered by the media solution. Additionally, a larger number of squares were counted on the hemocytometer in an effort to create a more consistent set of data. The procedure in detail follows.

22mm by 22mm carbon film wafers are placed in 35mm plastic Petri dishes and are sterilized by overnight exposure to UV light. In parallel, 35mm Petri dishes with bell glass slides are prepared and sterilized along with the carbon samples. Samples are coated with PL by suspending 30,000-70,000 molecular weight PL (Sigma-Aldrich) at a concentration of 50mg/ml. The substrates are set in 35mm Petri dishes to be exposed to the PL solution for 4 hours, at which point the PL solution is removed and the samples are washed three times with PBS.

Seeding cells are prepared grown in a Forma Scientific water jacketed series II Incubator at 37°C and 5% CO_2 in high glucose DMEM serum media (Invitrogen, Carlsbad CA). Changing the media every other day, cells are grown until they reach sufficient concentrations (around 2.2×10^6 cells/ml). Cell concentrations are determined using a hemocytometer and a VMR Vista Vision Inverted Microscope at 100x magnification. PC12 cells are seeded at a concentration of 6.0×10^5 cells/ml onto sterilized substrates in a 35mm Petri dish. 2ml of cell solution is pipetted into the dish and an addition 1ml of media is added to ensure that the substrate is covered with liquid. Cells are permitted to adhere to the surface for 1 day, at which point the media is replaced with DMEM high glucose serum free media (Invitrogen, Carlsbad CA). At this point, nerve growth factor (NGF) is added to the media of certain samples at a concentration of 1:1000 (v/v). The media is changed for fresh media of the same type after another two days, and after two more days the cells are counted. Cells are washed first in PBS, then treated with 0.5ml 0.5% trypsin and let to sit in an incubator at 37°C and 5% CO_2. Petri dishes are removed from the

incubator after 15 minutes exposure and 0.3ml DMEM high glucose serum free media (Invitrogen, Carlsbad CA) is added to the dish. With a pipette, the cells are washed thoroughly with the trypsin-media mixture to detach them from the surface. Cell concentrations are then determined by counting cell numbers using a hemocytometer with the use of a VMR Vista Vision Inverted Microscope at a 100x objective.

3.5. Cellular Morphology Assay

Cell morphology on each surface is evaluated not only as a means to evaluate cell-surface interaction on a qualitative level, but also to further explore possible explanations for the odd results in genetic assay 2. Indeed, this assay can serve as a baseline to explain further genetic assays in terms of morphology. Regrettably, this assay is not as quantitative as RT/PCR procedures. Since the substrates for cell growth (silicon, carbon and oxygen plasma treated carbon) are opaque, traditional transmission visual spectrum microscopy cannot be used. Thus, options are limited to more complicated techniques. Scanning electron microscopy (SEM) is a reasonable option, but it is a relatively challenging and time consuming procedure. Fluorescent microscopy does not offer the resolution or accuracy of SEM, but it is much easier and higher throughput.

Cells for this experiment were seeded at 3.7×10^5 cells in 3 ml of growth media. Glass, carbon, oxygen plasma treated carbon and silicon substrates are used for this experiment. Within each material group, there is a control sample seeded with only cells and media, a group with PL added to the surface using the aforementioned procedure, a group with NGF added and a group with PL and NGF. PL is coated on the surfaces prior to seeding cells, while NGF is added after a 24 hour adhesion period. After three days, the media is refreshed and after two more days the cells are prepared for microscopy.

To begin, DiI (Invitrogen) powder is suspended at a concentration of 1 µg/ml in ethanol. This stock solution is diluted 1:1000 by volume in ethanol for further use. 4 aliquots each of 1 ml were prepared for later use. Cell media is removed and cells are fixed for 5 minutes in 4% paraformaldehyde solution for 5 minutes. Enough paraformaldehyde is added to each of the 35 mm Petri dishes to ensure that the substrates are covered. The paraformaldehyde is disposed of and cells are washed 3 times in PBS. The 1:1000 DiI in ethanol solution is then pipetted in 20 µl quantities until the surface is covered and is added constantly to keep the surface from drying out over a 1 minute period. After 1 minute of exposure to the dye solution, the substrate is rinsed once in PBS and then mounted on a microscope slide. 20 µl of mounting media is added and a cover slip is applied.

3.6. Film Characterization

Film characterization is intended to place a focus on properties that may play a role in cell-surface interaction. The film mass and thickness loss is intended to demonstrate a change in density on the surface and is useful for comparison to previously documented work with other photoresist precursor materials. Film electrochemical properties analyzed with the use of cyclic voltammetry offer a hint at the surface's chemical properties, which may play a key role in a number of cell processes. Surface energy of the film lends insight regarding potential expectations for cell adhesion, as well as the films'

stability after experience to solvents and water. For an illustrated guide to cyclic voltammetry procedures, refer to Appendix H for the setup of the electrochemical cell and Appendix I for a guide to the software used to conduct the scan.

3.5.1. Film Loss Assessment

Film thickness and mass loss during fabrication are also quantified to provide better understanding of the film. Film thickness is measured using interfering phase microscopy. A Nikon microscope with a white light source and a 10X mirou type double beam CF Plan EPI DI objective mounted on a Physik Instrumente E-500.00 piezoelectric controller and measuring device is used to take measurements. By scraping a small area of the carbon film off with a razor blade, it is possible to measure the distance between the top of the remaining film and the wafer surface. Viewing the wafer through a microscope at a 100x objective, the wafer is aligned at a slight tilt so that it is not perpendicular to the microscope. The tilt of the sample makes phase contrast lines appear and distances may be measured by observing the change of phase between focusing on the top of the film and bare wafer surface.

Film mass loss is measured using a balance. Unpyrolyzed photoresist coated wafers cut into 22mm by 22mm wafers are weighed and then pyrolyzed. After the pyrolysis, the wafers are weighed again. The carbon films are removed from several wafers using an abrasive technique (rubbing with a kim wipe) and then are sonicated in ethanol. Resulting bare wafers are weighed, permitting film mass loss to be quantified.

3.5.2 Electrochemical Tests

Carbon films are characterized using cyclic voltammetry (CV) to confirm that the samples are indeed carbon. Using the PPF surface, the rectangular surfaces will first be cleaned by sonication in water, ethanol, and water again for five minutes each using the B25500A-MTH Ultrasonics Cleaner manufactured by VWR North America. The wafers are then allowed to dry in air. Using 3 mM 4-aminobenzoic acid (4-ABA) in a 1 M KCl deionized and distilled water solution. The carbon surface will act as a working electrode using a 3-electrode potentiostat with Ag/AgCl as the reference electrode using an AUTOLAB PGSTAT12 and utilizing the General Purpose Electrochemical System for Windows version 4.9.004. The surface in the water solution will be treated and monitored using four cycles of cyclic voltammetry scanning between 0.0 and +0.60 V at a rate of 100 mV/s.

3.5.3 Surface Energy Tests

Contact angles are estimated by simply placing a droplet on the surface and taking a photograph. Water, ethanol and toluene are used on bare silicon, silicon coated in s1813, an ordinary thin carbon film and an oxygen plasma treated thin carbon film. For water, a 25 µL droplet is used, 12 µL for ethanol and 8 µL for toluene. The differences in surface tension between the fluids allows for larger droplets to be more stable on the surface, where a larger droplet eases the task of measuring the contact angle. Photographs were taken of the droplets with a Nikon D80 with a Nikon AF Nikkor 50mm 1:1.8D reverse

mounted. A tangent line is drawn on each end of the droplet using Microsoft Paint and the angle is measured with a protractor.

4. Results and Discussion

4.1. Substrate Spin Coating

Wafers appear to have a very even coating of photoresist while spinning. Refraction of light along the surface of varying height creates a banding pattern of green and red that enlarges outwards as the wafer spins. This suggests an evening of the coating, with each band approximating a single wavelength height difference. As seen in Figure 4.4.1, the spinning wafer reflects light very well, suggesting a rather smooth surface.

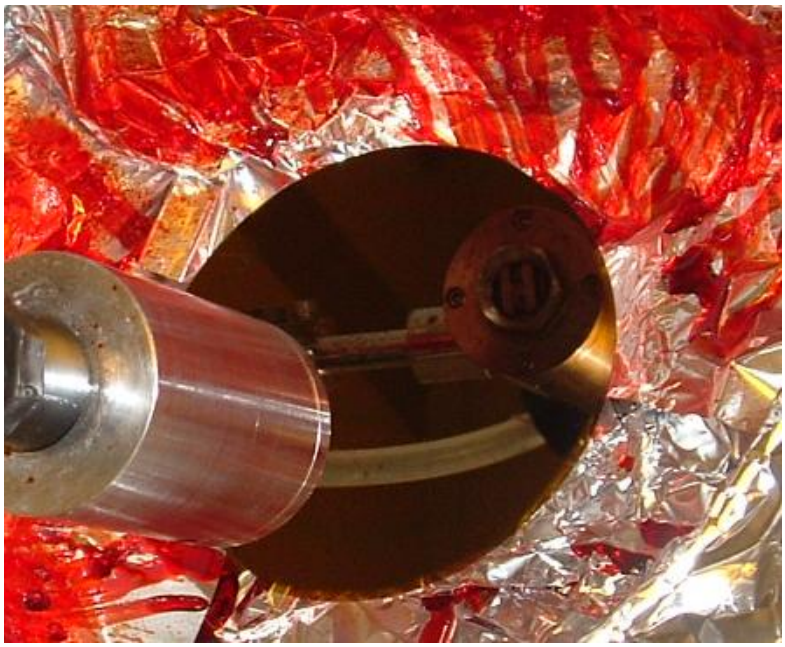

Figure 4.1.1: Wafer while being spin coated.
The wafer in this photograph is spinning at 3000 rpm to ensure a uniform coating. Each layer is approximately 2µ thick, resulting in a final thickness of 8-10 µm for four layers. The wafer appears mirror smooth while spinning, as may be seen by the reflection of the nozzle in the wafer.

After a single coating and soft bake, a banding pattern appears permanently on the wafers when subsequent photoresist layers are added. As seen in Figure 4.4.1, alternating green and red bands mark the surface of the wafer, though the wafer still does appear mirror smooth. With the addition of more coatings, the size and shape of the banding pattern grows more irregular, eventually appearing in a spotted pattern.

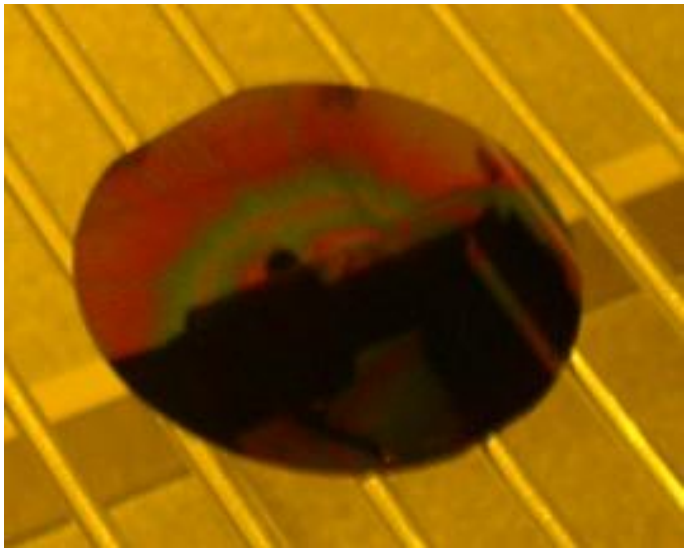

Figure 4.1.2: Banding pattern on a wafer with multiple coatings.
The banding pattern that appears on the wafer is due to differences in coating height. Each band represents a one half wavelength difference in height. More coatings results in a less even distribution of the banding pattern, and has consequences for local thickness. That said, changes in film thickness are not noticeable between different groups or different areas of the wafer.

Figure 4.1.3: Addition of photoresist to coated wafer.
2 ml of photoresist is pipetted into the center of the wafer prior to spinning. The wafer in this picture has been coated twice and the banding pattern is visible. Immediately after applying the photoresist to the wafer's surface the spin cycle is started.

When pipetting the photoresist onto the wafer for spin coating, the liquid photoresist expands evenly in a circle from the center of the wafer, as is expected (see Figure 4.1.3). When adding subsequent layers, however, droplets tend to pool preferentially in certain areas compared to others. The droplet

formation, though not quantified, seems to indicate slight variations in surface energy, with those photoresist-phobic regions forming nearly spherical droplets that roll along the surface rapidly, and photoresist-philic regions that see shallow droplets that pool together. This effect is exaggerated in the two 45 second step spin procedure. Though only observed qualitatively, it is believed that these variations in surface energy may play a role in adhesion between photoresist layers since the two 45 second step procedure seems to exhibit poor adhesion between layers.

The first spin procedure (3000 rpm for 90 seconds) results in a very thin (1.5-2.1 μm) coating (measured using the procedure in section 3.5.1) that is very consistent. By contrast, the second procedure (500 rpm for 45 seconds followed by 1000 rpm for 45 seconds) creates a visibly uneven coating. The edge effects are very noticeable and there is a clearly thicker layer in the center. Because of the inconsistencies in thickness, the wafers coated in this method did not produce good, consistent results when pyrolyzing, with samples cracking.

4.2. Substrate Pyrolysis

4.2.1. Pyrolysis Summary

Table 4.1.1: Substrate Preparation Methods organized chronologically

Method	Heat rate 1	Rest	Heat rate 2	Peak temperature, rest time		Photoresist
1	10°C/min	none	N/A	1000°C	60 min	SU-8
2	3°C/min	none	N/A	600°C	60 min	SU-8
3	**2°C/min**	**40 min at 300°C**	**10°C/min**	**900°C**	**60 min**	**SU-8**
4	2°C/min	40 min at 300°C	10°C/min	900°C	60 min	S1813
5	2°C/min	40 min at 300°C	10°C/min	1000°C	60 min	S1813
6	**2°C/min**	**0 min at 300°C**	**10°C/min**	**1000°C**	**60 min**	**S1813**
7	2°C/min	60 min at 300°C	10°C/min	1000°C	60 min	New SU-8
8	2°C/min	60 min at 300°C	10°C/min	800°C	60 min	New SU-8
9	2°C/min	60 min at 300°C	5°C/min	800°C	60 min	New SU-8
10	2°C/min	60 min at 300°C	5°C/min	700°C	60 min	New SU-8
11	2°C/min	60 min at 300°C	N/A	1000°C	60 min	New SU-8
12	2°C/min	none	N/A	1000°C	60 min	New SU-8
13*	2°C/min	none	N/A	800°C	300 min	New SU-8
14*	2°C/min	none	N/A	800°C	60 min	New SU-8
15*	2°C/min	none	N/A	800°C	0 min	New SU-8
16	**2°C/min**	**0 min at 300°C**	**10°C/min**	**1000°C**	**0 min**	**S1813**
17	**2°C/min**	**0 min at 300°C**	**8°C/min**	**1000°C**	**0 min**	**S1813**

* indicates 2°C/min cooling rate

Bolded rows indicate successful procedures

Defects in carbon surfaces are generally described as either peeling or cracking. Peeling is the delamination of the carbon film, which is believed to be caused by uneven thermal expansion of the wafer and carbon as proposed by Ranganathan et al. (2000). Cracking is a breakdown of the film itself,

presumably caused by film breakdown due to high temperature. Both defects may exist independently of one another, but may occur together. See Figure 4.2.1.1 for an example of cracking, Figure 4.2.1.2 for a depiction of peeling and Figure 4.2.1.3 for an example of a peeling and cracking film. In general, peeling refers to degradation of film adhesion, while cracking is the disintegration of the film itself. Other defects include deplating under electrical current and edge effects or edge pealing (depicted in Figures 4.2.1.4 and 4.2.1.5 respectively). Electrical deplating is observed with the film dissociates from the silicon wafer during a CV analysis. Edge effects seem to be caused largely by process used to cut the wafers and are exaggerated by exposure to water. Properly fabricated photoresist films may be seen in Figures 4.2.1.6 and 4.2.1.7. Photoresist films on wafers coated in "New SU-8" (SU-8 coated wafers received in the fall of 2008) remained intact when the wafer was broken. The result was pealing along the edges of a significant number of these samples due to the peeling off of edge areas.

Figure 4.2.1.1: Photograph of cracking of carbon film.
Cracking is defined as the breakdown of the film within itself, while maintaining adhesion to the silicon surface. Cracking is caused by a heat rate or cooling rate that is too rapid, resulting in differential rates of thermal expansion. The four ridges near the center of the image are from water induced edge effects (as depicted in Figure 4.2.1.5.

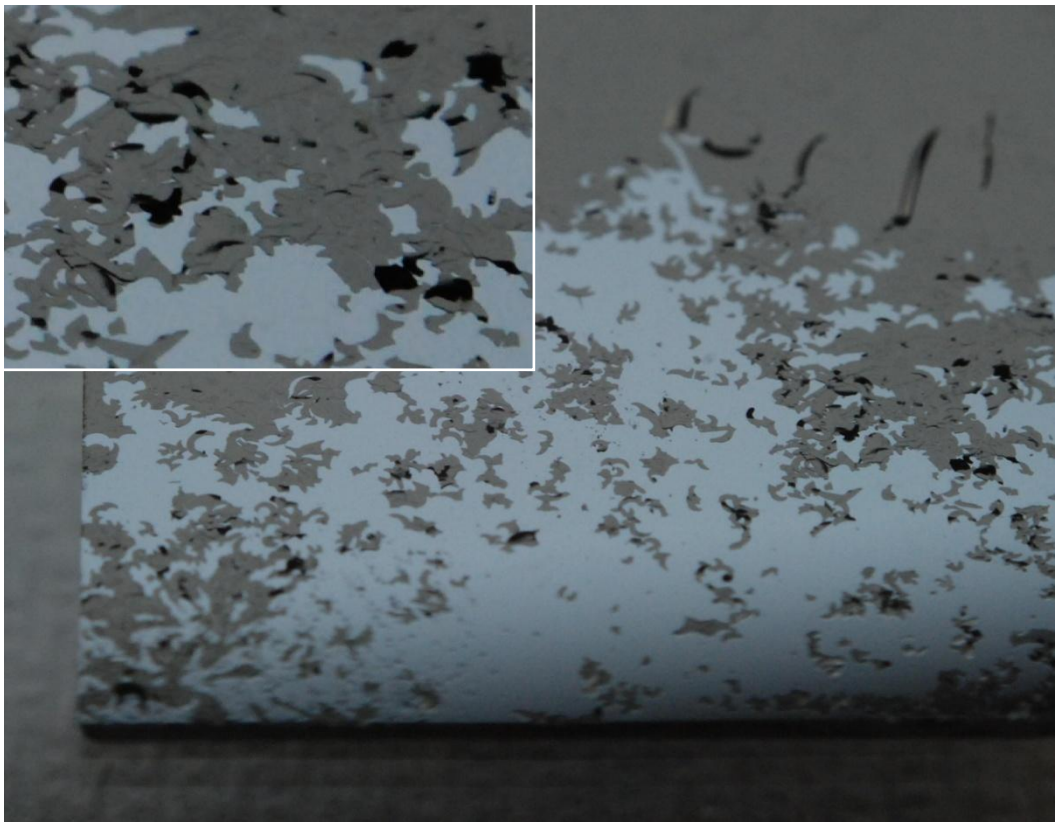

Figure 4.2.1.2: Photograph of peeling of carbon film.
Film peeling is the dissociation of the carbon film from the surface. Note the separation of the film from the surface and continued integrity of the film within itself. The insert highlights an area of particularly profound peeling. Peeling is caused by a maximum temperature that is too high. Ridges in the upper right of the wafer are caused by edge effects and exposure to water, highlighted in Figure 4.2.1.5.

Figure 4.2.1.3: Photograph of cracking and pealing of carbon film.
Cracking (disintegration of the carbon film) and peeling (separation of the film from the silicon surface) occur together when the heat rate is too high and the maximum temperature is too high. When exposed to water, these surfaces are often left as bare silicon wafers.

Figure 4.2.1.4: Photograph of electric deplating of carbon film.
Application of current to a seemingly stable film resulted in deplating of the film. The film was stable when left in water for 24 hours, but lifted off the surface after a single CV scan. Additionally, securing the wafer in the electrochemical cell broke the wafer along the edge depicted on the left of the photograph.

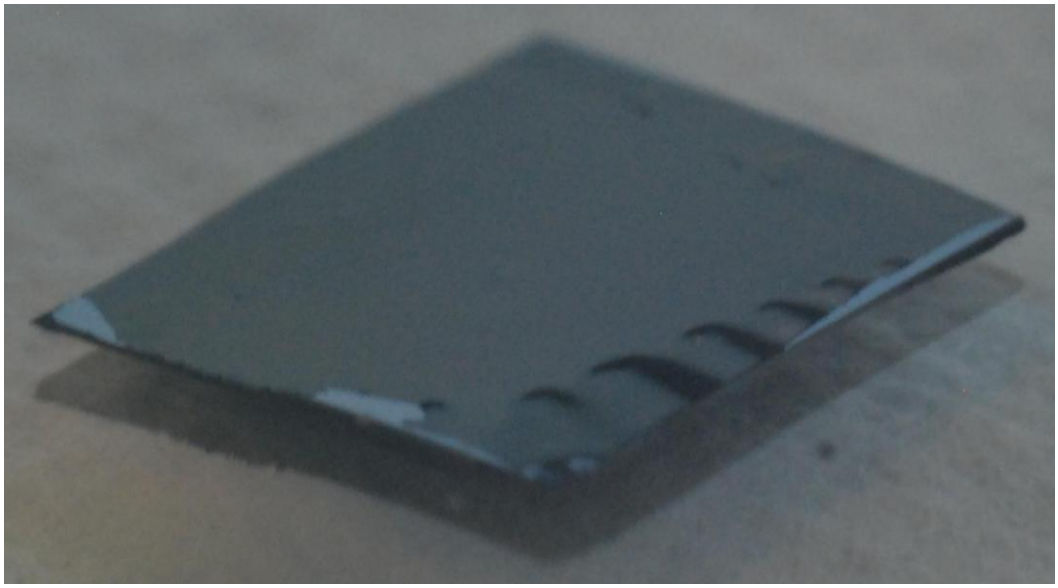

Figure 4.2.1.5: Photograph of edge effects of carbon film after exposure to water.
Slight defects along the edge of the wafer are caused by the wafer scoring and breaking process. Water infiltrates under the wafer along the edge and lifts the wafer from its silicon substrate, but the carbon film remains intact. It has been observed that this defect does not alter the substrate's ability to serve as a substratum for cell culture.

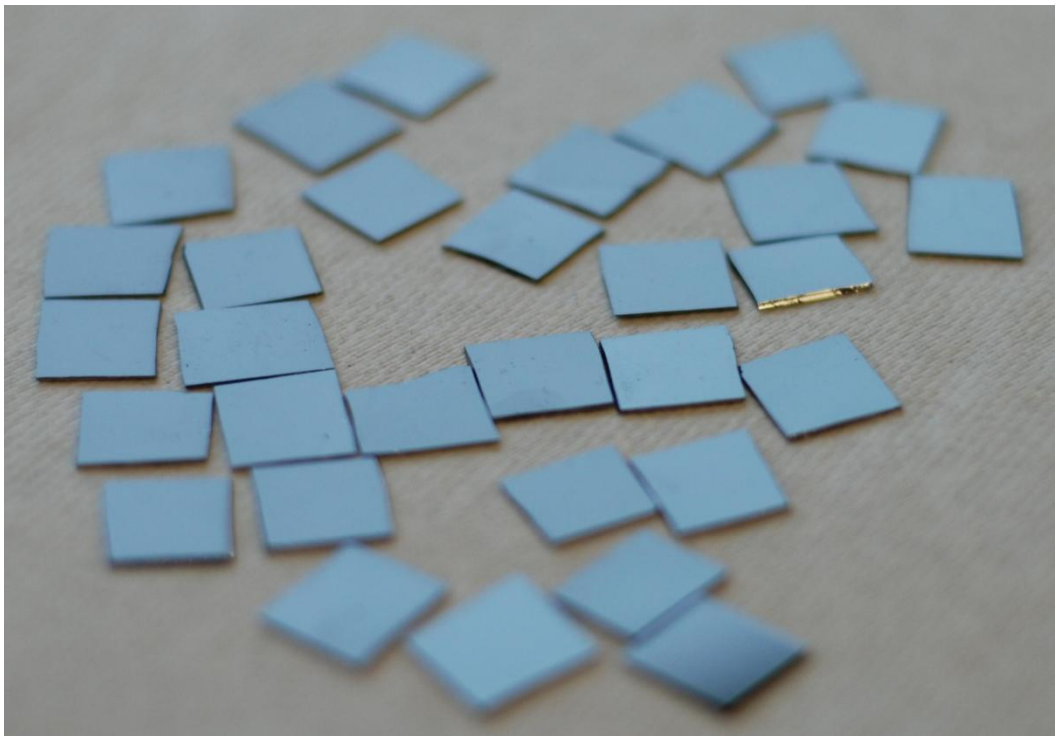

Figure 4.2.1.6: Photograph of properly fabricated thin carbon films.
These properly fabricated thin carbon films are consistent and free of defects. Integrity within the film itself and strong adhesion to the silicon substrate result in no visible cracking or peeling, creating the appearance of being a single, coherent layer.

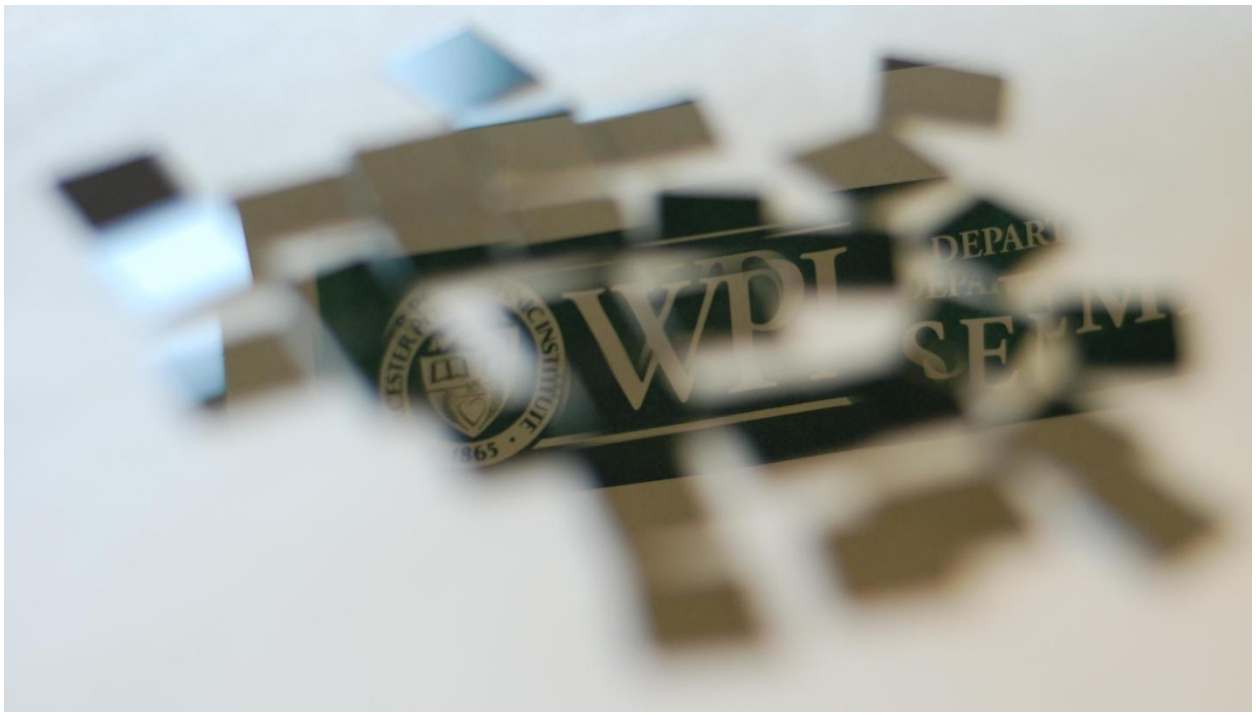

Figure 4.2.1.7: Photograph highlighting the reflective properties of properly fabricated carbon films.

4.2.2. Pyrolysis Method 1

Resulting substrates from method 1 were marked by a disappearance of photoresist from the surface. Retrieved samples appear to be pristine silicon wafers. The peak temperature of method 1 was within a range where the photoresist would be expected to still be stable and the predicted stability for different photoresists was assumed to hold true for SU8. Heat rate was selected as half of that used by Ranganathan et al., which was noticed to be somewhat higher than most other procedures (Ranganathan, McCreery, Majji, & Madou, 2000), (Renschler & Sylwester, Conductive, spin-cast carbon films from polyacrylnitrile , 1987), (Renschler, A.P., & Salgado, Carbon films from polyacrylnitrile, 1989), (Kostecki, Schnyder, Alliata, Song, Kinoshita, & Kotz, 2001). Thus, it was concluded that the heat rate for this method must be too high.

4.2.3. Pyrolysis Method 2

Desire to insure film stability and reduce film loss during heating motivated the creation of method 2. Samples prepared with this method appeared to have a consistent and smooth layer of carbon covering the surface. Results by Ranganathan et al. seemed to indicate that 600°C would be a sufficient peak temperature, albeit for AZ4330 (Ranganathan, McCreery, Majji, & Madou, 2000). A simple adhesion test (merely submerging the sample in tap water in a Petri dish for several days) indicated that the photoresist did not adhere well to the silicon wafer in aqueous environment. Thus, this method would not be suitable for creating a substrate to withstand biological conditions.

4.2.4. Pyrolysis Method 3

Learning from the failures of methods 1 and 2, method 3 combined the slow initial heat rate of method 2 with the high maximum temperature of method 1. The carbon film produced by method 3 appeared consistent and proved stable in water. This method was used to create the substrates used for the cell experiments using films from SU8. According to Ranganathan et al., the material loss was greatest around 300°C (Ranganathan, McCreery, Majji, & Madou, 2000). Thus, seeing that greatest material loss seemed to correlate with greatest rate of temperature increase in our experiments, it was decided that slowing or halting the rate of temperature of change in that period may curtail material loss. The procedure seemed to work, creating a layer with minimal surface loss and with desired stability. Method 3 was used to prepare samples for genetic assays done on SU8 based carbon films.

4.2.5. Pyrolysis Method 4

Method 4 was merely applying method 3 to the S1813 photoresist. The product of this procedure was a thin and visually consistent film. Despite appearances, the film did not prove stable in water, breaking into small pieces which floated to the surface of the water. These results paralleled results from method 2, suggesting that the peak temperature was not high enough.

4.2.6. Pyrolysis Method 5

With the failures of method 4, the peak temperature was increased in an effort to create a more carbon like character in the film. Samples created by method 5 were consistent thin films that appeared smooth. The carbon films were stable in water and proved suitable for cell cultures.

4.2.7. Pyrolysis Method 6

Method 6 was created merely as a means to decrease the time necessary to complete a pyrolysis procedure. It was hypothesized that S1813 would not need a rest because the film was much thinner than the previous coatings and may not need the rest period to form cross links to increase stability. Samples produced by method 6 were indistinguishable from samples from method 6. It was method 6 that was used to prepare carbon film samples for the cellular adhesion assay done on S1813 based carbon films.

4.2.7. Pyrolysis Method 7

After having run out of SU-8 and switching to S1813 for procedures 4 through 6, more SU-8 was ordered. Procedure 3, which was previously successful failed to create a carbon film with suitable stability. In particular, the film failed to adhere when exposed to water and when conducting CV analysis. It was assumed that the failures of procedure 3 were due to an inability to sufficiently convert the photoresist to carbon, and the film retained photoresist-like properties. Thus, 1000°C was chosen as a new peak temperature, as suggested by Ranganathan, McCreery, Majji, & Madou, 2000. The film appeared fractured and demonstrated poor adhesion in the same manner as previous high temperature results.

4.2.8. Pyrolysis Method 8

Assuming that the peak temperature for procedure 7 was too high, it was lowered in procedure 8. It was hoped that this method would indicate more photoresist like character than procedure 3 (900°C) and less carbon character than both procedures 3 and 7. The film, contrary to expectations pealed and was fractured in points, yet had some areas that adhered very well. Unfortunately, surface areas for these adhered points were not sufficient to conduct an electrochemical analysis of the surface. The fracturing in this case appeared similar to previous tests with heat rates that were too high.

4.2.9. Pyrolysis Method 9

Working on the hypothesis that the heat rate was too high for method 8, a lower (5°C/min) heat rate was used in method 9. The film appeared slightly more stable, but still failed to adhere, particularly around the edges. It appeared that the temperature may have been too high for this procedure.

4.2.10. Pyrolysis Method 10

Lowering the temperature of procedure 9 to 700°C was intended to test if procedure 9's maximum temperature was too high. The film appeared very stable and had good adhesion in air and in water, but did not qualitatively look the same as the film produced by procedure 9. Specifically, the film did not have the same dull black color and still appeared to refract light as the bare photoresist does. Yet, a CV analysis revealed no carbon like behavior, with eventual deplating of the photoresist. It was quite clear that the temperature for procedure 10 was not high enough to pyrolyze the photoresist.

4.2.11. Pyrolysis Method 11

It appeared from procedures 9 and 10 that the heat rates were too high and the maximum temperature was not high enough. Thus, method 11 was devised to have a lower heat rate and a higher maximum temperature. The 2°C/min heat rate had proven successful previously and thus was used again, while the 1000°C maximum temperature was selected to guarantee total pyrolysis, even if perhaps the film was unstable. Results indicated a film that was well adhered in some points, exhibiting pealing that is indicative of a maximum temperature that is too high.

4.2.12. Pyrolysis Method 12

Method 12 was conceived to test whether the cross linking rest had any effect on the film stability. No differences were observed between method 11 and method 12.

4.2.13. Pyrolysis Method 13

Consulting published sources (Singh, Jayaram, Madou and Akbar, 2002), method 13 emerged was selected. The heat profile was supposed to be 2°C/min to 800°C, followed by a 60 min rest at 800°C and then a 2°C/min cool to room temperature. An equipment malfunction, however, caused the temperature controller to not properly execute the planned procedure. The result was a 300 minute rest at 800°C with the desired heat rates up and down. The resulting film was fractured in very much

the same manner as procedures that use temperatures that are too high, yet it remained unclear whether this was due to the extended exposure at high temperature or the temperature itself.

4.2.14. Pyrolysis Method 14

To examine the role of rest time in method 13, method 14 was devised as a reduced rest time method. The film was somewhat more stable than method 13, but still failed to adhere after long term exposure to water and in the potentiostat.

4.2.15. Pyrolysis Method 15

With a better film from a shorter rest time between methods 13 and 14, method 15 was devised to test if a further reduction in rest time could improve film stability further. There were no noticeable differences between methods 14 and 15.

4.2.16. Pyrolysis Method 16

Following repeated failures using SU-8, S1813 was returned to again for its successes and ease of use. With the increased film stability with decreased rest time demonstrated by methods 13 and 14, method 16 was fashioned after method 6, but with no rest time. The films produced by method 6 and 16 are indistinguishable and thus method 16 was selected as a means to reduce process time. Films depicted in Figures 4.2.1.6 and 4.2.1.7 are created using method 16.

4.2.17. Pyrolysis Method 17

Method 17 is very similar to method 16, with the slightly lower second heat rate step yielding a slightly thicker film. No obvious differences in stability or chemical content are observed, but the film is nearly 1.0 µm thicker (see section 4.5.1 for detailed discussion of film thickness). Additionally, this heat profile produced a higher portion of high quality films, with around 90% of samples being usable for cell growth, compared to the approximately 65% using method 16. That said, those suitable samples made with method 16 appear to be a higher quality than those with 17, with fewer minor defects and a more consistent appearance.

4.2.18. Pyrolysis Method Summary

Early procedures using original SU-8 samples were successful once a two step heat profile was adopted. The rest temperature of 300°C was selected because it is a commonly used hard bake temperature for SU-8 (del Campo & Greiner, 2007). Movement to S1813 was done out of necessity, as the SU-8 samples had been consumed and S1813 was available. New SU-8 wafers were eventually obtained, but attempts to create an acceptable carbon film were unsuccessful. It was concluded that the new SU-8's failures were due to the wafers being fused silica rather than monocrystal silicon. S1813 was thus used again because it was available and effective. Samples prepared using Method 16 are treated with oxygen plasma etching. While film thickness was measured to be less than it's unmodified counterparts, there are no visible differences between oxygen plasma treated carbon and unmodified carbon.

4.3. Neurite Differentiation Genetic Assay

A genetic assay was selected as an easy means to gauge cell-surface interactions. Similar studies have used visual methods (SEM and fluorescent microscopy most notably) to assess cell-surface interactions (Zhou, Gupta, Zou, & Zhou, 2007; Li & Hoffman-Kim, 2008). These techniques are more expensive, time demanding and less quantitative than assessing gene expression, though it provides a much clearer view of cellular phenomena. Thus, it is desirable to develop a genetic assay that can offer insight regarding cell-surface interactions with greater ease and higher throughput.

Three genes were selected as a means of assessing cell-surface response. The first, Tau, is a protein that cross-links tubulin to stabilize microtubules (Weingarten, Lockwood, Hwo, & Kirschner, 1975). It has been observed previously that Tau genes are upregulated during the process of neuritogenesis (Drubin, Feinstein, Shooter, & Kirschner, 1985). Elevated levels of Tau expression should indicate a higher rate of neurite growth and more stable neurites as a result of assisting microtubule assembly (Esmaeli-Azad, McCarty, & Feinstein, 1994). The next gene, glyceraldehydes-3-phosphate dehydrogenase (GAPDH) codes for a cytosolic protein that plays a key role in glycolysis. Because of this gene's constitutive nature, its regulation is not expected to change between samples (Voet, Voet, & Pratt, 2006). GAPDH is to act as a housekeeping gene that is expected to be roughly constant in all samples. Finally, beta-actin expression is gauged. Beta-actin is a structural protein that plays a key role in cytosolic expansion and neuritogenesis. Previous studies have noted slightly elevated expression of this gene during neuritogenesis (Drubin, Feinstein, Shooter, & Kirschner, 1985).

4.3.1. Genetic Assay Method 1

Assay 1 sought to determine if neuritogenesis could be detected using a genetic assay on photoresist derived carbon surfaces. Tau proteins were chosen to detect neurite growth, while GAPDH would serve as a housekeeping gene that was presumed to be constant between cell populations. As expected, processes were observed on NGF treated cells removed from the substrate by trypsinization, and not observed on samples not treated with NGF. 1µg total RNA per sample was extracted and the cDNA library was created and amplified without any errors.

The results of the gel electrophoresis shown in Figure 4.3.1.1 demonstrate an upregulation of Tau genes in the presence of NGF. Additionally, the constant expression of GAPDH and equivalent starting quantities of mRNA indicate that the cell numbers are roughly constant and other genes are being expressed in normal levels. These results, considered along with observations of processes and previously published work indicate that Tau genes may be used as an indicator of neurite growth for these PPF substrates.

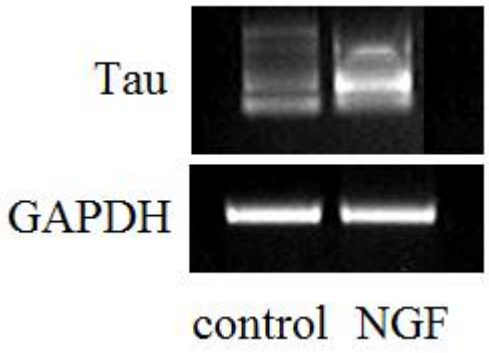

Figure4.3.1.1: Gel electrophoresis results for cells grown on carbon substrates using genetic assay 1. Note the upregulation of Tau genes while GAPDH standard remains constant. Enhanced expression of Tau in the context of constant GAPDH expression indicates that NGF does indeed cause neuritogenesis on PPF surfaces. These results are confirmed by observation of trypsinized cells (not shown).

Further experiments using this procedure in context of current alternatives (SEM or fluorescent microscopy) may provide a quantitative method to study neurite growth. Though the method will not provide the level of detail that alternatives possess (three dimensional visualization of neurite growth specifically), the assay may be used as an easy and high throughput screening method to compare cell-surface response at a superficial level. Additionally, genetic analysis methods permit an understanding of cell-surface interactions that is not apparent in other techniques. Specifically, genetic assays permit one to quantify gene expression levels.

4.3.2. Genetic Assay Method 2

Building on the success of Assay 1, it was hoped that a more encompassing study would further elucidate cell-surface interactions. Tau genes were selected to confirm that neuritogenesis was indeed taking place, while beta-actin was hoped to offer further insight regarding cytosolic expansion and GAPDH would act as a housekeeping gene again. As in the previous assay, neuritogenesis was noted when observing trypsinized cells from samples treated with NGF, but not from samples not treated with NGF. 1µg total RNA per sample was amplified.

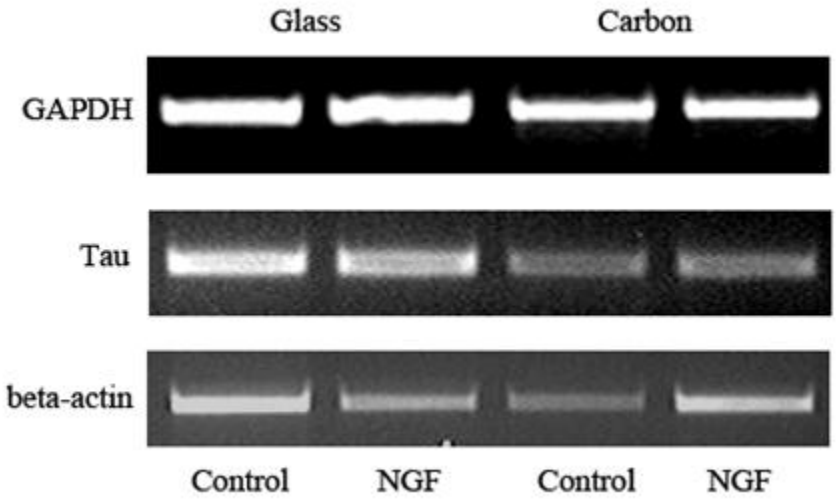

Figure 4.3.2.1: Merged image of gene expression levels as determined in genetic assay 2.
GAPDH genes show equal expression, demonstrating performance as a good housekeeping gene and suggesting that representative mRNA samples are accurate assessments of cell gene levels. Tau genes show little noticeable changes in expression level, with a slight upregulation in NGF on carbon samples and a slight downregulation on glass. Beta-actin behaves as expected on carbon surfaces, but is downregulated after treatment with NGF on glass surfaces.

The results for Assay 2 did not conform to expectations. Though the GAPDH control did behave as expected, showing a constant expression level, beta-actin and tau genes showed some puzzling results. Beta -actin, as a structural protein, would presumably be upregulated after NGF treatment, but actually shows a lower expression level on glass samples treated with NGF. Tau underexpression in NGF treated glass samples is very slight.

It was believed that the lower expression of Tau and beta-actin could be accounted for by different cytoskeletal conformations. This difference in cytosolic shape may perhaps have consequences for cellular adhesion. Such predictions make sense in context of previous findings of cell adhesion (Liliensiek, Campbell, Nealey, & Murphy, 2006; Teixidor, et al., 2008). Thus, a cell adhesion assay would be conducted in an effort to see if any correlation existed.

Examining the findings of this assay in context of cell adhesion assay 2 (see section 4.4.2) shows enhanced Tau and beta-actin expression on better adhering cells within surface material groups. In other words, the glass control group exhibits better adhesion and higher expression of tau and beta-actin genes, while the NGF treated carbon surface shows higher expression and adhesion. These results may be accounted for by different cell morphologies in each group.

4.3.3. Genetic Assay Method 3

It was believed that the results in Assay 2 may be elucidated by a cellular adhesion study. For this assay, only beta-actin and GAPDH are considered in an effort to simplify the experiment and because the Tau

genes appeared to coordinate strongly with beta-actin expression and it was believed that beta-actin would be a suitable indicator of possible changes in cell shape manifested in changes in adhesion. Adhesion data from Cell Adhesion Assay Method 2 is compared to findings from the genetic assay in an effort to better understand the results of Genetic Assay Method 2. As in previous assays, 1µg total RNA per sample was used as a means to normalize expression levels for each sample.

As in previous assays, cells were trypsinized and examined under a microscope to confirm that only those treated with NGF exhibited neuritogenesis. Results of the genetic assay are displayed in context of the cellular adhesion assay in Figure 4.3.3.1. GAPDH levels between all samples are constant as expected from previous experiments, demonstrating that GAPDH may again be used as a housekeeping gene for these genetic assays. Slight variations in beta-actin expression are observed.

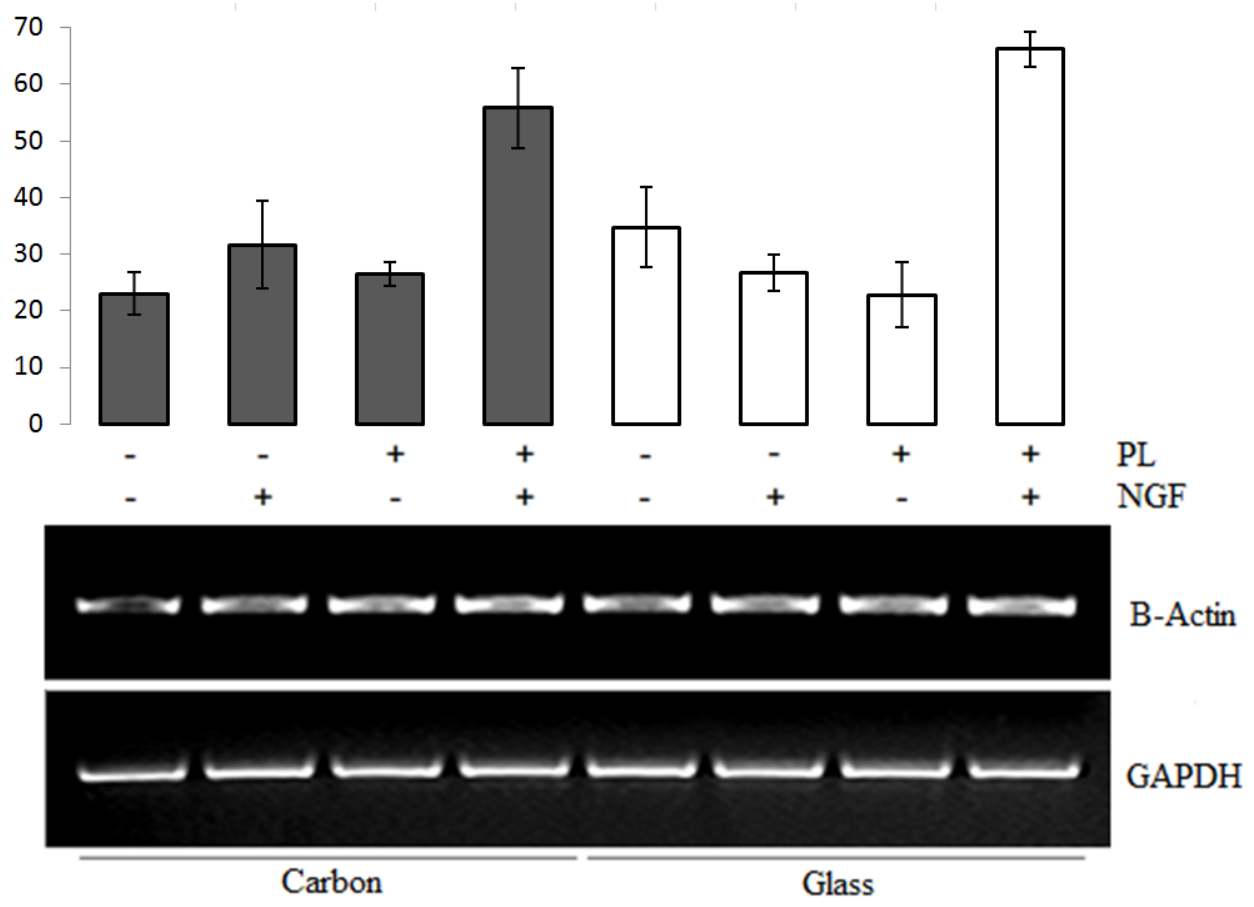

Figure 4.3.3.1: Merged image of gene expression levels from genetic assay 3 and cell adhesion data. A "+" in a row labeled PL or NGF indicates either coating with PL or exposure to NGF, conversely a "-" indicates an absence of PL or NGF. Bars indicate concentration of adhered cells in 10^5 cells/ml for each sample, where grey bars represent carbon samples and white bars denote glass substrates. Beta-actin expression differs only slightly between samples, showing very slight levels of upregulation on only PL coated surfaces compared to only NGF treated surfaces. This assay does not show the difference in expression observed in Method 2. Only samples without PL and without NGF show substantially lower

levels of expression. GAPDH expression is constant for all samples. Refer to Section 4.4.2 for a detailed discussion of cell adhesion data.

Results from Genetic Assay Method 2 were not repeated in Genetic Assay Method 3. While there is a clear upregulation of beta-actin in NGF treated carbon compared to non-NGF-treated carbon with no PL, the difference in expression of beta-actin between samples with and without NGF treatment on non-PL-coated surfaces is not notable. There are slightly elevated expression levels of beta-actin on surfaces that exhibit the greatest levels of adhesion. That is to say that samples treated with NGF on PL coated glass and carbon surfaces show clearly elevated levels of expression in context of other samples on carbon or glass surfaces. This may be explained by previous findings regarding morphological changes of nerve cells on differentially adhesive surfaces (Kleinfeld, Kahler, & Hockberger, 1988).

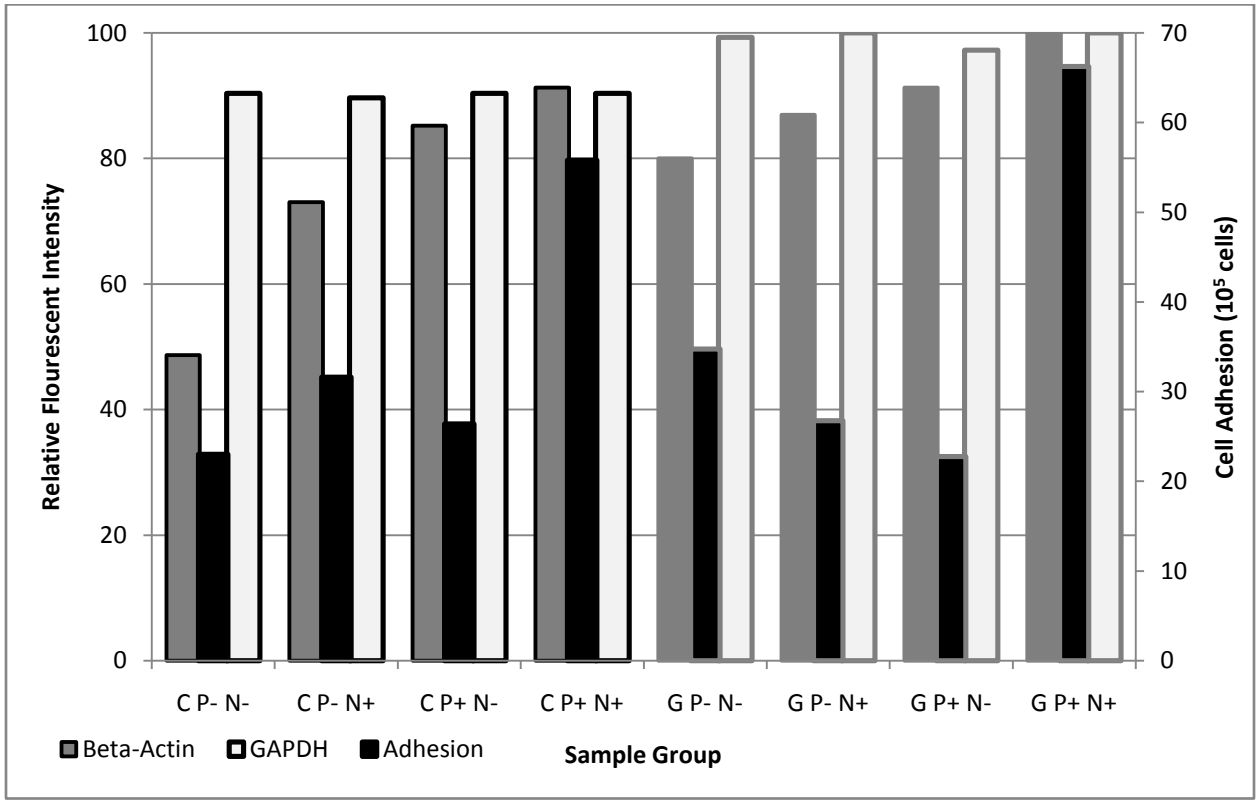

Figure 4.3.3.2: Semi- quantitative fluorescent intensities for beta-actin and GAPDH genes displayed in context of cell adhesion.
In this figure, "C" indicates carbon samples (bars outlined in black) while "G" signifies glass surfaces (gray bar outlines). "P-" denotes no PL treatment, where "P+" represents PL treatment, similarly, "N-" correlates to no NGF treatment and "N+" designates NGF treatment. GAPDH fluorescent intensities are normalized to the greatest fluorescent intensity (G P+ N+), and shows a high degree of consistency within each material group. Beta-actin expression is normalized to the maximum value also and adhered cell numbers are shown in units of 10^5 cells. It is important to note the consistency of GAPDH in each group and the lack of correlation between adhesion and beta-actin expression.

Levels of beta-actin expression do not exhibit any substantial differences between sample groups. Due to the semi-quantitative nature of the RT/PCR procedure, differences of 20% or more are considered significant. This cutoff means that only the reduced expression of beta-actin in carbon samples without PL and without NGF treatment is considered significant. Such findings correlate with expectations, since beta-actin expression is not controlled on a genomic level and actin monomers exist in substantial concentrations in the cytosol, with filament assembly controlled on the protein level (Voet, Voet, & Pratt, 2006).

Beta-actin (and perhaps tau as well) may not serve as a means to accurately compare levels of neurite growth between different surfaces without the ability to accurately account for changes in cellular morphology on each surface. It is exceedingly difficult to isolate each factor of cell-surface interaction between materials that differ on several very important properties. Differences between each surface in terms of chemistry, roughness, stiffness and several other parameters make it very difficult to, at this stage, develop a genetic assay that will isolate neuritogenesis as the dependent variable.

4.3.4 Genetic Assay Further Discussion

Findings from genetic assays demonstrated the difficulties of isolating variables in cell assays. The complicated nature of cell-surface interactions made it difficult to select genes that would indicate only neuritogenesis or neurite extension. Changes in cell shape due to cell-surface interaction are believed to account for a great deal of the differences in gene expression. Drastic differences in cell shape in response to surface adhesivity have profound consequences for gene expression, as may be seen in Figure 3.4.3.1.

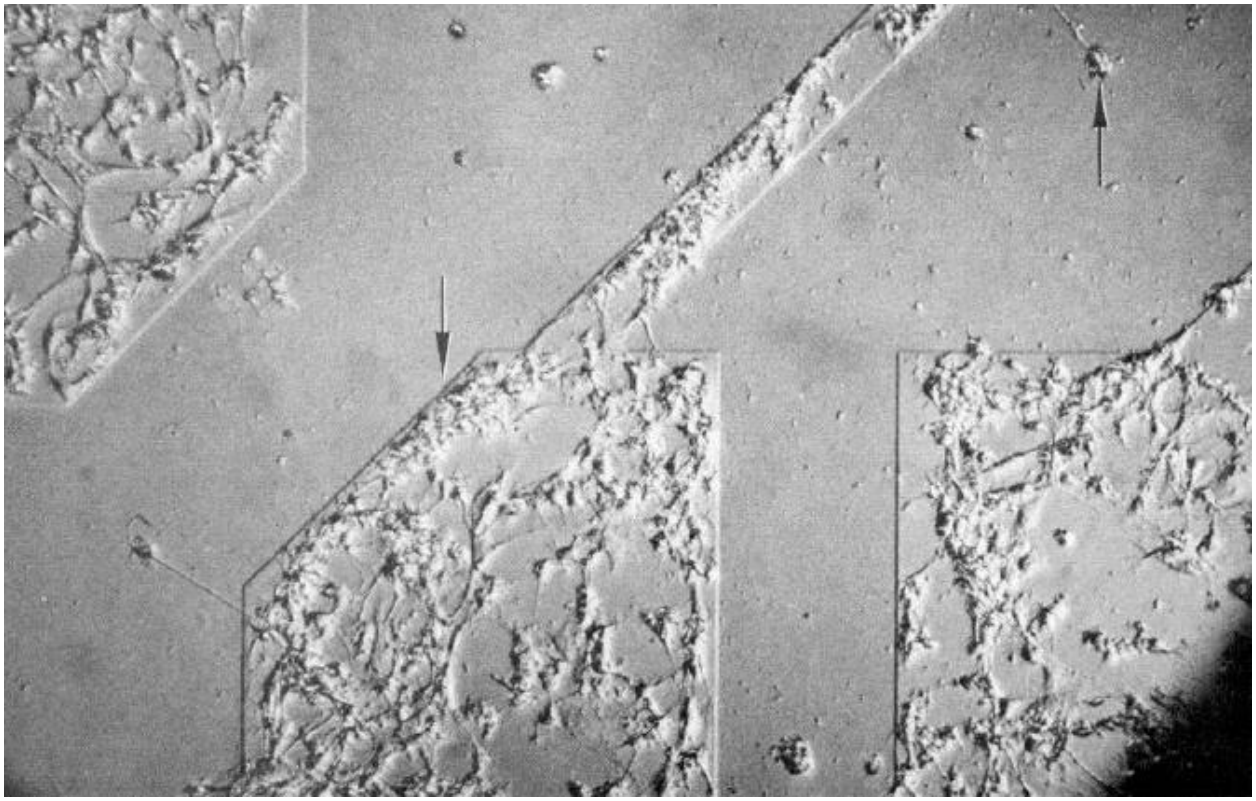

Figure 3.4.3.1: Figure of dissociated spinal cord cells grown on PL coated and uncoated regions from Kleinfeld et al. (1988).
PL coated regions appear as raised areas with high levels of cell adhesion, while uncoated (remaining area) surfaces show lower levels of adhesion. Note the drastic differences in morphology between the PL coated and uncoated areas. Cells grown on PL coated surfaces adopt a familiar neurite geometry, with a flat cell body and extending neurites, where cells on uncoated surfaces have a nearly spherical morphology with very few if any neurites are visible.

The extensive differences between glass and carbon surfaces in chemistry, topography and other influential factors make gene selection difficult for this assay. The opaque nature of the carbon surface makes visualization of cells very difficult, leaving very few techniques to view cells on the surface with a high level of detail. Typical methods include scanning electron microscopy (SEM) and fluorescent microscopy. The latter involves fluorescently dying the cell membrane and visualizing fluorescent emissions from the flouropores embedded in the membrane. Indeed, to further elucidate potential cell-surface interaction that could not be accounted for by mere genetic and adhesion assays, a morphology study was conducted (See Section 4.5).

4.4. Cellular Adhesion Assay

Results from Genetic Assay Method 2 were believed to be accounted for by differences in cell morphology, which may perhaps manifest in differences in cell adhesion on each surface. An adhesion assay was devised as a means to measure cell number for each surface and see if any correlation between cell number and genetic assay results could be noticed. This is not to mention the fact that cell

adhesion is an important facet of cell-surface interaction. Differences in adhesion may shed light on the importance of surface chemistry or roughness among other factors between different materials (Liliensiek, Campbell, Nealey, & Murphy, 2006). This procedure will only remove cells that are not adhered strongly. More specifically, this assay is a measure of removable cells and may say very little about the total number of cells or cell density per unit area on the substrate.

4.4.1 Cellular Adhesion Assay Method 1

Judging cellular adhesion rates permits a greater understanding of the interactions between PC12 cells and the photoresist derived carbon substrate. Cells in silicon samples not coated in PL but treated in NGF exhibited very low numbers because these samples were contaminated in this trial. A total of 52×10^4 cells were seeded on each plate Additionally, cell seeding numbers were quite low, leaving standard deviations that represent rather large portions of the total seed number. Figure 4.4.1 illustrates the results of the test.

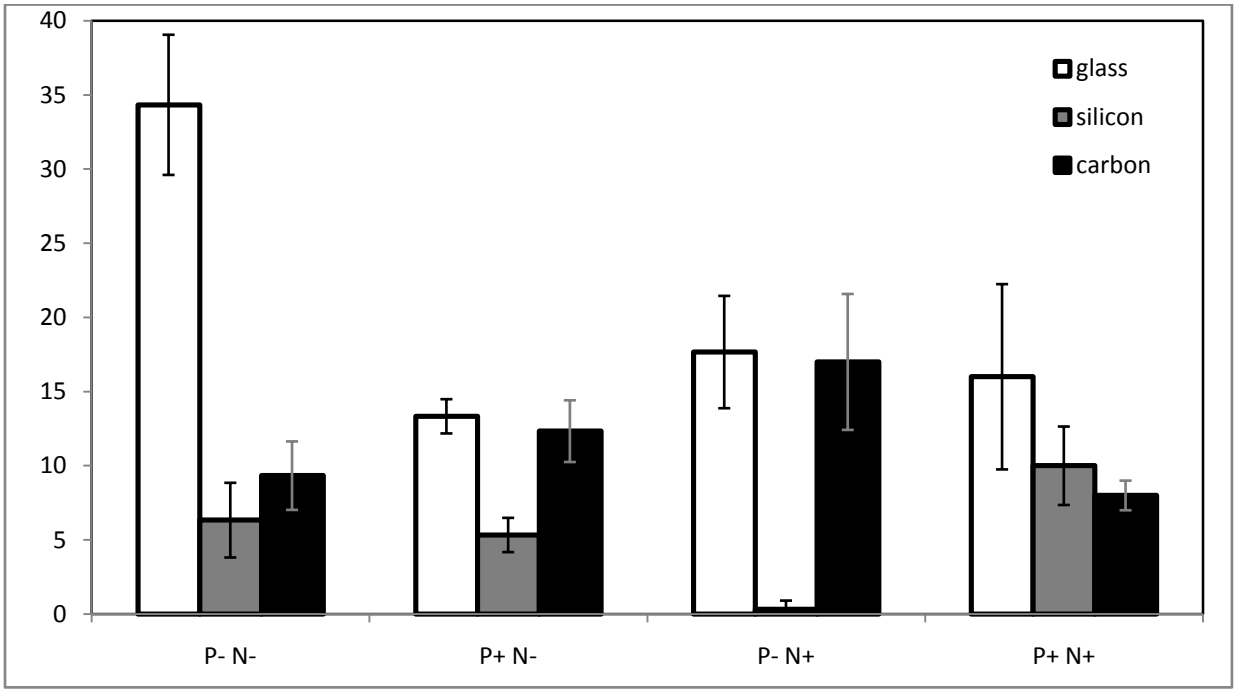

Figure 4.4.1.1: Results from cellular adhesion assay method 1.
Cell concentration (10,000 cells/ml) for each sample evaluated for each surface configuration. Data represents mean and standard deviation for each of the samples. G indicates glass substrates, S silicon substrates and C carbon substrates. P- represents surfaces not coated in PL, while P+ is surfaces coated in PL. Similarly, N- denotes samples not treated with NGF and N+ marks samples treated with NGF.

It was expected that both PL and NGF would promote adhesion on all surfaces. Glass presents the most peculiar results, with the sample lacking both PL and NGF exhibiting the highest rate of adhesion. This is believed to be due to elevated proliferation rates during the initial adhesion period. The lack of significant difference between three glass samples (P+N-, P-N+ and P+N+) was unexpected. These observations seem to be due in large part to

A simple analysis of variation (using the ANOVA test) offers further insight regarding the adhesive properties of each surface. Groups that have a statistically significant separation share a p value less than 0.05 (Refer to Appendix B for detailed p value calculations). No statistically significant difference is observed between any of the surfaces coated with PL and treated with NGF. This appears to be due largely to the large variation in the glass values and obvious similarity between carbon and silicon. Glass and carbon are significantly different than silicon for PL coated surfaces not treated with NGF, while carbon and glass are not significantly different.

The most important implication from these findings is the promise to parallel behavior on somewhat similar substrates. A study by Gabay et al. in 2005 demonstrated the ability for neuronal cells to migrate and self assemble into organized networks given proper surface qualities. Using isolated islands of carbon nanotubes on a silicon substrate, a previous experiment using PL islands on quartz was paralleled with new materials. Both experiments relied on local regions of high and low affinity to create self organizing neuronal networks. The cells tend to migrate, pulled by surface tension into clusters on high adhesion surfaces with bridges between clusters crossing the low adhesion surfaces. In the case of carbon nanotubes and silicon dioxide, the carbon nanotubes represent areas of high affinity upon which clusters form (Gabay, Jakobs, & Ben-Jacob, 2005). Similar patterns of migration have been witnessed in dorsal root ganglion bridging gaps on MEMS surfaces (Goldner, Bruder, Li, Gazzola, & Hoffman-Kim, 2006).

Judging by differences in adhesion between photoresist derived carbon and bare silicon, it may be possible to create self organizing clustered networks of neurons with the use of small islands of carbon. The potential for surface modification in terms of topological roughness and chemical markers may further increase the carbon's adhesive abilities, just as reaction with silane based compounds with specific active groups or a metallic coating below the photoresist may decrease cellular affinity for the non-carbon surfaces. Increasing affinity in certain areas while decreasing it in others creates the requisite high and low adhesion profiles for designing self organizing neuronal networks.

4.4.2 Cellular Adhesion Assay Method 2

Learning from the flaws of method 1 (low cell seeding number most notably), Cellular Adhesion Assay Method 2 was designed with a larger initial seeding number in hopes of generating a set of data with a smaller percentage variation. Additionally, bare silicon surfaces were omitted as a means to simplify the experiment and allow faster repeat experiments from seeding colonies. A total of 120×10^4 cells are seeded onto the samples at a concentration of 40×10^4 cells/ml.

When cells were being removed from glass substrates, they were examined under the microscope to confirm that the cells were indeed detaching from the surface. Samples treated with NGF were observed on the hemocytometer to be growing rather small processes regardless of surface of PL treatment. For glass samples, a noticeable decrease in neurite length between the cells in the Petri dish and in the hemocytometer (before and after trypsinization) was noted but not measured. A substantially longer term of trypsinization compared to that in Method 1 was used as cells were observed to remain attached to the glass substrate after 5 minutes.

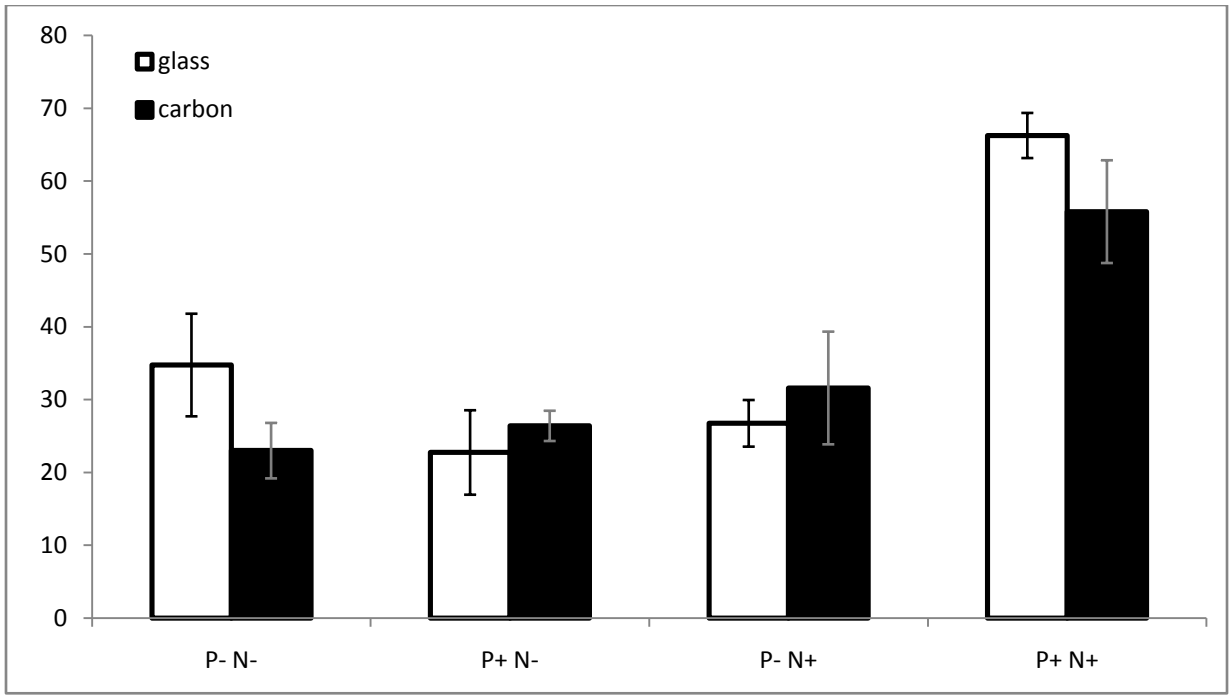

Figure 4.4.2.1: Results from cellular adhesion assay method 2.
Recovered cell concentration (10,000 cells/ml) for each sample evaluated for each surface configuration. Data represents mean and standard deviation for each of the samples. P- indicates no poly-lysine (PL) treatment, while P+ represents PL treatment, conversely N- denotes no NGF treatment and N+ marks NGF treated samples. For P+N- and P-N+ groups, glass and carbon are not significantly different and there is no statistically significant difference between P+N- and P-N+ ($p>0.05$).

It has been long understood that both NGF and PL promote cell adhesion in PC12 cells (Ranganathan, McCreery, Majji, & Madou, 2000; Schubert, 1977). Statistical analysis of the cell adhesion assay results reveals no significant difference between Poly-lysine (PL) coatings on carbon surfaces not treated in NGF and no difference in NGF treatment on glass surfaces not treated with PL ($p >0.05$). Moreover, there is no statistical significance between glass and carbon surfaces that are either treated with PL and no NGF or no PL and NGF. Further analysis reveals that there is no significant difference between only treatment with NGF and only coating with PL.

Glass not coated in PL and not treated with NGF shows a 51.0% higher cell recovery rate than its carbon based counterpart. This may be due to either (as suspected in the previous assay) a higher proliferation rate prior to firm adhesion, or a failure to adhere so strongly that the trypsin treating cannot remove the cells. The observations of high clustering rates in the morphology assay seems to suggest that the second hypothesis may be true.

The lack of statistical significance between NGF and PL holds application in self organizing neuronal networks. Findings by Gabay et al. demonstrate the ability to create self assembling neuronal networks with patterned surfaces with varying adhesive properties (Gabay, Jakobs, & Ben-Jacob, 2005). While their results demonstrate network assembly on silicon patterned with nanotube islands, preliminary

findings and observed cell migration by Kleinfeld et al. suggest that PL on glass or agarose may hold similar promise for network assembly (Kleinfeld, Kahler, & Hockberger, 1988). Given that the adhesive properties of NGF and PL are virtually indistinguishable, it may be possible to create self assembling neuronal networks with surface immobilized NGF patterns.

While self assembling neuronal networks on nanotube-silicon surfaces have been shown to exhibit neurite growth on non-desired areas, surface immobilized NGF has been shown to have the ability to induce neurite differentiation only in desired areas (Gabay, Jakobs, & Ben-Jacob, 2005; Kleinfeld, Kahler, & Hockberger, 1988). Qualitative investigation of similar PPF substrates has demonstrated the capacity for neuron cell migration and clustering on PPF-silicon patterned surfaces (Teixidor, et al., 2008). Coupling patterned PPF and immobilized NGF patterns may yield the capacity to produce self assembling neuronal networks where individual cell neuritogenesis may be controlled. Differences apparent adhesive properties manifested in clustering rates in the cell morphology assay seem to support this idea of use of carbon as a means to create self assembling neuronal networks.

Fabrication techniques for selected materials permit the creation of features with a resolution as high as 0.48µm, while the use of more elaborate fabrication techniques may permit the creation of intricate three-dimensional carbon structures (Yamada & Chang, 2008). The high resolution and potential for advanced structures of PPF permit the creation of multielectrode arrays. While some multielectrode arrays have been successfully used to measure neuronal cell activity, they have been quite primitive and lacked the ability to adequately pattern cell growth (Gabay, Jakobs, & Ben-Jacob, 2005; Ito, 1998). Carbon nanotube (CNT) based multielectrode arrays may have cytotoxic effects, whereas results thus far suggest that PPF has a high degree of biocompatibility—though admittedly not much work has been done to investigate the biocompatibility of PPF (Zhou, Gupta, Zou, & Zhou, 2007; Teixidor, et al., 2008).

4.4.3 Cell Adhesion Assay Common Observations

Bare glass not treated with NGF was not expected to perform as well as it did in either experiment. It appears that higher proliferation rates during initial seeding are the cause of the observed behavior, but this has yet to be tested. Additionally, the method used only dissociates moderately well attached cells, leaving very strongly adhered cells on the substrate, measuring only the number of cells which would be collected via trypsinization. The lack of significant difference between only PL coated surfaces and only NGF exposed surfaces is shown in both methods. An exact explanation for this observation remains elusive, but holds promise for the use of immobilized NGF as a means to preferentially control adhesion and differentiation.

In either case, the elevated adhesion of NGF treated cells on bare glass compared to carbon and the statistically insignificant difference between NGF treated bare surfaces is observed. These results are in agreement with Teixidor et al., who observe a slight preference for glass by nerve cells (2008). Additional results indicate a preference for carbon substrates over silicon, results that appear reasonable even in light of Method 1's failures and coincide with previous findings (Teixidor, et al., 2008; Gabay, Jakobs, & Ben-Jacob, 2005).

4.5. Cellular Morphology Study

Cellular morphology was determined for a total of eighteen samples composed of four substrate groups, each with four PL and NGF configurations and a repeat of two of the groups. As may be observed in the images of the cells, the DiI was successfully absorbed into the cell membranes with a low level of background noise. Fixing the cells and addition of the dye appear to preserve morphologies of the cells, as confirmed qualitatively by comparing the view of cells in an ordinary inverted microscope to the fluorescent micrographs.

This procedure allows qualitative comparison of cell shape and relative adhesion numbers between each of the sample groups. While some of these observations permit one to draw conclusions about cell-surface interactions, the qualitative nature of these data limits the range of analysis. A selection of figures follows, refer to Appendix G for more detailed images of each sample group.

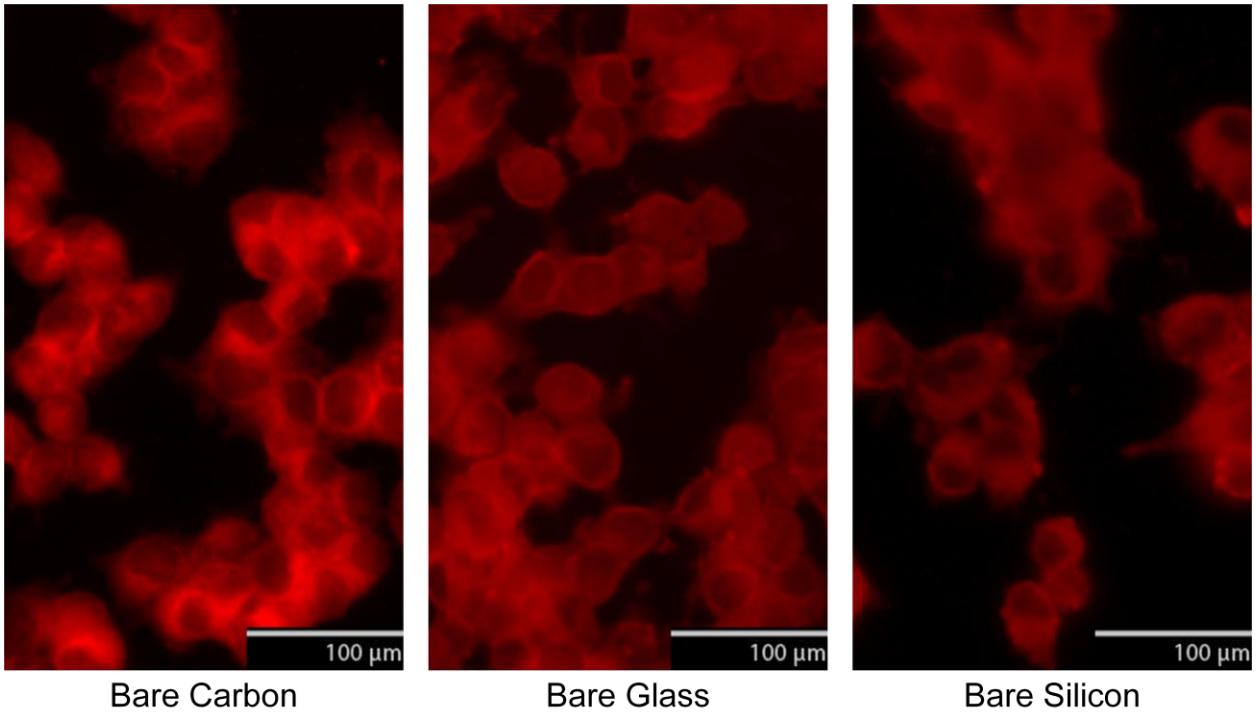

Figure 4.5.1: Undifferentiated cells seeded on carbon, glass and silicon surfaces.
It is important to observe here that the bare glass sample exhibits higher rates of clustering of cells (better illustrated by figures in Appendix G).

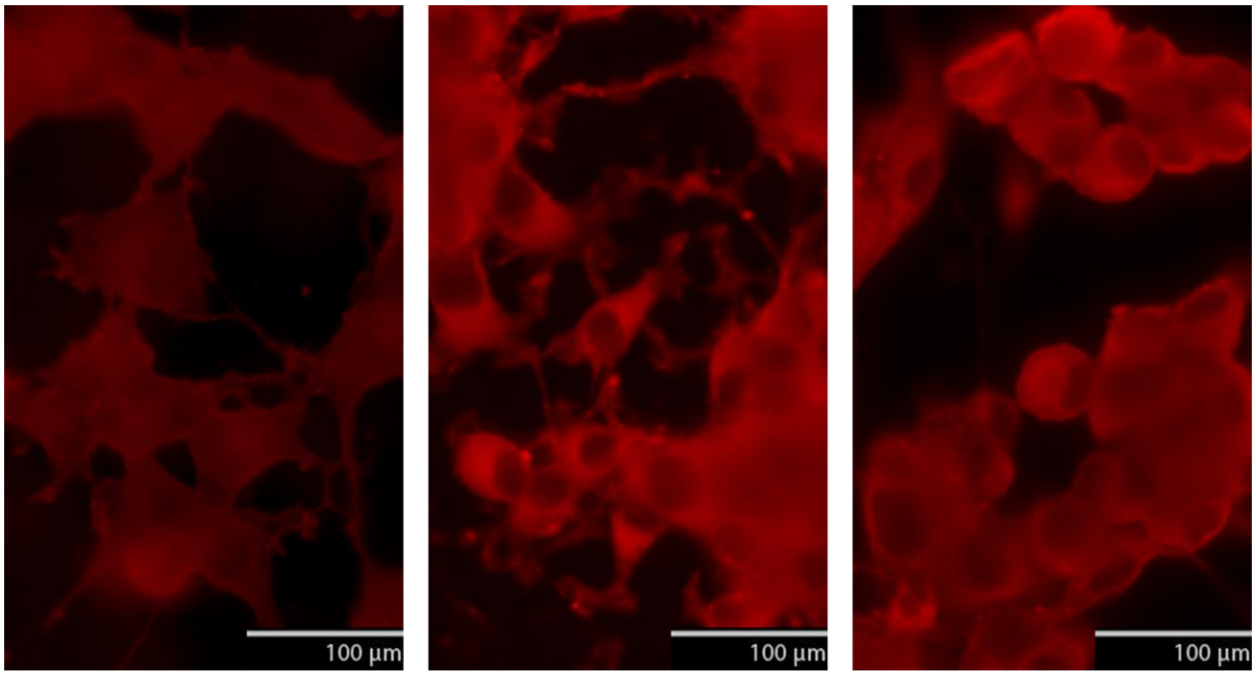

Figure 4.5.2: NGF treated PC12 cells seeded on unmodified carbon, glass and silicon surfaces.
Here, with the addition of NGF, it is easy to see that the cells adopt a distinctly different morphology than the blank control. Slight changes in cell adhesion are expected, and clustering rates, as a consequence, are altered slightly.

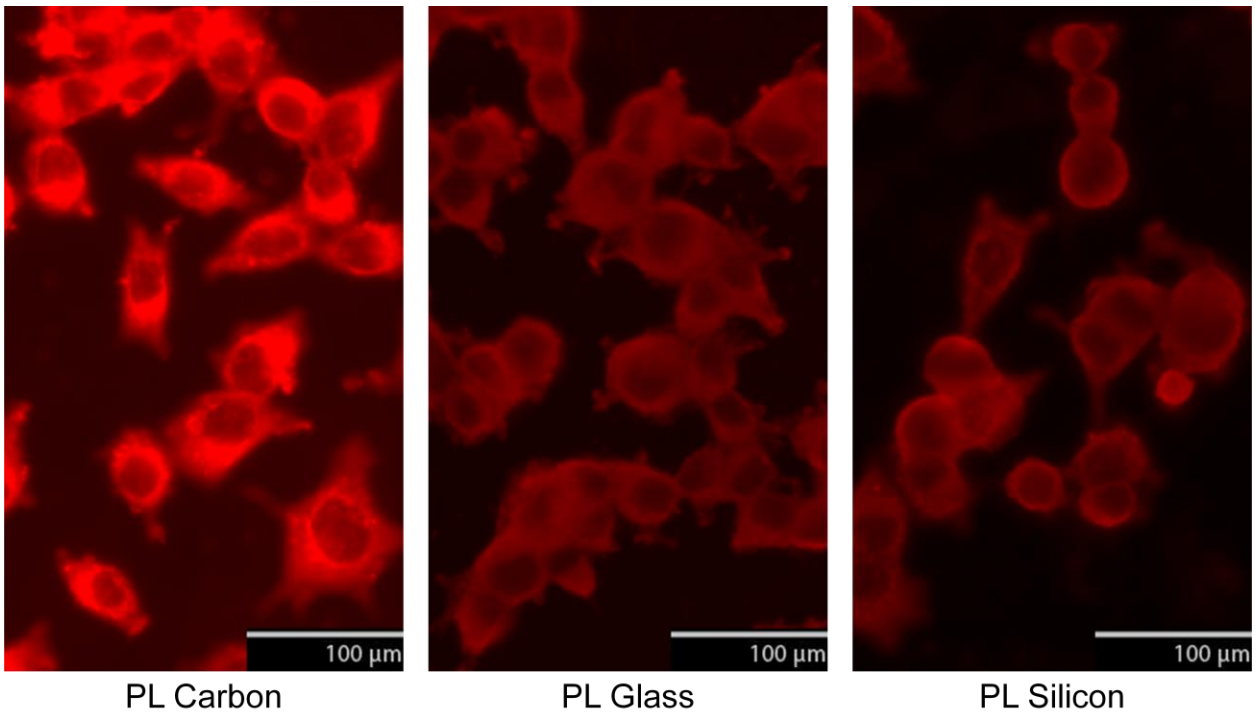

Figure 4.5.3: PC12 cells on PL coated carbon, glass and silicon surfaces.
Coating surfaces with PL promotes cell adhesion and decreases clustering slightly compared to samples without PL. This suggests that more adhesive surfaces permit less cell migration as a means to clustering.

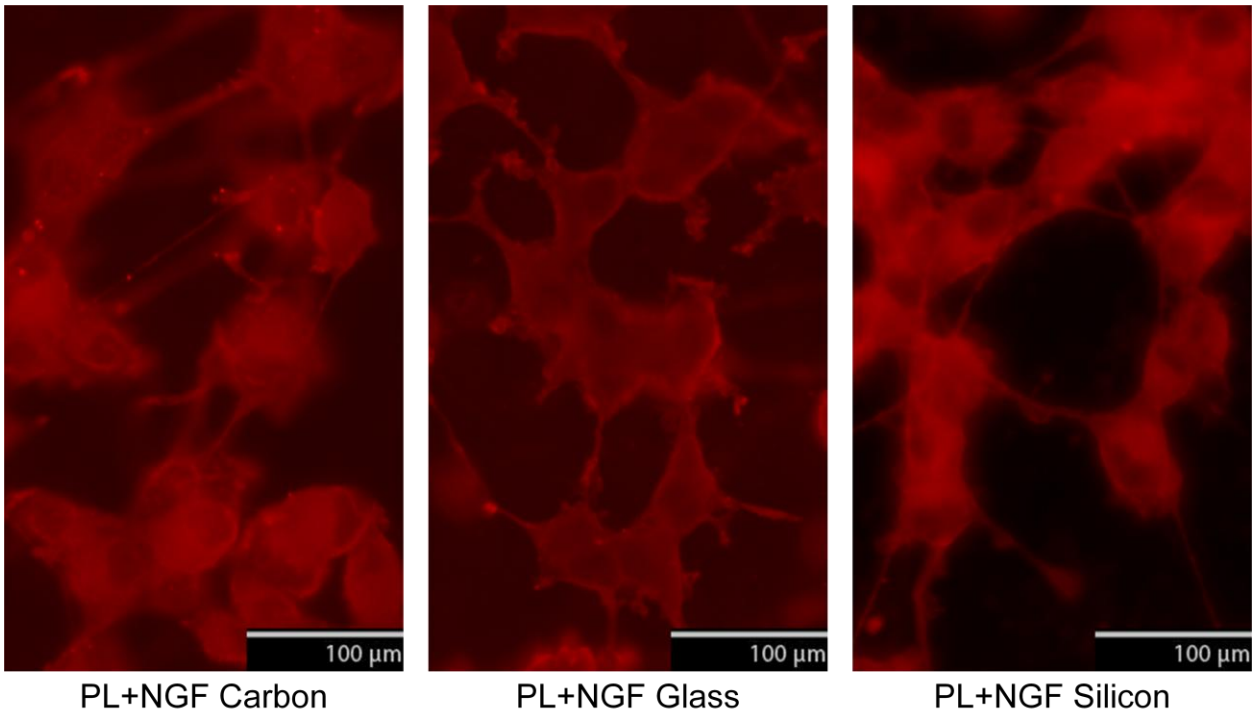

Figure 4.5.4: NGF treated PC12 cells on PL coated carbon, glass and silicon surfaces.
Addition of NGF and PL differentiates neuronal cells on a highly adhesive surface. As in previous additions of PL, a reduction in clustering compared to the NGF only group is observed, in addition to the apparent ability to form long neurites.

Figures 4.5.1, 4.5.2, 4.5.3 and 4.5.4 depict cells seeded on bare substrates, cells treated with NGF on bare substrates, untreated cells on PL coated substrates and NGF treated cells on PL coated substrates respectively. NGF serves to differentiate the cells into forming processes and adopting an expected neuronal cell morphology. PL increases cellular adhesion on each surface, serving as a basis against which adhesion may be judged on a surface

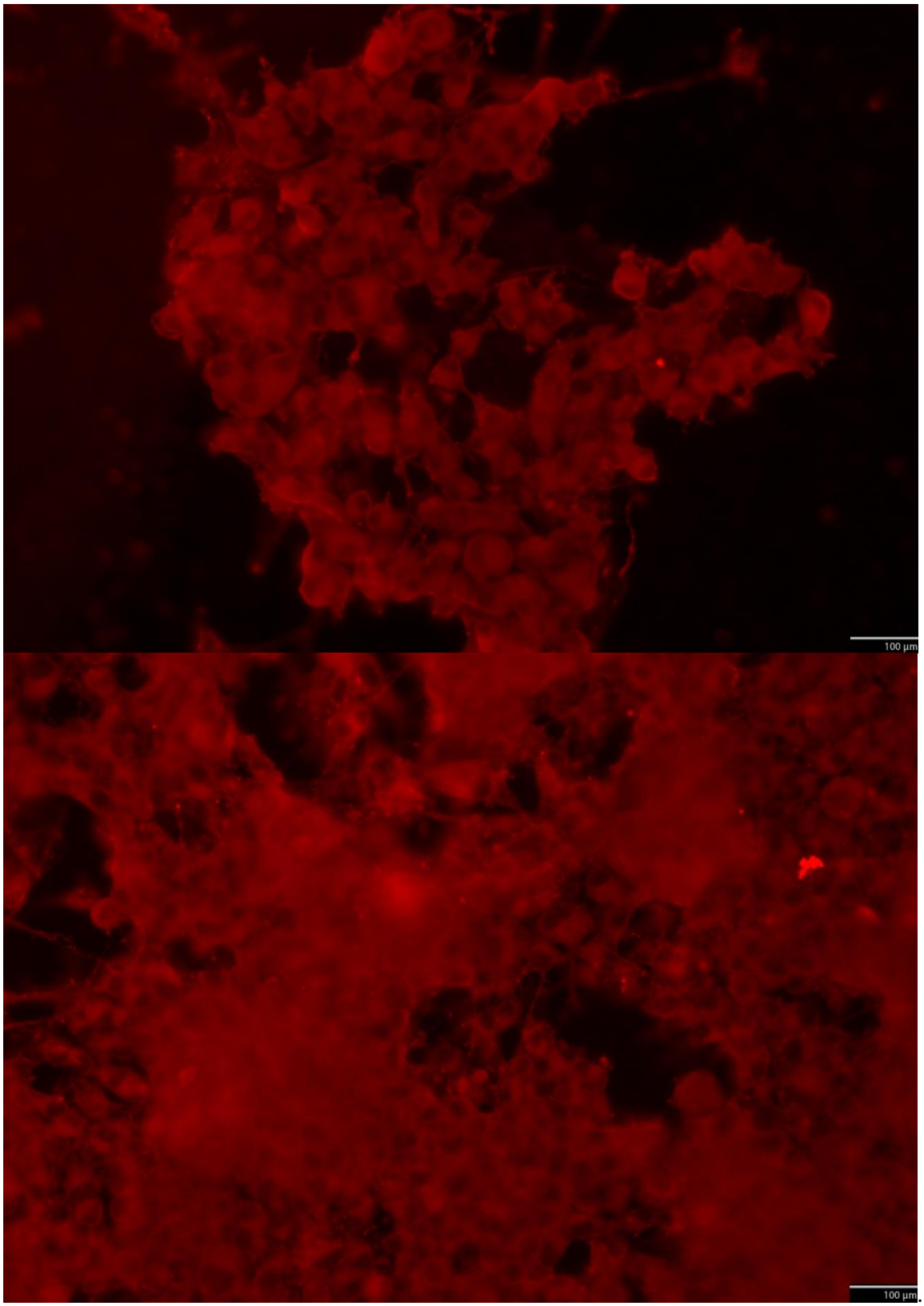

Figure 4.5.5: Dense clustering of NGF treated PC12 cells on carbon (above) and glass (below)

The scale bar indicates 100 µm. Note the increased cell density and total area on the glass substrate. Though not pictured, the glass substrate featured more barren area than the carbon counterpart, with clusters as depicted in the figure appearing at seemingly isolated intervals over the surface. By contrast, the carbon surface saw smaller clusters with less distance over the surface of the substrate.

Clustering of PC12 cells on carbon occurs at a much lower rate than on glass. As demonstrated in Figure 4.5.5, dense clusters are much larger on glass than carbon. Other large vacant areas (not pictured), are seemingly larger on glass than on carbon, suggesting perhaps a longer distance of migration brought about by a perhaps lower level of adhesion. This hypothesis could perhaps be supported if one considers that the trypsinization procedure used to gauge adhesion (in fact gauging recoverable adhesion) detaches only loosely attached cells, in cell adhesion method 2 shows a greater proportion of cells detaching from glass.

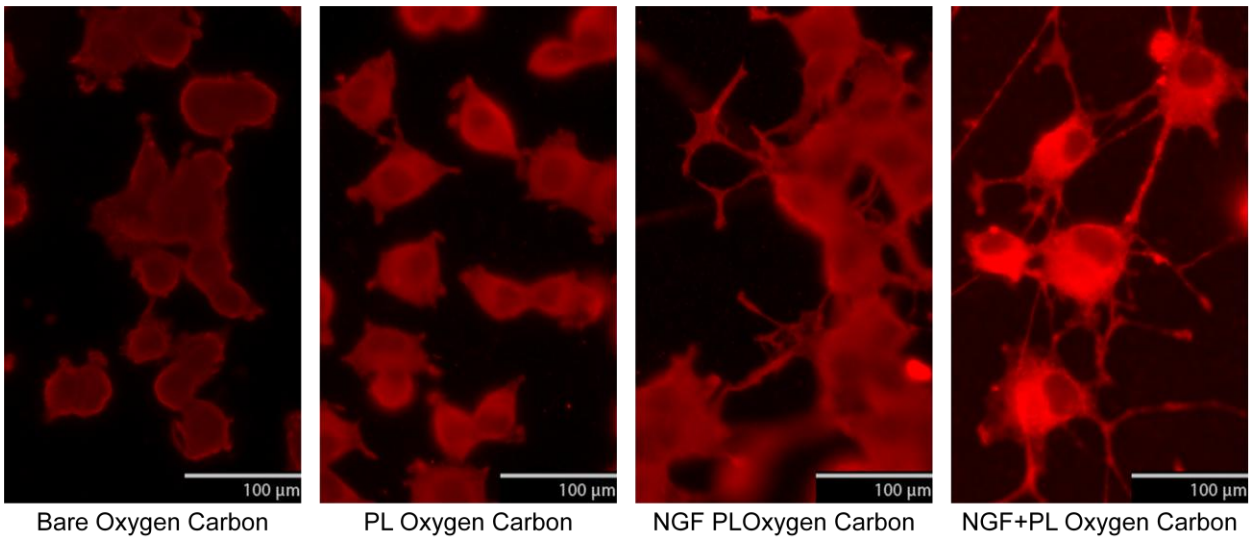

Figure 4.5.6: Cell morphologies on oxygen plasma treated carbon samples.
These PC12 cells seeded on oxygen plasma treated carbon samples demonstrate quite well the morphological consequences for cells seeded on each surface. The cells seeded on oxygen plasma treated carbon not treated with NGF and not coated in PL show roughly spherical morphologies. Coating surfaces with PL preserves the roughly spherical morphology, with a slight increase in cell surface area from flattening the cell due to non specific adhesion to the surface as well as a slight reduction in cell clustering. Addition of NGF results in clear formation of neurites, with a clear clustering of cells. Addition of NGF to cells seeded on PL coated oxygen plasma treated surfaces shows clear neurite formation with a slight reduction in cell clustering, suggesting an elevation in cell-surface adhesion.

Comparison of morphologies on a single surface with different treatments is quite easy, as is illustrated in Figure 4.5.6, but comparisons between surfaces proves a bit more challenging since the consequences of different surface properties are far less pronounced than the dramatic differences imparted by coating with PL or treating with NGF. That consideration, coupled with the qualitative nature of examining cell morphologies, makes definitive conclusions about cell-surface interactions difficult. Of

course, profound differences between each of the surfaces are sufficient to draw conclusions about cell-surface interactions.

4.6. Film Characterization

To study cell-surface interactions, it is necessary not only to understand cellular response, but also surface characteristics that may influence cell response. Material loss plays an important role in understanding the fabrication process' effectiveness. Specifically, a film that is too thin or too inconstant will not provide good surface coverage and will allow cells to contact the silicon substrate below. Additionally, surface chemistry (as discussed in detail earlier) plays a very important role in cell adhesion and cell-surface response. Electrochemical analysis demonstrates that the carbon film behaves electrochemically as carbon. Electrical behavior may also play a role in influencing nerve cell behavior, thus surface electrical resistance is measured.

4.5.1. Film Loss

Film thickness measurements reveal an average initial film thickness of 10.1µm and a final pyrolyzed film thickness of 1.8 µm. Film thickness measurements show an 82.2% loss in film thickness. Similar findings have been reported, though admittedly with a different resist (Ranganathan et al., 2000).

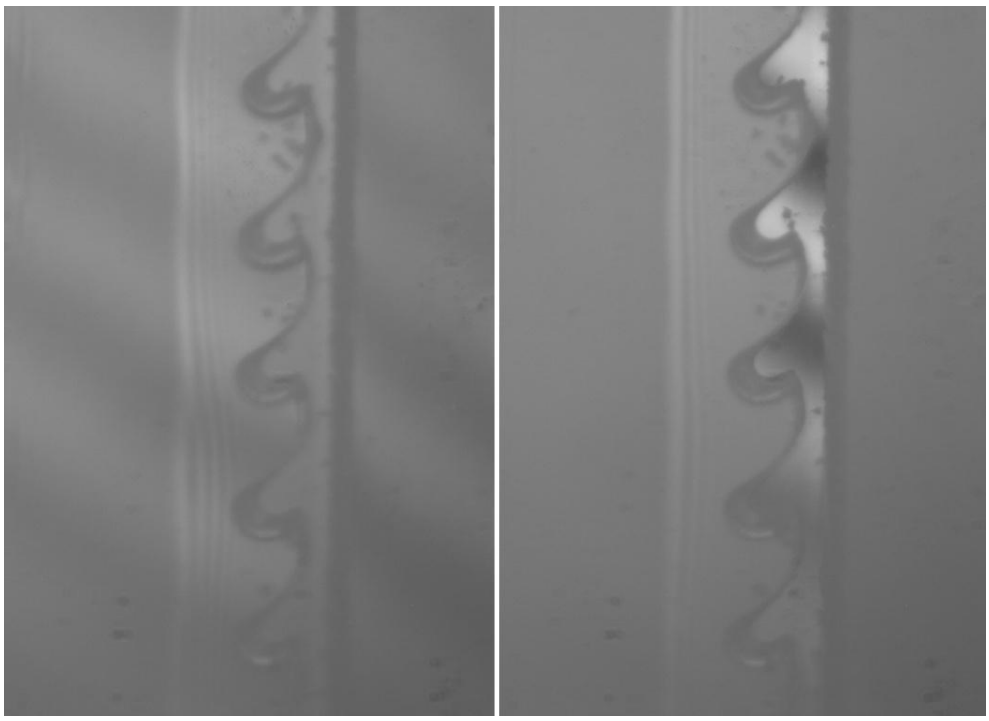

Figure 4.5.1.1: Phase contrast micrographs of unpyrolyzed S1813 coated surfaces.
The focal length of the peak contrast on the top of the films (left) is measured and compared to the focal length of the underlying substrate (right). The contrast lines or fringes denote a single wavelength

difference in height, correlating to about 250 nm in the case of the white light source and filters used, creating very high levels of contrast. A razor blade is used to remove the photoresist layer down to the silicon substrate, leaving an unusual pattern as seen above.

Table 4.5.1.1: Film Thickness Measurements

Type	Film distance (μm)	Substrate distance (μm)	Film thickness (μm)	% loss
Pyrolyzed S1813 (10°C/min heat rate second step)	153.6	151.8	1.8	82.2%
Unpyrolyzed S1813 (4 coats)	131.5	121.4	10.1	
Oxygen Plasma Treated Pyrolyzed S1813	100.1	99.34	0.76	90.2%
Unpyrolyzed S1813 (4 coats)	109.5	101.7	7.8	
Pyrolyzed S1813 (8°C/min heat rate second step)	131.0	128.1	2.9	62.8%
Unpyrolyzed S1813 (4 coats)	109.5	101.7	7.8	

As was expected, the oxygen plasma treated carbon film exhibited a greater amount of surface loss. Reactions at the surface forming carbon monoxide and carbon dioxide reduce the film thickness. Additionally, the 8°C/min heat rate for the second heat step was observed to drastically increase film thickness. It appears that the slower heat rate (particularly at lower temperatures) increases the film's stability during the pyrolysis procedure. The slight increase in exposure time at high temperatures appears to not have noticeable effects on the film's stability.

Table 4.5.1.2: Film Mass Loss Measurements

Sample	Unpyrolyzed (g)	Pyrolyzed (g)	Bare Wafer (g)	Photoresist (g)	Carbon (g)	Mass Loss %
1	0.6934	0.6877	0.6826	0.0108	0.0051	52.8%
2	0.6789	0.6741	0.6712	0.0077	0.0029	62.3%

Film mass loss for Method 16 (10°C/min heat rate for second heat step) averaged between 47.2% and 37.6%. Considering the change in mass in context in the change in film thickness, it is easy to see that the material left on the wafer after pyrolysis has a different density than the photoresist precursor. The carbon film is roughly 2.5 times denser than the photoresist film. Film densities are 0.916 mg/μm thickness for the photoresist and 2.22 mg/μm thickness for the pyrolyzed product.

4.5.2. Electrochemical Analysis

Cyclic voltammetry (CV) analysis of pyrolyzed photoresist films (PPF) is intended to indicate that the substrate does indeed behave chemically as carbon. For certain pyrolysis methods that appeared stable in water, the samples did not prove adherent under conditions of the CV test. Some samples broke apart during sonication to clean the surface, while others did not adhere well either in the $Fe(III)(CN)_3$ solution or when voltage was applied, causing the carbon film to deplate. The final stable method used for cell growth tests is stable under CV conditions and is the method used to prepare samples for characterization.

Characterization with the use of CV reveals that the pyrolyzed S1813 is very much akin to the glassy carbon standard. Figure 4.5.2 shows a plot of current against voltage for the thin carbon film and glassy carbon standard. ΔE_p values of 118mV and 137mV for glassy carbon and PPF respectively. The difference of 19mV between ΔE_p values for each material is very similar to findings from procedures using similar temperature ranges (a ΔE_p of 25mV has been reported for SU8 derived PPF) (Ranganathan, McCreery, Majji, & Madou, 2000).

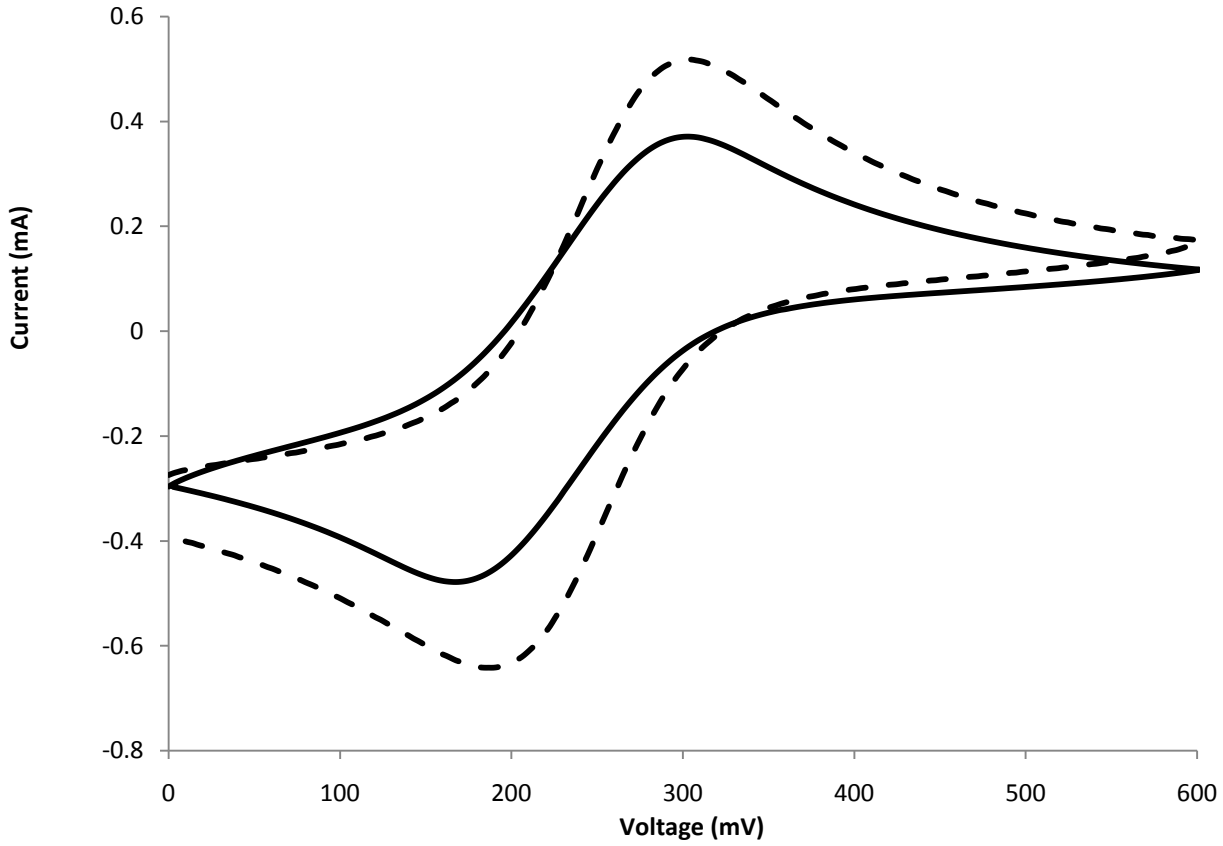

Figure 4.5.2: Cyclic voltammetry results for pyrolyzed S1813 wafer.

The solid line depicts the CV for the carbon sample, while the dashed line is the glassy carbon standard. Scans were conducted between 0.0V and +0.60 V at a rate of 100 mV/s in a 0.005 M $Fe(II)(CN)_3$ and a 0.005 M $Fe(III)(CN)_3$ solution of PBS. Peaks appear at 302mV and 168mV for cathode and anode respectively in the PPF and at 304 mV and 184 mV for the glassy carbon standard. Resulting ΔE_p values are 2mV on the cathode side and 16 mV.

4.5.3. Surface Energy

As may be seen in figure 4.5.3.1, the contact angle of water is greatest on the plain carbon surface. Contact angles are less on the unmodified S1813 surface, followed by the silicon surface; while the oxygen plasma treated carbon surface has the lowest contact angle. A greater contact angle indicates a more hydrophobic surface, while a lower contact angle correlates to a hydrophilic surface. The bare carbon surface was not expected to be more hydrophobic than the untreated S1813 nor the silicon wafer. It was expected that unmodified S1813 would probably have the greatest contact angle because it is composed of aromatic polymer chains and it is cast in an organic solvent.

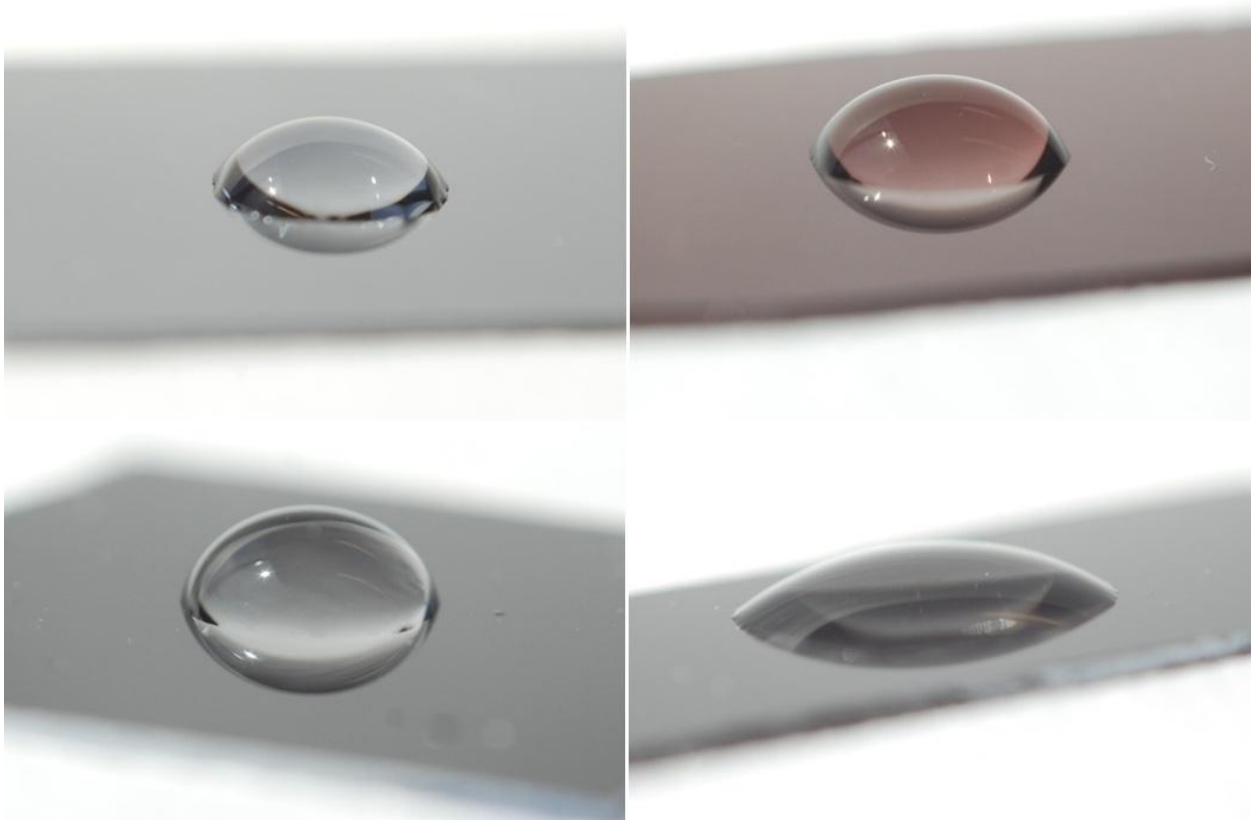

Figure 4.5.3.1: Image of droplet contact with surface samples.
Silicon (top left), untreated S1813 (top right), bare carbon (bottom left) and oxygen plasma treated carbon (bottom right) are pictured. Bare carbon clearly exhibits the largest contact angle, followed by S1813, silicon and oxygen plasma treated carbon in descending order. The larger contact angle indicates greater hydrophobic behavior, while a smaller contact angle indicates more hydrophilic character. Glass and tissue culture plastic are not pictured, with glass appearing completely wettable (no defined droplet shape and a very low contact angle) and tissue culture having a more spherical droplet than carbon. See Figure 4.5.3.2 for quantitative measurements of surface energy.

Angles are measured by drawing a tangent line and using a protractor to estimate the contact angle of the droplet. Surface energies are calculated with the use of Young's Equation, where the surface energy S is calculated as $S = \gamma_{LG}(\cos(\theta) + 1)$, where γ_{LG} is the contact energy between the liquid and the gas surroundings (or surface tension) and θ is the contact angle between the solid and fluid. The surface energy, S, is calculated in dynes/cm (or mN/m), forming an analogue to surface tension between the fluid and the solid phases, indicating an attractive force between the two substances. Using measured contact angles and a surface tension of 71.9 dyne/cm (based on a temperature of roughly 25°C in the laboratory), surface energies are measured. These values are used for relative comparisons of surface energy between samples. It is important to note that the method of measuring angles is accurate only to within about ±2 degrees, resulting in a potential error of about 5%.

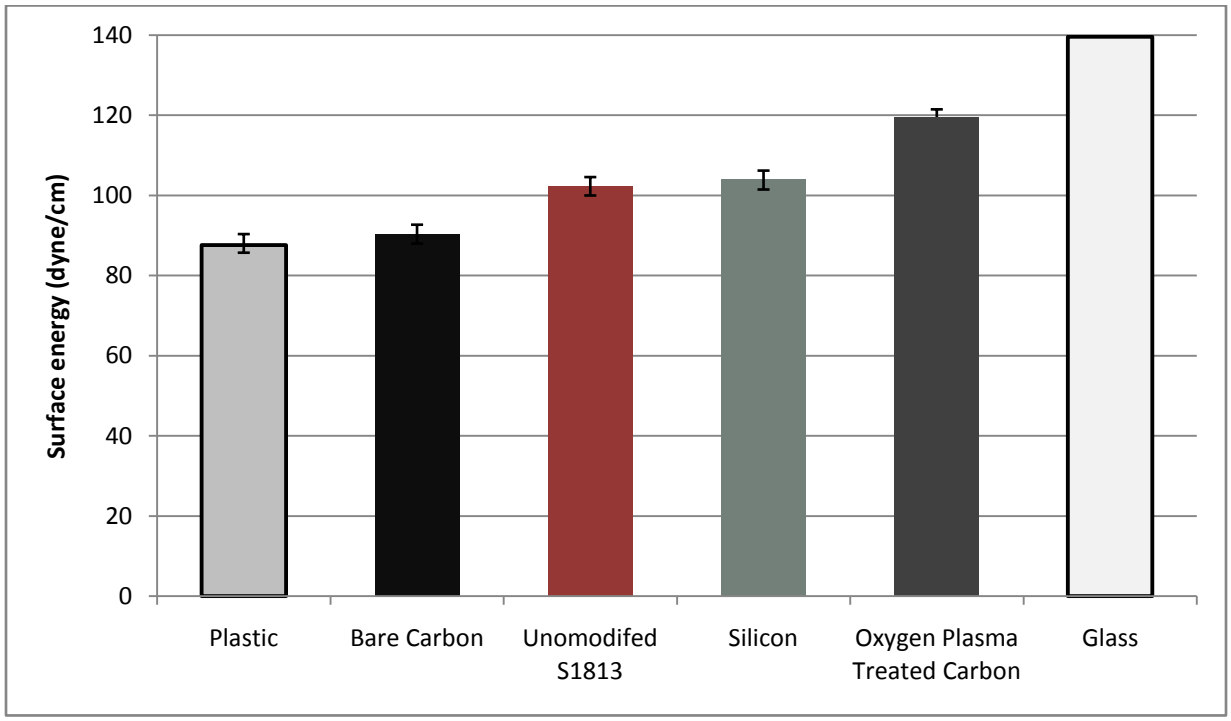

Figure 4.5.3.2: Energy of interaction between a water droplet and surface samples.
A greater surface energy correlates to a more hydrophilic surface, with glass being almost completely wettable in these tests. It is important to note that due to the margin of error in measuring droplet contact angles, tissue culture plastic and bare carbon are not significantly different. Similarly, unmodified S1813 and a bare silicon surface are effectively identical. It is easy to see correlations in surface energy between Figure 4.5.3.2 and measured values of surface energy.

Qualitative observations of droplet shape yield insight regarding the interaction between the fluid and the surface, and calculation of relative surface energy values confirms qualitative observations. As shown in Figure 2, within the degree of accuracy of the measuring methods, silicon and unmodified S1813 are effectively equal, while bare carbon has a much lower energy and oxygen plasma etched carbon has a much higher energy.

In the case of ethanol and toluene, all surfaces were completely wettable by solvents. Contact angles were far too small to measure and the droplets were not uniform in shape. Droplets as small as 4 µL were tried, but the camera used had trouble resolving such small images. The S1813 actually dissolved in the ethanol, leaving a colorful pattern as the ethanol evaporated. Additionally, toluene dissolved tissue culture plastic, leaving a hole in the dish.

5. Conclusions

Once film flaws were correlated with different causes of the flaw, it was possible to easily optimize the procedure for film quality. Films created using the developed procedure are free of cracking, peeling and delamination. Most importantly, these films are stable in water and growth media, permitting cell culture. Comparing film thickness and mass loss measurements demonstrates the creation of a thin and dense carbon film on the silicon wafer. Additional surface modification in the form of oxygen plasma etching modifies the chemical nature of the carbon film.

Completed films are characterized for electrochemistry and surface energy in hopes of identifying properties relevant to cell-surface interactions. Unmodified thin carbon films are observed to have electrochemical behavior that is virtually identical to a glassy carbon standard. Surface energy of unmodified carbon is shown to be nearly identical to that of tissue culture plastic, while oxygen plasma etched carbon is similar to glass. The deposition of oxygen groups on the surface of the carbon films drastically increases the surface energy by imparting the ability to form hydrogen bonds with water.

PC12 cells are grown on carbon and oxygen plasma treated carbon and are compared to silicon and glass surfaces. Examining gene expression of PC12 cells grown and differentiated on carbon surfaces, it is observed that neuritogenesis may be identified in a semi-quantitative manner. Further efforts to identify cell-surface responses via gene expression remained inconclusive. While neuritogenesis could be identified, the semi- quantitative nature of RT-PCR and agarose gel electrophoresis prevents any definitive judgments from being made beyond very obvious observations.

Measuring recoverable cell adhesion on surfaces via trypsinization demonstrates that each surface and each sample group elicits a different adhesive response from cells. Examining morphologies of cells on each surface, however qualitative, lends further insight regarding the cells' behavior on each surface. In addition to being able to visualize individual cell shape, the interactions between cells shows very different interactions between cells and each surface than was shown in either the genetic assay and adhesion assay. Focus in this case is placed on apparent adhesive properties of the surface and consequences for cell network assembly and migration.

Ultimate hopes of using this material in regenerative medicine are less elusive after this study. Building upon previous work demonstrating biocompatibility of photoresist derived carbon and considering a new context of cell-surface interaction studies, photoresist derived carbon has emerged as a stronger potential material for neuronal cell network substrata. The adhesive properties in comparison to the silicon substrate illustrated in the morphological study draw clear parallels to similar materials composed of carbon nanotubes that have proven capable of creating self assembling neuronal networks. The increased ease of manufacture in contrast to the nanotube based materials offers a clear advantage, in addition to the lower cost (Gabay, Jakobs, & Ben-Jacob, 2005).

Modification of the carbon film with oxygen plasma etching leaves a surface that is ripe for further modification via immobilization of key biomolecules or virtually any molecule of interest. This capability, coupled with the material's capacity of being patterned easily offers benefits over alternative soft

materials in its ease of manufacture and potential for application. Properly patterned substrates could create two dimensional gradients of immobilized molecules, offering a unique test platform for the study of neuronal guidance with respect to molecular gradients. Indeed, the material's electrical properties offer the capacity to measure action potentials between cells grown on the substrates, a feat not possible with PDMS and PEG based soft materials.

Similar materials have proven capable of guiding neurite growth when properly patterned. Given the chemical similarity between carbon nanotubes and photoresist derived carbon, it may be expected that non-specific interactions between cells and these two key materials may be virtually very similar. The largely non-amorphous sp^2 configurations of these materials (though carbon nanotubes are demonstrably less amorphous), may mean that photoresist derived carbon is a viable alternative to carbon nanotubes for cell-length scale applications (Harris, 2005). This assertion holds greater potential when considering the cytotoxic consequences of using nanotubes and the fact that the structural advantages of carbon nanotubes are not significant when considering the desired scale of interaction between cells and these substrates in neuronal network applications (Hu, Ni, Montana, Haddon, & Parpura, 2004).

In contrast to traditional approaches to neuronal network assembly and study, photoresist derived carbon microstructures may be fabricated merely from patterned photoresist, eliminating a complex series of steps to produce a MEMS structure with metal cell-surface interfaces (Zeck & Fromherz, 2001). Photoresist derived carbon thus not only eases the difficulty and cost of manufacturing such platforms, but the adhesive properties and easy modification of carbon structures further facilitates deliberate network assembly and cell adhesion. The ability to manufacture complex three dimensional carbon structures with relative ease furthers this material's advantages as well (Yamada & Chang, 2008).

With respect to further work, both fabrication and cell growth hold promise for further development. Doping thin carbon films with metal nanoparticles or ions that may diffuse out gradually holds promise for imparting unique properties to the surface. Sufficient concentrations of metal nanoparticles may alter the surface's electric and electrochemical properties, not to mention physical characteristics (roughness and hardness among others), to a sufficient degree where consequences for cell growth may be measured. Immobilizing salts in the structure of photoresist derived carbon may permit them to gradually diffuse out, which may be useful for cell growth. Of particular interest in this case is divalent metal cations, which are known to influence neuron cell growth, and such applications of photoresist derived carbon may permit the creation of a fixed two dimensional gradient enabling further study.

Cell growth on these substrates must be studied further to better understand the cell-surface interactions and consequences of modifications. In seeking to deliberately guide neurite growth and elicit very specific cell response to surface conditions, it is necessary to understand how cells respond to certain chemical and topographic cues so that a platform for nerve study may be fabricated. Better understanding of cell-surface interaction and modification capabilities will permit the creation of a platform for studying neurite response to not only surface cues, but gradients—offering a great advantage over existing materials and filling a large void in current research practices.

Works Cited

Bear, M. F., Connors, B. W., & Paradiso, M. A. (2007). *Neuroscience: Exploring the Brain.* New York: Williams & Wilkins.

Belanger, M., & Marois, Y. (2001). Hemocompatibility, Biocompatibility, Inflammatory and in Vivo Studies of Primary Reference Materials Low-Density Polyethylene and Polydimethylsiloxane: A Review. *Journal of Biomedical Materials Research* , 467-477.

Berdondini, L., van der Wal, P., Guenat, O., de Rooij, N., Koudelka-Hep, M., & Seitz, P. (2005). High-density electrode array for imaging in vitro electrophysiological activity. *Biosensors and Bioelectronics* , 167-174.

Dalby, M., Riehle, M., Johnstone, H., Affrossman, S., & Curtis, A. (2003). Nonadhesive nanotopography: Fibroblast response to poly(n-butyl methacrylate)-poly(styrene)demixed surface features. *Journal of Biomedical Materials Research* , 1025-1032.

Dalby, M., Yarwood, S., Riehle, M., Johnstone, H., Affrossman, S., & Curtis, A. (2002). Increasing Fibroblast Response to Materials Using Nanotopography: Morphological and Genetic Measurmements of Cell Response to 13-nm-High Polymer Demixed Islands. *Experimental Cell Research 276* , 1-9.

David, S., & Lacroix, S. (2003). Molecular Approaches to Spinal Cord Repair. *Annual Review Neuroscience* , 411-440.

del Campo, A., & Greiner, C. (2007). SU-8: a photoresist for high-aspect-ratio and 3D submicron lithography. *J. Micromech. Microeng* , R81-R95.

Drubin, D., Feinstein, S., Shooter, E., & Kirschner, M. (1985). Nerve Growth Factor-induced Neurite Outgrowth in PC12 Cells Involves the Coordinate Induction ofMicrotubule Assembly and Assembly-promoting Factors. *The Jounal of Cell Biology* , 1799-1807.

Esmaeli-Azad, B., McCarty, J., & Feinstein, S. (1994). Sense adn antisense transfection analysis fo tau function: tau influences net microtubule assembly, neurite outgrowth and neuritic stability. *Journal of Cell Science 107* , 869-879.

Folch, A., & & Toner, M. (2000). Microengineering of Cellular Interactions. *Annual Review Biomedical Engineering* , 227-256.

Fox, S. (2008). *Human Physiology 10th Edition.* New York: McGraw-Hill.

Francisco, H., Yellen, B., Halverson, D. S., Friedman, G., & Gallo, G. (2007). Regulation of axon guidance and extension by three-dimensional constraints. *Biomaterials* , 3398-3407.

Gabay, T., Jakobs, E., & Ben-Jacob, E. a. (2005). Engineered self-organization of neural networks using. *Physica A* , 611.

Gomez, N., Lu, Y., Chen, S., & Schmidt, C. (2007). Immobilized nerve growth factor adn microtopography have distinct effects on polarization versus axon elongation in hippocampal cells in culture. *Biomaterials* , 271-284.

Gonsalves, K. E., Halberstadt, C. R., Laurencin, C. T., & Nair, L. S. (2007). *Biomedical Nanostructures.* Hoboken, NJ: John Wiley & Sons.

Greene, L. A. (1976). Establishment of a noradrenergic clonal line of rat adrenal pheochromocytoma cells which respond to nerve growth factor. *Proceedings of National Academy of Sciences USA* , 2424-2428.

Harris, P. F. (2005). New Perspectives on the Structure of Graphitic Carbons. *Critical Reviews in Solid State and Materials Sciences 30* , 235–253.

Hu, H., Ni, Y., Montana, V., Haddon, R., & Parpura, V. (2004). Chemically Functionalized Carbon Nanotubes as Substrates for Nueronal Growth. *Nano Letters* , 507-511.

Ito, Y. (1998). Regulation of cellular gene expression by. *Jpn J Artif Org* , 541.

Jiguet, S., Bertsch, A., Hofmann, H., & Renaud, P. (2004). Conductive SU9-Silver COmposite Photopolymer. 125-128.

Johnansson, F., Carlberg, P., Danielson, N., Montelius, L., & Kanje, M. (2006). Axonal outgrowth on nano-imprinted patterns. *Biomaterials 27* , 1251-1258.

Kapur, T., & Shoichet, M. (2004). Immobilized concentration gradients of nerve growth factor guide neurite outgrowth. *Journal of Biomedical Materials Research* , 235-241.

Karuri, N. W., Liliensiek, S., Teixeira, A. I., Abrams, G. C., Nealey, P. F., & Murphy, C. J. (2004). Biological length scale topography enhances cell-substratum adhesion of human corneal epithelial cells. *Journal of Cell Science* , 3153-3164.

Kleinfeld, D., Kahler, K. H., & Hockberger, P. E. (1988). Controlled Outgrowth of Dissociated Neurons on Patterned Substrates. *Journal of Neuroscience* , 4098-4120.

Kostecki, R., Schnyder, B., Alliata, D., Song, X., Kinoshita, K., & Kotz, R. (2001). Surface studies of carbon films from pyrolyzed photoresist. *Thin Solid Films* , 36-43.

Kostecki, R., Song, X. Y., & Kinoshita, K. (2000). Influence of Geometry on the Electrochemical Response of Carbon Interdigitated Microelectrodes. *Journal of the Electrochemical Society* , 1878-1881.

Kostecki, R., Song, X., & Kinoshita, K. (2002). Fabrication of Interdigitated Carbon Structures by Laser Pyrolysis of Photoresist. *Electrochemical and Solid-State Letters* , 29-31.

Koukharenko, E., Kraft, M., Ensell, G., & Hollinshead, N. (2005). A comparative study of different thick photoresists for MEMS applications. *Journal of Materials Science: Materials in Electronics* , 741-747.

Li, G. N., & Hoffman-Kim, D. (2008). Tissue-Engineered Platforms of Axon Guidance. *Tissue Engineering: Part B* , 33-51.

Li, N., & Folch, A. (2005). Integration of topographical and biochemical cues by axons during growth on micorfabricated 3-D substrates. *Experimental Cell Research 311* , 307-316.

Liliensiek, S., Campbell, S., Nealey, P., & Murphy, C. (2006). The scale of substratum topographic features modulates proliferation of corneal epithelial cells and corneal fibroblasts. *Journal of Biomedical Materials Research Part A* , 185-192.

Lyons, A., Hale, L., & Wilkins, C. J. (1985). Photodefinable carbon films: Control of image quality. *Journal of Vacuume Science and Technology* , 447-452.

Marieb, E. N., & Hoehn, K. (2007). *Human Anatomy and Physiology, 7th Edition.* San Fransisco: Pearson Educaiton.

Morgado-Valle, C., Verdugo-Diaz, L., Garcia, D. E., Morales-Orozco, C., & Rene, D.-C. (1998). The role of voltage-gated Ca2+ channels in neurite growth of cultured chromaffin cells induced by extremely low frequency (ELF) magnetic field stimulation. *Cell Tissue Research 291* , 217-230.

Ranganathan, S., McCreery, R., Majji, S. M., & Madou, M. (2000). Photoresist-Derived Carbon for Microelectromechanical Systems and Electrochemical Applicaitons. *Journal of the Electrochemical Society* , 277-282.

Renschler, C., & Sylwester, A. (1987). Conductive, spin-cast carbon films from polyacrylnitrile. *Applied Physics Letters* , 1420-1422.

Renschler, C., A.P., S., & Salgado, L. (1989). Carbon films from polyacrylnitrile. *Journal of Materials Research* , 452-457.

Schubert, D. &. (1977). Alteration of cellular adhesion by nerve growth factor. *Proceedings of the National Academy of Sciences* , 4055-4058.

Shipley. (2005). *Microposit® S1800® series photo resists.* Marlborough, MA: Shipley.

Singh, A., Jayaram, J., Madou, M., & Akbar, S. (2002). Pyrolysis of Negative Photorests to Fabricate Carbon Structures for Microelectromechanical Systems and Electrochemical Applications. *Journal of the Electrochemical Society* , 78-83.

Sorribas, H., & Padeste, C. (2002). Photolithographic generation of protein micropatterns for neuron culture applications. *Biomaterials* , 893-900.

Sorribas, H., Braun, D., Leder, L., Sonderegger, P., & Tiefenauer, L. (2001). Adhesion proteins for a tight neuron--electrode contact. *Journal of Neuroscience Methods* , 133-141.

Teixidor, G., Gorkin III, R., Tripathi, P., Bisht, G., Kulkarni, M., Maiti, T., et al. (2008). Carbon microelectromechanical systems. *Biomedical Materials* .

Uttayarat, P., Toworfe, G. K., Dietrich, F., Lelkes, P. I., & Composto, R. J. (2005). Topographic guidance of endothelial cells on silicone. *Journal of biomedical materials research A* , 668-680.

Voet, D., Voet, J. G., & Pratt, C. W. (2006). *Fundamentals of Biochemistry: Life At The Molecular Level.* Danvers: John Wiley & Sons Inc.

Walther, F., Davydovskaya, P., Zurcher, S., Kaiser, M., Herberg, H., Gigler, A., et al. (2007). Stability of the hydrophilic behavior of oxygen plasma activated SU-8. *J. Micromech. Microeng.* , 524-531.

Weingarten, M., Lockwood, A., Hwo, S., & Kirschner, M. (1975). A protein factor essential for microtubule assembly. *Proceedings of the National Academy of Sciences* , 1858-1862.

Yamada, Y., & Chang, D. (2008). Three-dimensional microstructuring of carbon by thermoplastic spacer evaporation during pyrolysis. *Carbon 16* , 1765-1772.

Yavin, E., & Yavin, Z. (1974). Attachment and Culture of Dissociated Cells From Rat Embryo Cerebral Hemispheres on Polylysine-Coated Surface. *The Journal of Cell Biology* , 540-546.

Zeck, G., & Fromherz, P. (2001). Noninvasive neuroelectronic interfacing with synaptically connected snail neurons immobilized on a semiconductor chip. *Proceedings of the National Academy of Sciences* , 10457-10462.

Zhou, H., Gupta, A., Zou, T., & Zhou, J. (2007). Photoresist Derived Carbon for Growth and Differentiation of Neuronal Cells. *International Journal of Molecular Sciences* , 884-893.

APPENDIX A: Detailed Pyrolysis Procedure Summary

Table A.1: Detailed Pyrolysis Procedure Summary

Date	Photoresist	Procedure	Results
	S-1813	0 → 300°C @ 2°C/min 300 → 1000°C @ 10°C/min Hold 1 hr Cool to Room Temperature	▪ Less Peeling than previous
	New SU-8	0 → 800°C @ 2°C/min Hold 6 hr Cool to Room Temperature	▪ Very good carbonization ▪ Not very stable
	SU-8	0 → 800°C @ 3°C/min Cool to Room Temperature	▪ A lot of cracking ▪ Not very good adhesion
	SU-8	0 → 300°C @ 2°C/min Hold 1 hr 300 → 800°C @ 5°C/min Cool to Room Temperature	▪ Cracking ▪ Not stable in water
November 29, 2007	SU-8	0 → 600°C @ 2°C/min Hold 1 hr Cool to Room Temperature	▪ Not pyrolyzed ▪ Not stable in water – forms a gel in water
December 6, 2007	SU-8	0 → 300°C @ 10°C/min 300 → 900°C @ 10°C/min Cool to Room Temperature	▪ Little scratching near edges – probably from cutting. ▪ No obvious splotching or pealing ▪ Stable in water
December 6, 2007	SU-8	0 → 300°C @ 10°C/min Hold 40 min 300 → 900°C @ 10°C/min Hold 1 hr Cool to Room Temperature	▪ No Visible Flaws ▪ Some scratching in storage
February 20, 2008	SU-8	0 → 600°C @ 2°C/min Hold 1 hr Cool to Room Temperature	▪ Spotty ▪ Not stable in water – forms a get in water
March 20, 2008	SU-8	0 → 800°C @ 3°C/min Hold 1 hr	▪ Peeling when placed in cloth

		Cool to Room Temperature	(Damaged in storage)
April 8, 2008	SU-8	0 → 300°C @ 2°C/min Hold 1 hr 300 → 800°C @ 10°C/min Hold 1 hr Cool to Room Temperature	▪ Some peeling on edges, otherwise appears very good
April 17, 2008	SU-8	0 → 300°C @ 2°C/min Hold 1 hr 300 → 800°C @ 10°C/min Hold 1 hr Cool to Room Temperature	▪ 1 small area of peeling – appears cutting
June 25, 2008	SU-8	0 → 300°C @ 2°C/min Hold 1 hr 300 → 900°C @ 10°C/min Wait 1 hr Cool to Room Temperature	▪ Perfect Film ▪ No visible flaws
July 10, 2008	SU-8	0 → 300°C @ 2°C/min Hold 1 hr 300 → 900°C @ 10°C/min Hold 1 hr Cool to Room Temperature	▪ Stable Carbon ▪ Good adherent layer
August 4, 2008	S-1813	0 → 300°C @ 2°C/min Hold 1 hr 300 → 900°C @ 10°C/min Hold 1 hr Cool to Room Temperature	▪ No problems ▪ Very stable
September 4, 2008	S-1813		▪ Appears consistent ▪ Some spotting and scratching, more pronounced along an edge ▪ Shiny surface
September 11, 2008	S-1813	0 → 300°C @ 2°C/min Hold 1 hr 300 → 1000°C @ 10°C/min Hold 1 hr Cool to Room Temperature	▪ Very consistent ▪ Reflective ▪ No obvious silicon viewable ▪ Some areas darker than others
September 13, 2008	S-1813	0 → 300°C @ 2°C/min 300 → 1000°C @	▪ Some edge effects on two of the

		10°C/min Hold 1 hr Cool to Room Temperature	samples, probably cutting ▪ Consistent ▪ Reflective
September 17, 2008	S-1813	0 → 300°C @ 2°C/min 300 → 1000°C @ 10°C/min Hold 1 hr Cool to Room Temperature	▪ 45/45 Very unstable, significant cracking ▪ Also unstable in water ▪ Film cast – Peeling, very loose structure
September 18, 2008	New SU-8		▪ Inconsistent surface between wafers ▪ Bad edge effects – disintegration along some corners ▪ Looks suitable otherwise
November 4, 2008	New S-U8	0 → 300°C @ 2°C/min Hold 1 hr 300 → 1000°C @ 10°C/min Hold 1 hr Cool to Room Temperature	▪ Significant cracking and peeling ▪ Not stable in water ▪ Bubbling up at points
November 6, 2008	New SU-8	0 → 300°C @ 2°C/min Hold 1 hr 300 → 1000°C @ 10°C/min Cool to Room Temperature	▪ Unstable in water ▪ Some odd line formations on surface
November 12, 2008	New SU-8	0 → 800°C @ 2°C/min 800 → 25°C @ 2°C/min	▪ Some edge from cutting ▪ Very unstable in water and when CV is performed
November 13, 2008	New SU-8	0 → 800°C @ 2°C/min Cool to Room Temperature	▪ Bad cracking ▪ Flow removal ▪ Bubbling up
December 11, 2008	S-1813	0 → 300°C @ 2°C/min 300 → 1000°C @ 10°C/min Cool to Room Temperature	▪ Peeling in water after significant time in water ▪ Striations on surface – appear to be from spinning process ▪ Otherwise very stable carbon

			▪ Bubbled areas are easily removed
December 14, 2008	New SU-8	0 → 300°C @ 10°C/min 300 → 1000°C @ 10°C/min Cool to Room Temperature	▪ Significant cracking and peeling
December 16, 2008	S-1813	0 → 300°C @ 2°C/min 300 → 1000°C @ 10°C/min Cool to Room Temperature	▪ Cracking in middle of one wafer; however, rest appear stable ▪ One has small bubbling

APPENDIX B: Detailed Statistical Analysis of Cell Adhesion Assay 1

Anova: Single Factor

SUMMARY

Groups	*Count*	*Sum*	*Average*	*Variance*
G P- N-	3	103	34.33333	22.33333
S P- N-	3	19	6.333333	6.333333

ANOVA

Source of Variation	*SS*	*df*	*MS*	*F*	*P-value*	*F crit*
Between Groups	1176	1	1176	82.04651	**0.000823**	7.708647
Within Groups	57.33333	4	14.33333			
Total	1233.333	5				

Anova: Single Factor

SUMMARY

Groups	*Count*	*Sum*	*Average*	*Variance*
G P+ N-	3	40	13.33333	1.333333
S P+ N-	3	16	5.333333	1.333333

ANOVA

Source of Variation	*SS*	*df*	*MS*	*F*	*P-value*	*F crit*
Between Groups	96	1	96	72	**0.001058**	7.708647
Within Groups	5.333333	4	1.333333			
Total	101.3333	5				

Anova: Single Factor

SUMMARY

Groups	*Count*	*Sum*	*Average*	*Variance*
G P- N+	3	53	17.66667	14.33333
C P- N+	3	51	17	21

ANOVA

Source of Variation	*SS*	*df*	*MS*	*F*	*P-value*	*F crit*
Between Groups	0.666667	1	0.666667	0.037736	**0.855441**	7.708647
Within Groups	70.66667	4	17.66667			
Total	71.33333	5				

Anova: Single Factor

SUMMARY

Groups	*Count*	*Sum*	*Average*	*Variance*
G P+ N+	3	48	16	39
S P+ N+	3	30	10	7

ANOVA

Source of Variation	*SS*	*df*	*MS*	*F*	*P-value*	*F crit*
Between Groups	54	1	54	2.347826	**0.200223**	7.708647
Within Groups	92	4	23			
Total	146	5				

Anova: Single Factor

SUMMARY

Groups	*Count*	*Sum*	*Average*	*Variance*
C P- N-	3	28	9.333333	5.333333
S P- N-	3	19	6.333333	6.333333

ANOVA

Source of Variation	*SS*	*df*	*MS*	*F*	*P-value*	*F crit*
Between Groups	13.5	1	13.5	2.314286	**0.202837**	7.708647
Within Groups	23.33333	4	5.833333			
Total	36.83333	5				

Anova: Single Factor

SUMMARY

Groups	*Count*	*Sum*	*Average*	*Variance*
G P+ N-	3	40	13.33333	1.333333
C P+ N-	3	37	12.33333	4.333333

ANOVA

Source of Variation	*SS*	*df*	*MS*	*F*	*P-value*	*F crit*
Between Groups	1.5	1	1.5	0.529412	**0.507158**	7.708647
Within Groups	11.33333	4	2.833333			
Total	12.83333	5				

Anova: Single Factor

SUMMARY

Groups	*Count*	*Sum*	*Average*	*Variance*
G P- N+	3	53	17.66667	14.33333
S P- N+	3	1	0.333333	0.333333

ANOVA

Source of Variation	*SS*	*df*	*MS*	*F*	*P-value*	*F crit*
Between Groups	450.6667	1	450.6667	61.45455	**0.00143**	7.708647
Within Groups	29.33333	4	7.333333			

Total	480	5

Anova: Single Factor

SUMMARY

Groups	*Count*	*Sum*	*Average*	*Variance*
S P+ N+	3	30	10	7
C P+ N+	3	24	8	1

ANOVA

Source of Variation	*SS*	*df*	*MS*	*F*	*P-value*	*F crit*
Between Groups	6	1	6	1.5	**0.287864**	7.708647
Within Groups	16	4	4			
Total	22	5				

Anova: Single Factor

SUMMARY

Groups	*Count*	*Sum*	*Average*	*Variance*
C P- N-	3	28	9.333333	5.333333
G P- N-	3	103	34.33333	22.33333

ANOVA

Source of Variation	*SS*	*df*	*MS*	*F*	*P-value*	*F crit*
Between Groups	937.5	1	937.5	67.77108	**0.001187**	7.708647
Within Groups	55.33333	4	13.83333			
Total	992.8333	5				

Anova: Single Factor

SUMMARY

Groups	*Count*	*Sum*	*Average*	*Variance*
C P+ N-	3	37	12.33333	4.333333
S P+ N-	3	16	5.333333	1.333333

ANOVA

Source of Variation	*SS*	*df*	*MS*	*F*	*P-value*	*F crit*
Between Groups	73.5	1	73.5	25.94118	**0.007016**	7.708647
Within Groups	11.33333	4	2.833333			
Total	84.83333	5				

Anova: Single Factor

SUMMARY

Groups	*Count*	*Sum*	*Average*	*Variance*
S P- N+	3	1	0.333333	0.333333
C P- N+	3	51	17	21

ANOVA

Source of Variation	*SS*	*df*	*MS*	*F*	*P-value*	*F crit*
Between Groups	416.6667	1	416.6667	39.0625	**0.003341**	7.708647
Within Groups	42.66667	4	10.66667			
Total	459.3333	5				

Anova: Single Factor

SUMMARY

Groups	*Count*	*Sum*	*Average*	*Variance*
G P+ N+	3	48	16	39
C P+ N+	3	24	8	1

ANOVA

Source of Variation	*SS*	*df*	*MS*	*F*	*P-value*	*F crit*
Between Groups	96	1	96	4.8	**0.093599**	7.708647
Within Groups	80	4	20			
Total	176	5				

Anova: Single Factor

SUMMARY

Groups	*Count*	*Sum*	*Average*	*Variance*
G P- N-	3	103	34.33333	22.33333
S P- N-	3	19	6.333333	6.333333
C P- N-	3	28	9.333333	5.333333

ANOVA

Source of Variation	*SS*	*df*	*MS*	*F*	*P-value*	*F crit*
Between Groups	1418	2	709	62.55882	**9.58E-05**	5.143253
Within Groups	68	6	11.33333			
Total	1486	8				

Anova: Single Factor

SUMMARY

Groups	*Count*	*Sum*	*Average*	*Variance*
G P+ N-	3	40	13.33333	1.333333
S P+ N-	3	16	5.333333	1.333333

C P+ N-	3	37	12.33333	4.333333

ANOVA

Source of Variation	*SS*	*df*	*MS*	*F*	*P-value*	*F crit*
Between Groups	114	2	57	24.42857	**0.001308**	5.143253
Within Groups	14	6	2.333333			
Total	128	8				

Anova: Single Factor

SUMMARY

Groups	*Count*	*Sum*	*Average*	*Variance*
G P- N+	3	53	17.66667	14.33333
S P- N+	3	1	0.333333	0.333333
C P- N+	3	51	17	21

ANOVA

Source of Variation	*SS*	*df*	*MS*	*F*	*P-value*	*F crit*
Between Groups	578.6667	2	289.3333	24.33645	**0.001322**	5.143253
Within Groups	71.33333	6	11.88889			
Total	650	8				

Anova: Single Factor

SUMMARY

Groups	*Count*	*Sum*	*Average*	*Variance*
G P+ N+	3	48	16	39
S P+ N+	3	30	10	7
C P+ N+	3	24	8	1

ANOVA

Source of Variation	*SS*	*df*	*MS*	*F*	*P-value*	*F crit*
Between Groups	104	2	52	3.319149	**0.107001**	5.143253
Within Groups	94	6	15.66667			
Total	198	8				

Anova: Single Factor

SUMMARY

Groups	*Count*	*Sum*	*Average*	*Variance*
G P+ N-	3	40	13.33333	1.333333
G P- N+	3	53	17.66667	14.33333

ANOVA

Source of Variation	*SS*	*df*	*MS*	*F*	*P-value*	*F crit*
Between Groups	28.16667	1	28.16667	3.595745	**0.130804**	7.708647
Within Groups	31.33333	4	7.833333			
Total	59.5	5				

Anova: Single Factor

SUMMARY

Groups	*Count*	*Sum*	*Average*	*Variance*
G P- N+	3	53	17.66667	14.33333
G P+ N+	3	48	16	39

ANOVA

Source of Variation	*SS*	*df*	*MS*	*F*	*P-value*	*F crit*

Between Groups	4.166667	1	4.166667	0.15625	**0.712807**	7.708647
Within Groups	106.6667	4	26.66667			
Total	110.8333	5				

Anova: Single Factor

SUMMARY

Groups	*Count*	*Sum*	*Average*	*Variance*
S P- N-	3	19	6.333333	6.333333
S P+ N-	3	16	5.333333	1.333333

ANOVA

Source of Variation	*SS*	*df*	*MS*	*F*	*P-value*	*F crit*
Between Groups	1.5	1	1.5	0.391304	**0.565533**	7.708647
Within Groups	15.33333	4	3.833333			
Total	16.83333	5				

Anova: Single Factor

SUMMARY

Groups	*Count*	*Sum*	*Average*	*Variance*
C P- N-	3	28	9.333333	5.333333
C P+ N-	3	37	12.33333	4.333333

ANOVA

Source of Variation	*SS*	*df*	*MS*	*F*	*P-value*	*F crit*
Between Groups	13.5	1	13.5	2.793103	**0.16999**	7.708647
Within Groups	19.33333	4	4.833333			

Total	32.83333	5

Anova: Single Factor

SUMMARY

Groups	*Count*	*Sum*	*Average*	*Variance*
C P+ N-	3	37	12.33333	4.333333
C P- N+	3	51	17	21

ANOVA

Source of Variation	*SS*	*df*	*MS*	*F*	*P-value*	*F crit*
Between Groups	32.66667	1	32.66667	2.578947	**0.183567**	7.708647
Within Groups	50.66667	4	12.66667			
Total	83.33333	5				

Anova: Single Factor

SUMMARY

Groups	*Count*	*Sum*	*Average*	*Variance*
C P- N-	3	28	9.333333	5.333333
C P+ N+	3	24	8	1

ANOVA

Source of Variation	*SS*	*df*	*MS*	*F*	*P-value*	*F crit*
Between Groups	2.666667	1	2.666667	0.842105	**0.41072**	7.708647
Within Groups	12.66667	4	3.166667			
Total	15.33333	5				

Anova: Single Factor

SUMMARY

Groups	*Count*	*Sum*	*Average*	*Variance*
S P+ N+	3	30	10	7
S P+ N-	3	16	5.333333	1.333333

ANOVA

Source of Variation	*SS*	*df*	*MS*	*F*	*P-value*	*F crit*
Between Groups	32.66667	1	32.66667	7.84	**0.048812**	7.708647
Within Groups	16.66667	4	4.166667			
Total	49.33333	5				

Anova: Single Factor

SUMMARY

Groups	*Count*	*Sum*	*Average*	*Variance*
S P- N-	3	19	6.333333	6.333333
S P+ N+	3	30	10	7

ANOVA

Source of Variation	*SS*	*df*	*MS*	*F*	*P-value*	*F crit*
Between Groups	20.16667	1	20.16667	3.025	**0.156975**	7.708647
Within Groups	26.66667	4	6.666667			
Total	46.83333	5				

APPENDIX C: Detailed Statistical Analysis of Cell Adhesion Assay 2

Anova: Single Factor

SUMMARY

Groups	*Count*	*Sum*	*Average*	*Variance*
glass PL- and NGF-	4	139	34.75	49.58333
glass PL+ and NGF-	4	91	22.75	33.58333

ANOVA

Source of Variation	*SS*	*df*	*MS*	*F*	*P-value*	*F crit*
Between Groups	288	1	288	6.925852	**0.038971**	5.987378
Within Groups	249.5	6	41.58333			
Total	537.5	7				

Anova: Single Factor

SUMMARY

Groups	*Count*	*Sum*	*Average*	*Variance*
glass PL+ and NGF-	4	91	22.75	33.58333
glass PL- and NGF+	4	107	26.75	10.25

ANOVA

Source of Variation	*SS*	*df*	*MS*	*F*	*P-value*	*F crit*
Between Groups	32	1	32	1.460076	**0.272376**	5.987378
Within Groups	131.5	6	21.91667			
Total	163.5	7				

Anova: Single Factor

SUMMARY

Groups	*Count*	*Sum*	*Average*	*Variance*
glass PL- and NGF+	4	107	26.75	10.25
glass PL+ and NGF+	4	265	66.25	9.583333

ANOVA

Source of Variation	*SS*	*df*	*MS*	*F*	*P-value*	*F crit*
Between Groups	3120.5	1	3120.5	314.6723	**2.06E-06**	5.987378
Within Groups	59.5	6	9.916667			
Total	3180	7				

Anova: Single Factor

SUMMARY

Groups	*Count*	*Sum*	*Average*	*Variance*
glass PL- and NGF-	4	139	34.75	49.58333
glass PL- and NGF+	4	107	26.75	10.25

ANOVA

Source of Variation	*SS*	*df*	*MS*	*F*	*P-value*	*F crit*
Between Groups	128	1	128	4.278552	**0.084066**	5.987378
Within Groups	179.5	6	29.91667			
Total	307.5	7				

Anova: Single Factor

SUMMARY

Groups	*Count*	*Sum*	*Average*	*Variance*

glass PL+ and NGF+	4	265	66.25	9.583333
glass PL+ and NGF-	4	91	22.75	33.58333

ANOVA

Source of Variation	*SS*	*df*	*MS*	*F*	*P-value*	*F crit*
Between Groups	3784.5	1	3784.5	175.3436	**1.15E-05**	5.987378
Within Groups	129.5	6	21.58333			
Total	3914	7				

Anova: Single Factor

SUMMARY

Groups	*Count*	*Sum*	*Average*	*Variance*
carbon PL- and NGF-	5	115	23	14.5
carbon PL+ and NGF-	5	132	26.4	4.3

ANOVA

Source of Variation	*SS*	*df*	*MS*	*F*	*P-value*	*F crit*
Between Groups	28.9	1	28.9	3.074468	**0.11762**	5.317655
Within Groups	75.2	8	9.4			
Total	104.1	9				

Anova: Single Factor

SUMMARY

Groups	*Count*	*Sum*	*Average*	*Variance*
carbon PL+ and NGF-	5	132	26.4	4.3
carbon PL- and NGF+	5	158	31.6	59.8

ANOVA

Source of Variation	*SS*	*df*	*MS*	*F*	*P-value*	*F crit*
Between Groups	67.6	1	67.6	2.109204	**0.18448**	5.317655
Within Groups	256.4	8	32.05			
Total	324	9				

Anova: Single Factor

SUMMARY

Groups	*Count*	*Sum*	*Average*	*Variance*
carbon PL- and NGF+	5	158	31.6	59.8
carbon PL+ and NGF+	5	279	55.8	49.7

ANOVA

Source of Variation	*SS*	*df*	*MS*	*F*	*P-value*	*F crit*
Between Groups	1464.1	1	1464.1	26.74155	**0.000852**	5.317655
Within Groups	438	8	54.75			
Total	1902.1	9				

Anova: Single Factor

SUMMARY

Groups	*Count*	*Sum*	*Average*	*Variance*
carbon PL- and NGF-	4	97	24.25	8.916667
carbon PL- and NGF+	4	137	34.25	32.91667

ANOVA

Source of Variation	*SS*	*df*	*MS*	*F*	*P-value*	*F crit*

Between Groups	200	1	200	9.561753	**0.021328**	5.987378
Within Groups	125.5	6	20.91667			
Total	325.5	7				

Anova: Single Factor

SUMMARY

Groups	*Count*	*Sum*	*Average*	*Variance*
carbon PL+ and NGF+	5	279	55.8	49.7
carbon PL+ and NGF-	5	132	26.4	4.3

ANOVA

Source of Variation	*SS*	*df*	*MS*	*F*	*P-value*	*F crit*
Between Groups	2160.9	1	2160.9	80.03333	**1.94E-05**	5.317655
Within Groups	216	8	27			
Total	2376.9	9				

APPENDIX D: Detailed Clean Room Preparation Procedure

Prior to being able to spin coat within the clean room, some basic procedures need to be observed for functionality. Initially, the nitrogen gas, water, and vacuum supplies must be opened and initiated. On the side of the clean room, a small inlet is present in which the ddH_2O pump, the vacuum, and the nitrogen tanks are kept Figure D.1.

Figure D.1: Clean Room Supply Inlet

First, the water supply should be turned on and opened. The pump's power supply is disconnected after every use to prevent overheating. To begin, plug the pump in (behind the nitrogen tanks), followed by opening the water supply and turning the power switch on the pump to "on." All water pump and water supply areas that need adjusting are displayed in Figure D.2.

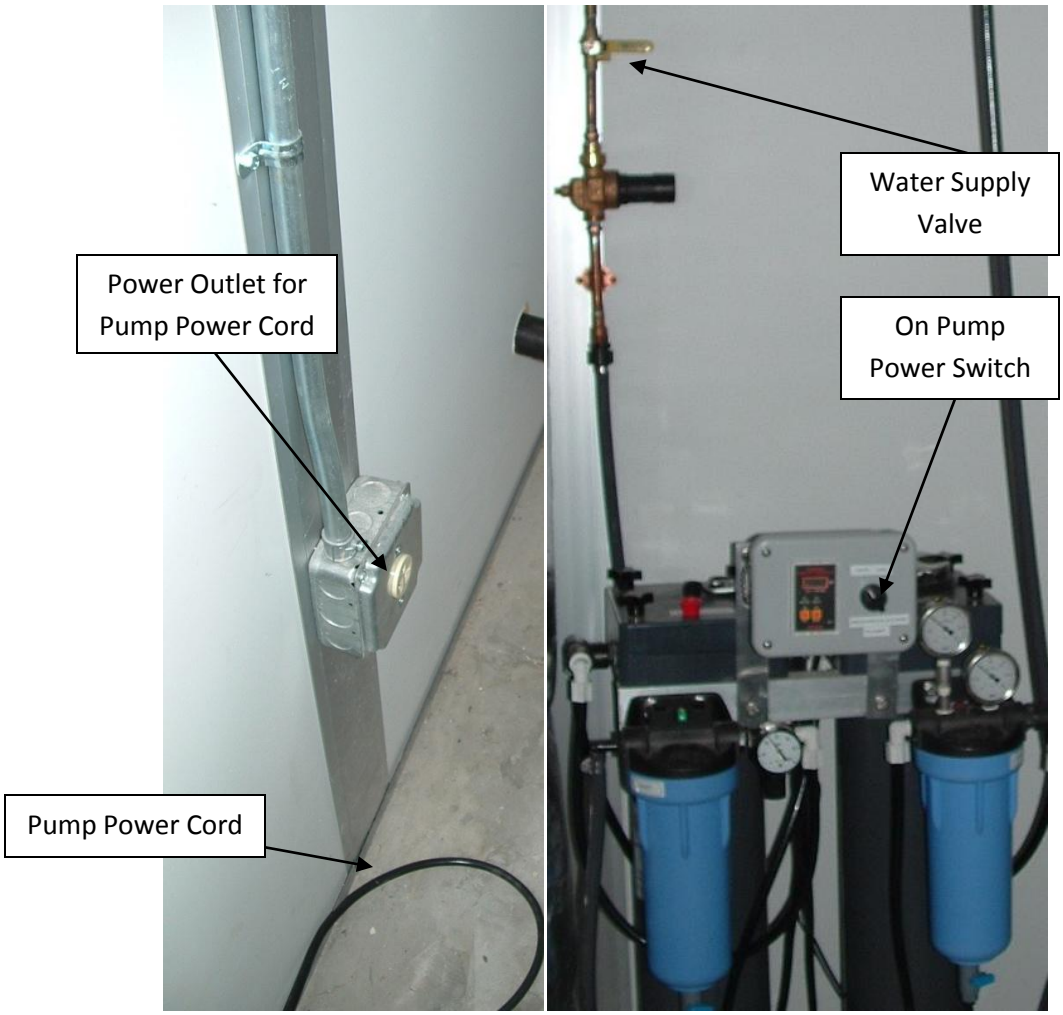

Figure D.2: Water Supply and Pump Points of Interest

The nitrogen gas supply and the vacuum are easily activated. The vacuum uses a simple switch and the nitrogen gas requires two valves to be opened fully. All of these activators are displayed in Figure D.3.

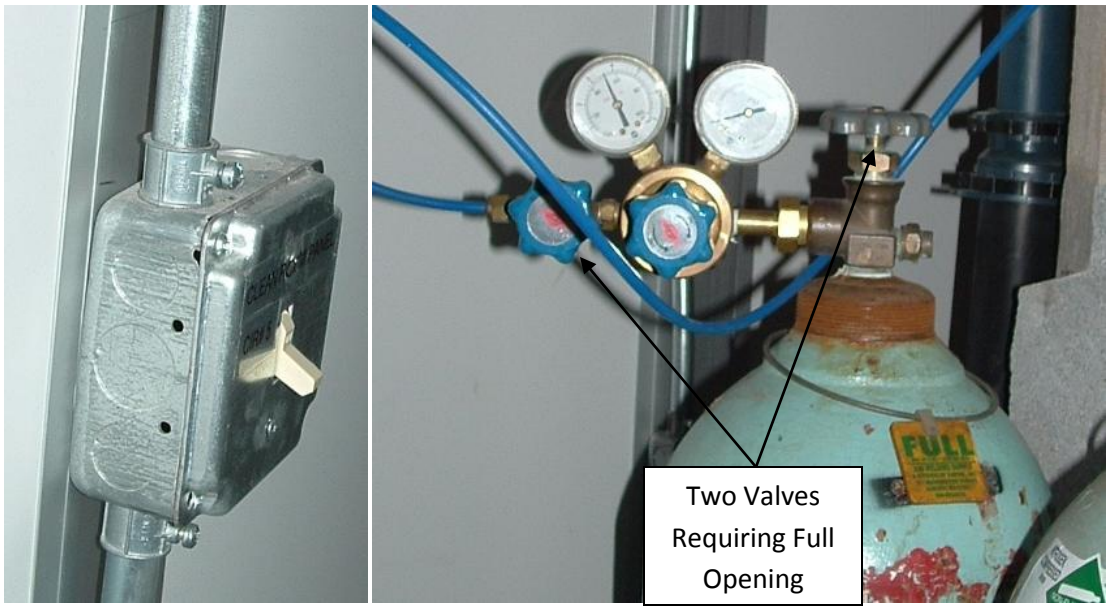

Figure D.3: Vacuum Switch and Nitrogen Gas Valves

After suiting up in the clean suits and entering the clean room, several machines and valves need to be immediately started so that spin coating can run smoothly and cleanly. First the supplies of water, nitrogen, and the vacuum must be opened to the hood and the spin coater. The supplies to the hood are located at the far left behind the hood and the supplies to the spin coater are located directly above the machine. All valves need to be opened for the equipment to function (Figure D.4).

Figure D.4: Hood Supply Lines (Left) and Spin Coater Supply Lines (Right)

Next, the water within the hood should be opened and allowed to flow for ten minutes before being used. Additionally the oven should be turned on so that the operating temperature of 110°C can be reached. Figure D.5 shows the oven's power switch and control panel.

Figure D.5: Oven Control Panel

At this time the air analyzer within the clean room can be started to determine the quality of air content within the room. To do this, the air collector on the top of the machine must be opened and the cone must be inserted into the opening. Additionally the green power button followed by the blue arrow must be pressed for the analyzer to begin its process.

Figure D.6: Clean Room Air Analyzer

Finally the methanol and acetone must be set up for the spin coating process. This requires methanol to be placed in the sonicator within the hood, acetone be placed in a petri dish, and a Petri dish to be placed under the water flow in the hood sink. Figure D.7 displays the approximate amount to put in each of the containers.

Figure D.7: Spin Coating Fluid Setup

The far left is the methanol within the sonicator. The middle picture contains acetone within a large Petri dish. Enough of both materials should be placed into the containers so that a wafer is guaranteed

to be covered. Finally, the right picture displays the water flow rate and the placement of the Petri dish under the water.

APPENDIX E: Detailed Spin Coating Procedure

The spin coating process begins with removing the silicon wafer from the storage container and rinsing the wafer in an acetone bath for five minutes. After being rinsed in acetone, the wafer is sonicated in methanol for an additional five minutes. These two processes are conducted to ensure the remove of all contaminates on the wafer surface. Following the sonication, the wafer is blown dry with nitrogen gas and placed in a flowing water bath for another five minutes.

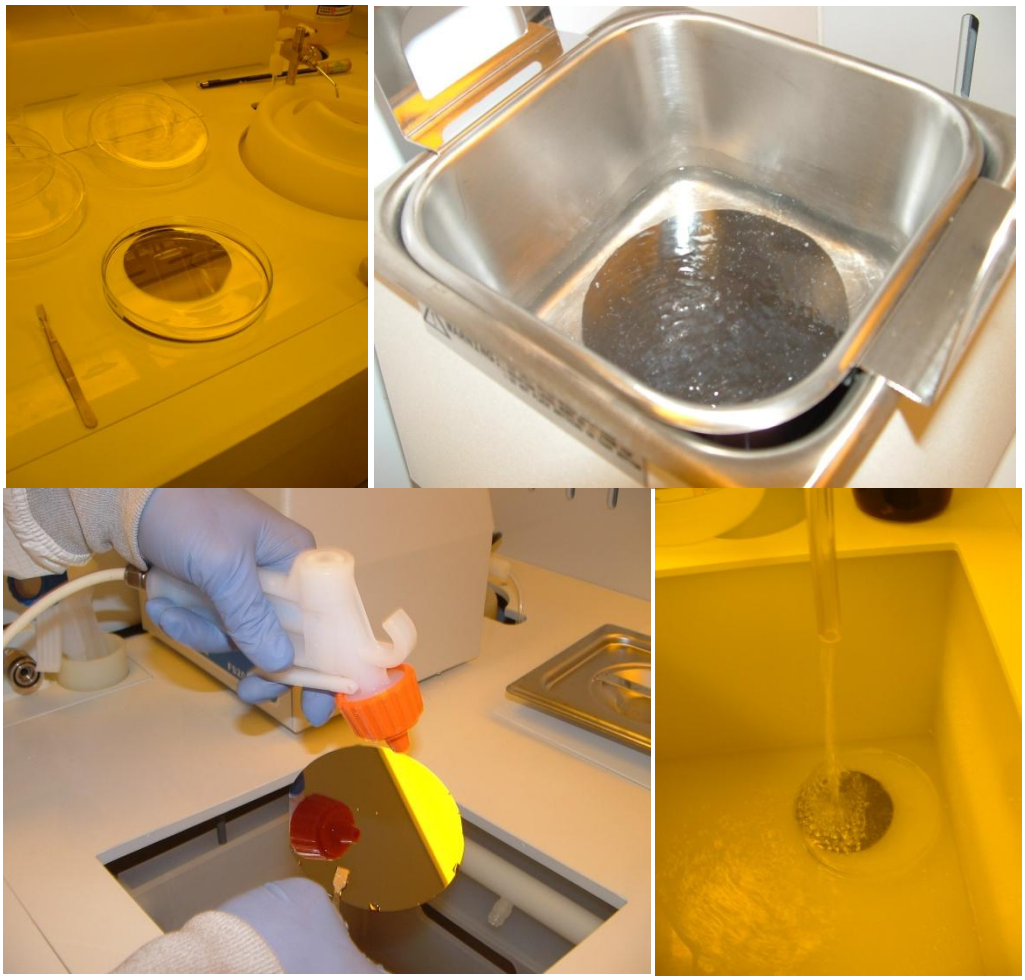

Figure E.8: Spin Coating Liquid Cleaning Treatment
Upper left depicts the acetone bath. Upper right is the sonicator with methanol as the fluid for cleaning the wafer. The bottom left is the method for cleaning all cleaning fluids off of the wafer before being placed in the water bath (bottom right). All liquid treatments are conducted for five minute intervals.

After being cleaned in the water bath, the wafer is first blown dry with the nitrogen gas as after the acetone and methanol treatments. Additionally, the wafer is dried in the 110°C oven for one minute to complete remove all fluids from the wafer surface. The goal of the cleaning process is to ensure a smooth, contaminate-free surface for photoresist attachment. After removing the wafer from the oven,

it is placed on a cooling rack for one minute to ensure that the photoresist does not begin to be heated during the spin coating process.

First begin by supplying power to the spin coater via the power switch (Figure E.12). Prior to beginning spin coating, the rotations per minute has to be set along with the spinning time. To adjust the RPM, under the "SPIN" heading there is a circular dial, this must be slightly pressed inward and turned in a clockwise direction to increase the RPM. The time for total spin coating is shown below the RPM adjustment knob, and is in seconds.

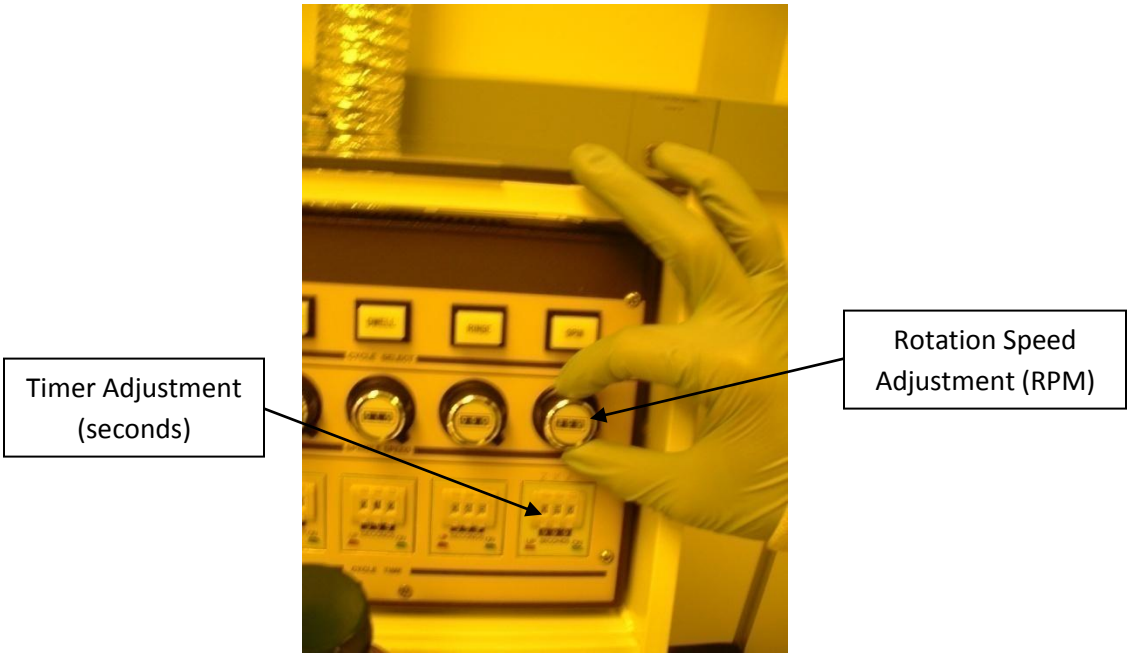

Figure E.9: Spin Coater Rotation Setup Control Panel.

Now the actual spin coating process can be completed. First, the vacuum supply to the spin coater must be turned off, otherwise positioning the wafer will be impossible. This is done by turning the vacuum valve above the spin coater to off. Next, using the right angled wafer placement bar (Figure E.10), the wafer is centered on the spin coater and the vacuum supply is restored. In order to center the wafer you must not use the side which is partially linear, only circular edges should be placed against the right angled placement bar.

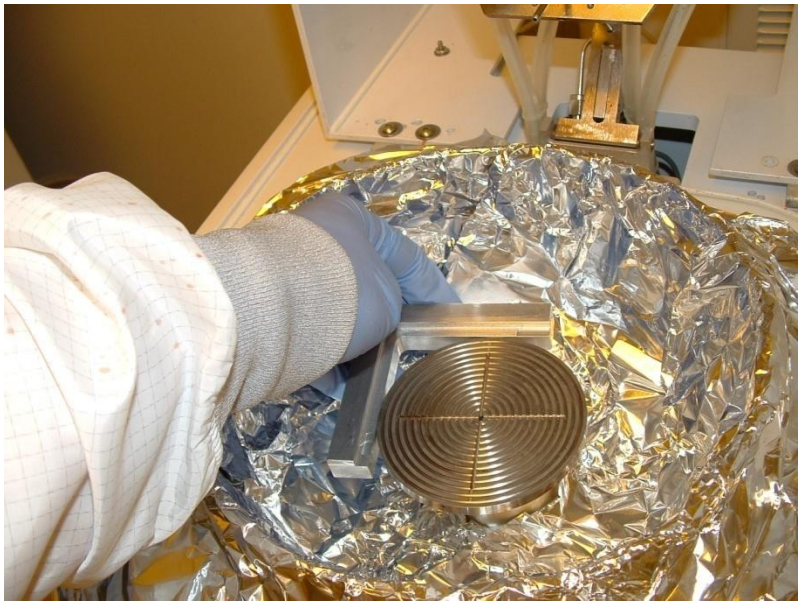

Figure E.10: Placement of the Right Angled Wafer Positioning Bar

After the wafer has been placed on the spin coater, the photoresist can be pipetted onto the surface. This is done using two pipettes almost entirely filled with photoresist (Figure E.11). Both are emptied simultaneously in the center of the wafer and the spin coater is activated immediately after the photoresist is completely emptied onto the surface.

Figure E.11: Spin Coating Photoresist Application Technique

The spin coater is activated by hitting the "START" button on the control consol. The spin coater will follow the predetermined and entered procedure and will automatically stop. After the spin coater has stopped and the applicator head has risen, remove the vacuum supply to the spin coater.

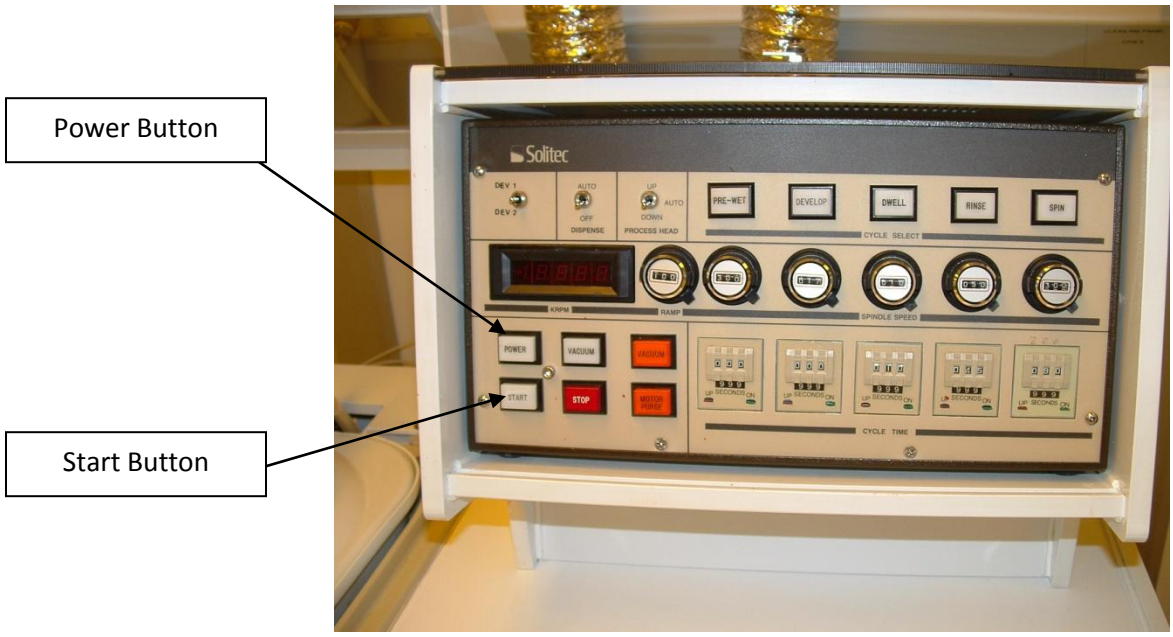

Figure E.12: Spin Coater Consol.

Transfer the wafer to the oven for three minutes of heating. Again cool to room temperature, and apply the photoresist as necessary following the same application, heating, and cool procedures described above.

APPENDIX F: Detailed Pyrolysis Procedure

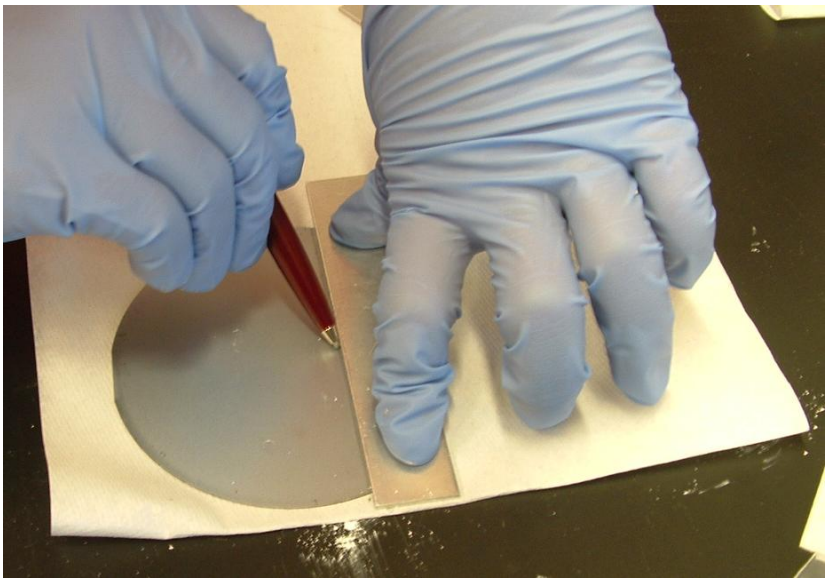

Figure F.1: Wafer Cutting Procedure

First, the wafers are cut to the correct size. For cell growth, the wafer is cut into 22mm by 22mm squares, and into 11mm by 22mm rectangles for electrochemical studies. The wafer is positioned on a paper cloth with the photoresist side facing downward and the wafer is scored with a diamond-tipped pen. An aluminum cutting guide (Figure F.F.1) is aligned with the larger flat cut on the wafer's edge and the wafer is scored from end to end. After scoring, the wafer is broken along the scored line and the process is repeated to yield a number of small chips of the desired size.

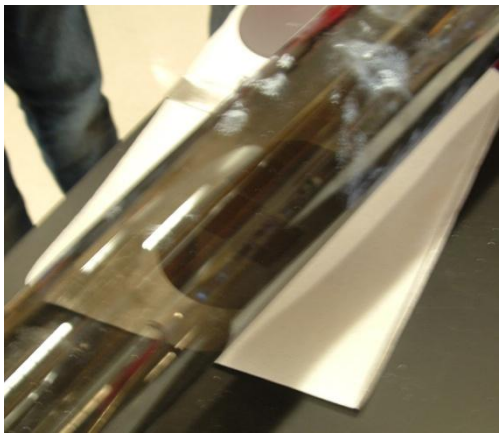

Figure F.2: Wafer Tray Placement

Wafer pieces are placed on a silicon sled and are slid into the open end of the fused quartz furnace tube. The sled is placed slightly past half way in the tube to place it close to center of the heating elements where the most consistent heat is and to place it far from the gas inlet to be sure that the nitrogen reaches the system temperature before being flowed over the wafer pieces (Figure).

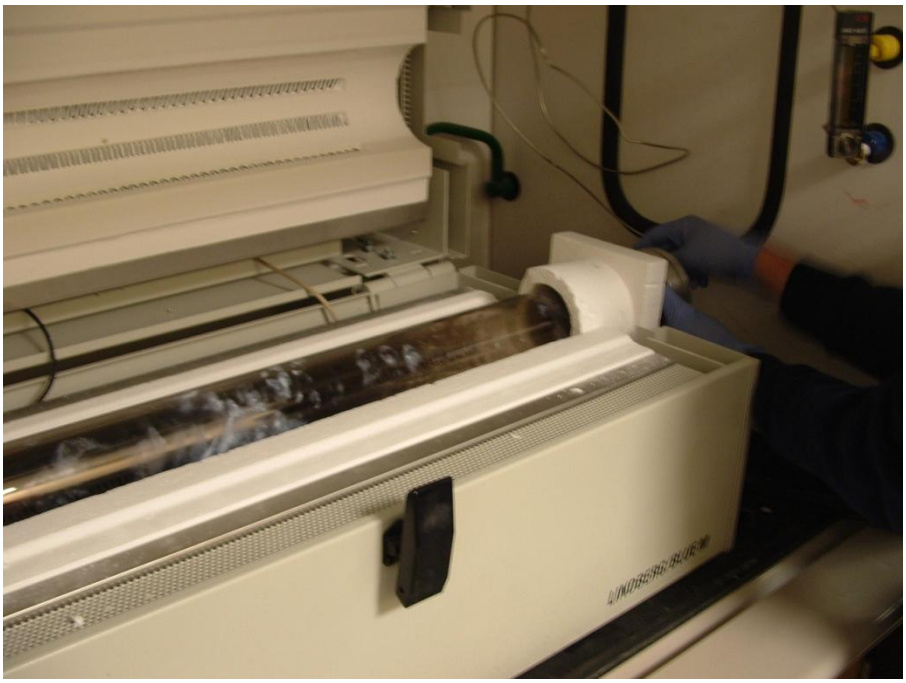

Figure F.3: Tube Placement in the Furnace

The tube is placed in the furnace as shown and the end is capped with the cover attached to the nitrogen gas line (Figure). The furnace is closed and the nitrogen is turned on.

Figure F.4: Nitrogen Supply Valves

Figure F.5: Nitrogen Control Valve and Flow Meter

Nitrogen is then flowed through the furnace tube for 10 minutes to evacuate all oxygen. Valves on the nitrogen tank and regulator are opened (FigureF.4 left) and the valve on the distribution line is opened all the way (Figure F.4 right). The blue valve on the hood (FigureF.5 left) is adjusted so that the flow rate indicated by the flow meter (Figure right) reads 100 sccm. After at least 10 minutes of flow, the furnace is turned on and the heat process begins.

Figure F.6: Tube Furnace Control

The furnace controller is turned on with the switch on the left of the machine's front side (Figure F.6 left). The target temperature is set by simply pressing the arrow keys on the control unit (Figure F.6 right). For this procedure, the maximum temperature is set to 1000°C. For the two step heat procedure, the initial heat rate must be set to 2°C/minute. This is done by holding down the blue button for 5 seconds until the options display appears and then pressing the blue button to cycle through the options until LoC (level of control) is displayed (FigureF.7 left). Using the arrow keys, set LoC to -1 (FigureF.7 left) and then press the blue button repeatedly to cycle through the options until UPr (up rate) is reached. The arrow keys are used to adjust the heat rate to the desired value. For the initial heat rate, UPr will be set to 2 (FigureF.7 center). The blue button is then held down to return to the

normal display screen (Figure F.7 right). Once the furnace reaches 300°C (displayed in the red letters on the display, shown as 21 in Figure F.6 right), UPr is then changed to 10 (Figure F.7 right).

Figure F.7: Tube Furnace Adjustments

Once the furnace reaches 1000°C, the controller is turned off by flipping the switch used previously to turn it on and is left to cool for several hours with the gas still flowing. Once the furnace has reached room temperature (which may be confirmed by turning the furnace on for a brief period and observing the temperature reading), the tube may be removed from the furnace and the samples removed.

APPENDIX H: Electrochemical Cell Assembly and Preparation

To prepare the electrochemical cell for the cyclic voltammetry and the electrochemical impedance spectroscopy, the cell must first be cleaned. The cell, including the connection screws and the copper working electrode supply, are sonicated for ten minute intervals of water, ethanol, and water once more. This is done in a 250 mL beaker. The cell then is allowed to air dry on a paper towel until all moisture is free of the surface.

Figure H.1: All Aspects of the Electrochemical Cell Being Allowed to Dry

The cell is assembled by placing the copper working electrode supply on the upper half of the plate, and placing the 10 mm by 22 mm carbon electrode over this and covering the o-ring in the center of the cell.

Figure H.2: Three Initial Steps to the Electrochemical Cell Assembly
The far left picture displays the placement of the o-ring within the cell, followed by the copper supply in the center photograph. Finally the carbon rectangle is placed on top of both the o-ring and the copper supply. The carbon rectangle must be centered both horizontally and vertically to ensure that the cell is completely sealed when assembled.

The cell is assembled by placing the two halves of the cell together, and tightening each of the four screws and equal distance (this means to rotate through each screw periodically so that all are tightened within one turn of one another).

After assembling the cell and if the cell is going to be store for an extended period of time before use, the interior of the cell should be filled with some pH stable solution (PBS) to maintain the integrity of the cell and the carbon within the cell.

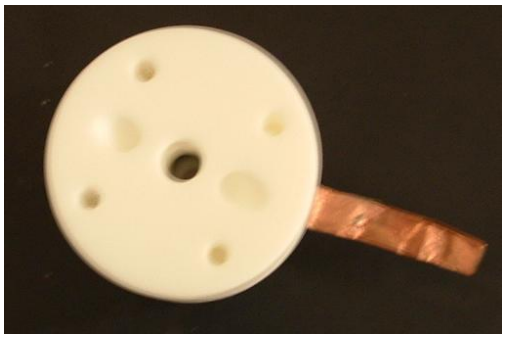

Figure H.3: Assembled Electrochemical Cell

If the cell is going to immediately attached to the potentiostat, the potentiostat needs to be turned on, simply by pressing the "POWER" button. Afterwards, the three electrode system should be assembled as shown in Figure . The reference electrode serves to negate the noise presented by the fluid, while the working and counter electrodes function as the current supply and return. This setup is maintained for both cyclic voltammetry and electrochemical impedance spectroscopy.

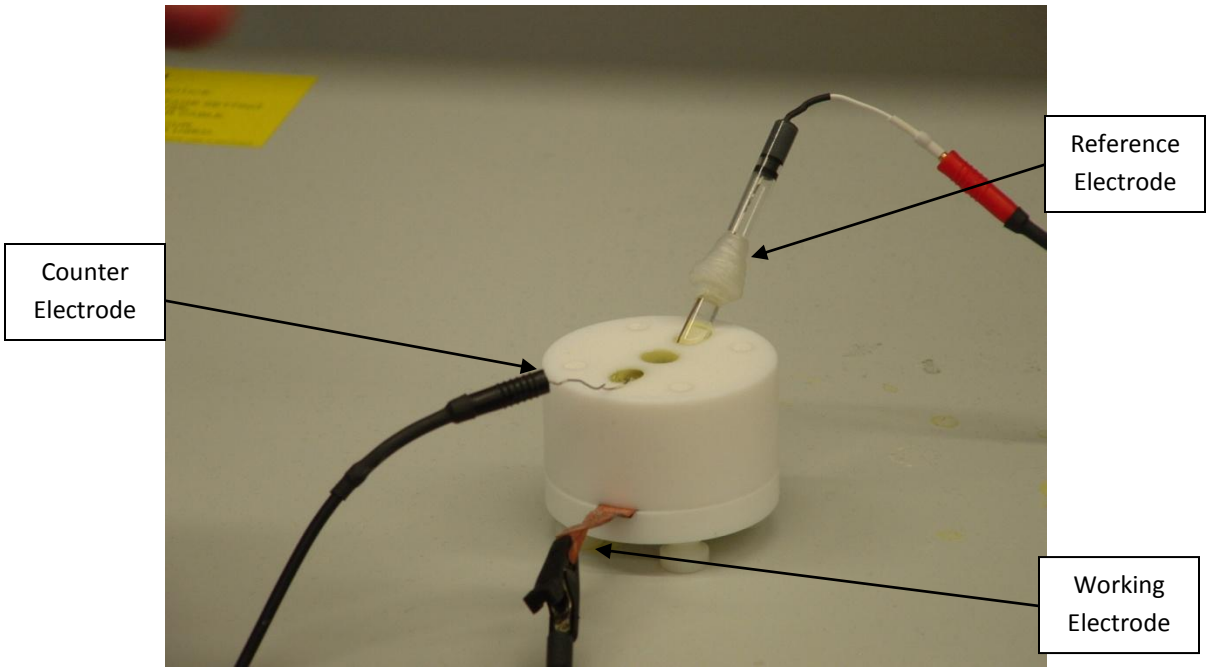

Figure H.4: The Three Electrode Assembly for the Electrochemical Cell

APPENDIX I: Detailed Cyclic Voltammetry Scan Procedure

The computer system will not allow the use of the potentiostat software without the credentials of an administrator. In order to use the machine an "ADMIN" must log onto the computer. To being cyclic voltammetry, open the GPES module within the programs menu (Figure).

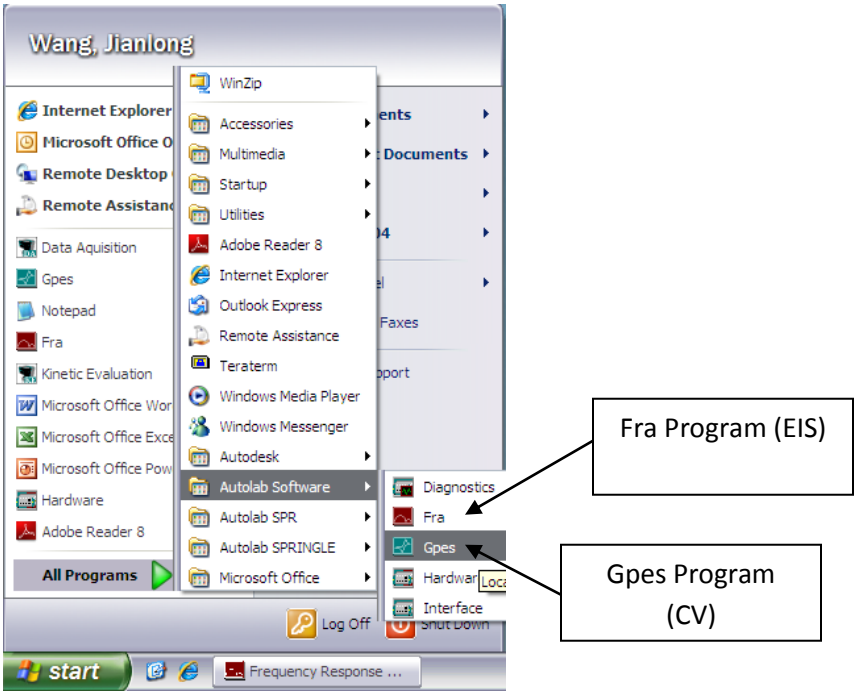

Figure I.1: Programs Menu Depicting CV and EIS Programs

The screen that appears (Figure I.2) contains all of the options that are capable for manipulation. The "Edit Procedures" window is the area in which the cyclic voltammogram scan is predefined. "Pretreatment" is created to hold the electrochemical cell at a certain potential before scanning, for our purposes this was not done. An equilibration time of 5 seconds was routinely used. "Measurement" allows for the possibility of running many sequential scans on the same cell, and to adjust the potential that the cell is held at after the scan is complete, for the purposes of these experiments the potential was 0.

"Potentials" is where the user is allowed to truly alter the scan. Under this tab, the scan potentials can be altered as well as the scan rate and the step the machine takes while scanning. The cyclic voltammetry scan encompasses beginning at one potential (Start Potential), scanning at a certain voltage step (Step Potential) to another potential (First Vertex Potential), and finally continuing to a final potential (Second Vertex Potential). Figure I.2 displays the values used for the general scanning of the biosensor. For the ABA treatment, the first vortex potential was changed to 1.4 and the scan rate was changed to 0.01.

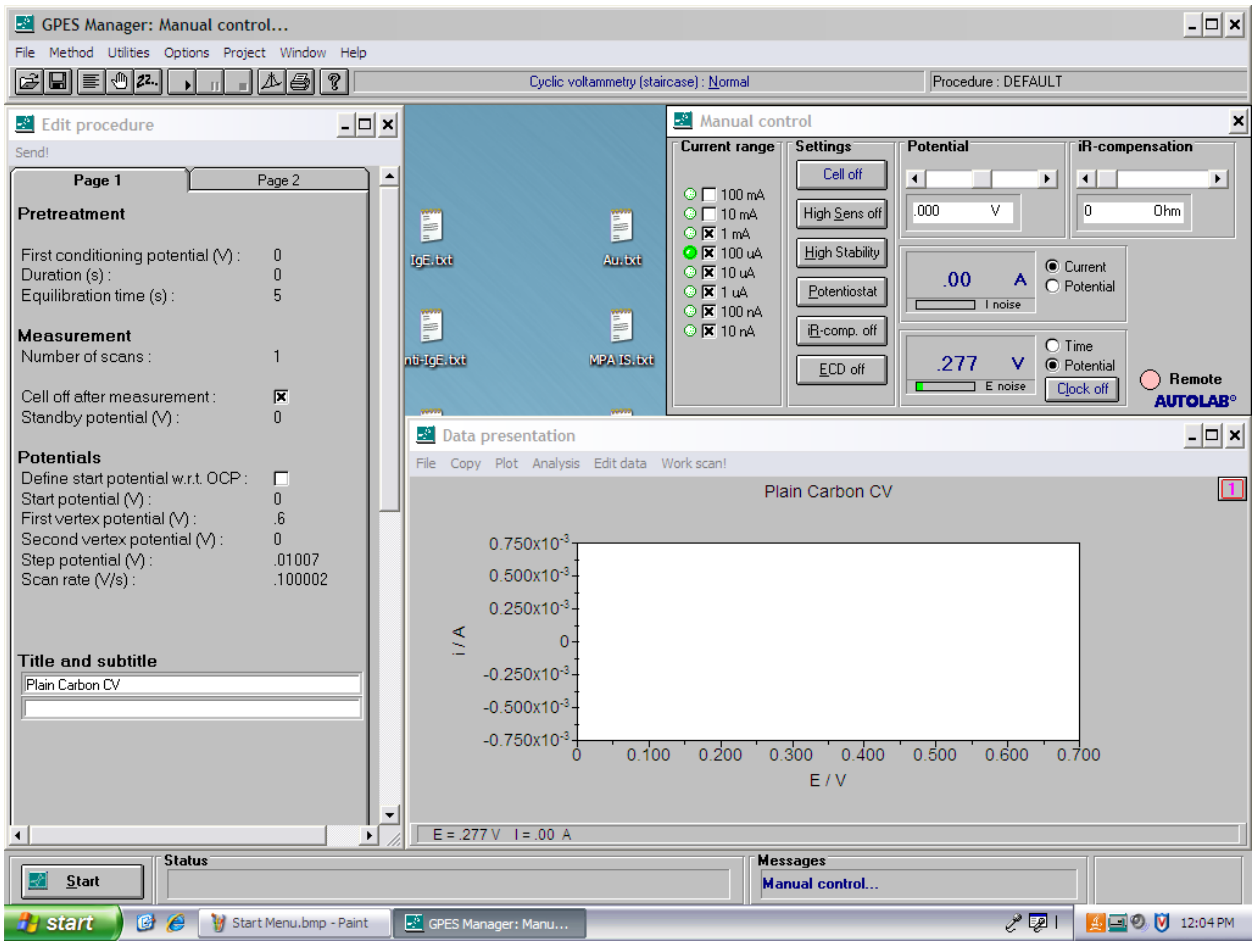

Figure I.2: Gpes (CV) Program Menu and Base Screen

APPENDIX J: Images From Cell Morphology Assay

A selection of images from the cellular morphology assay follows. The scale bar in the lower right of each image indicates 100 µm. Particularly bright spots are probably due to precipitation of the fluorescent dye (DiI), and differences in intensity between cells or groups have no physical significance.

J.1 Carbon

J.1.1 Bare Carbon

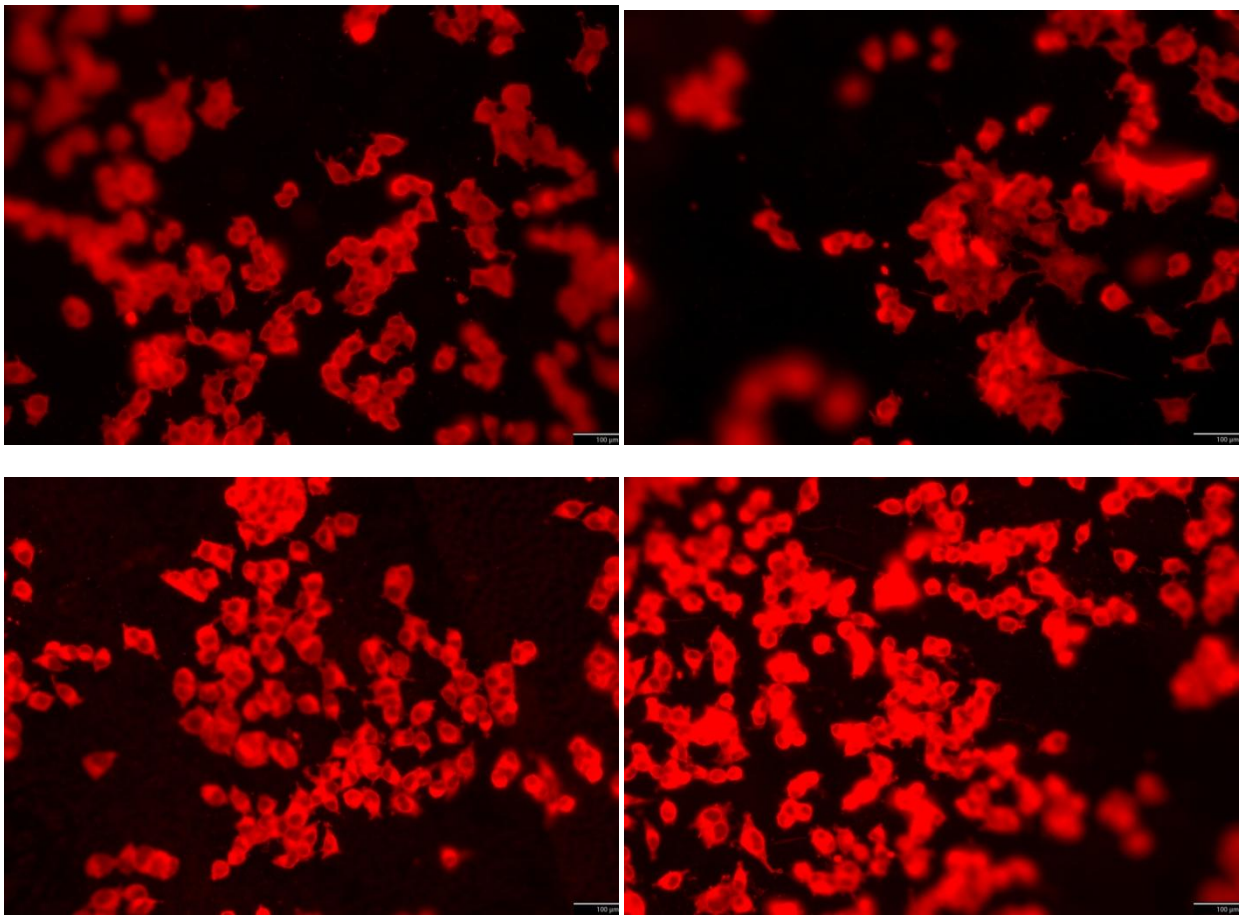

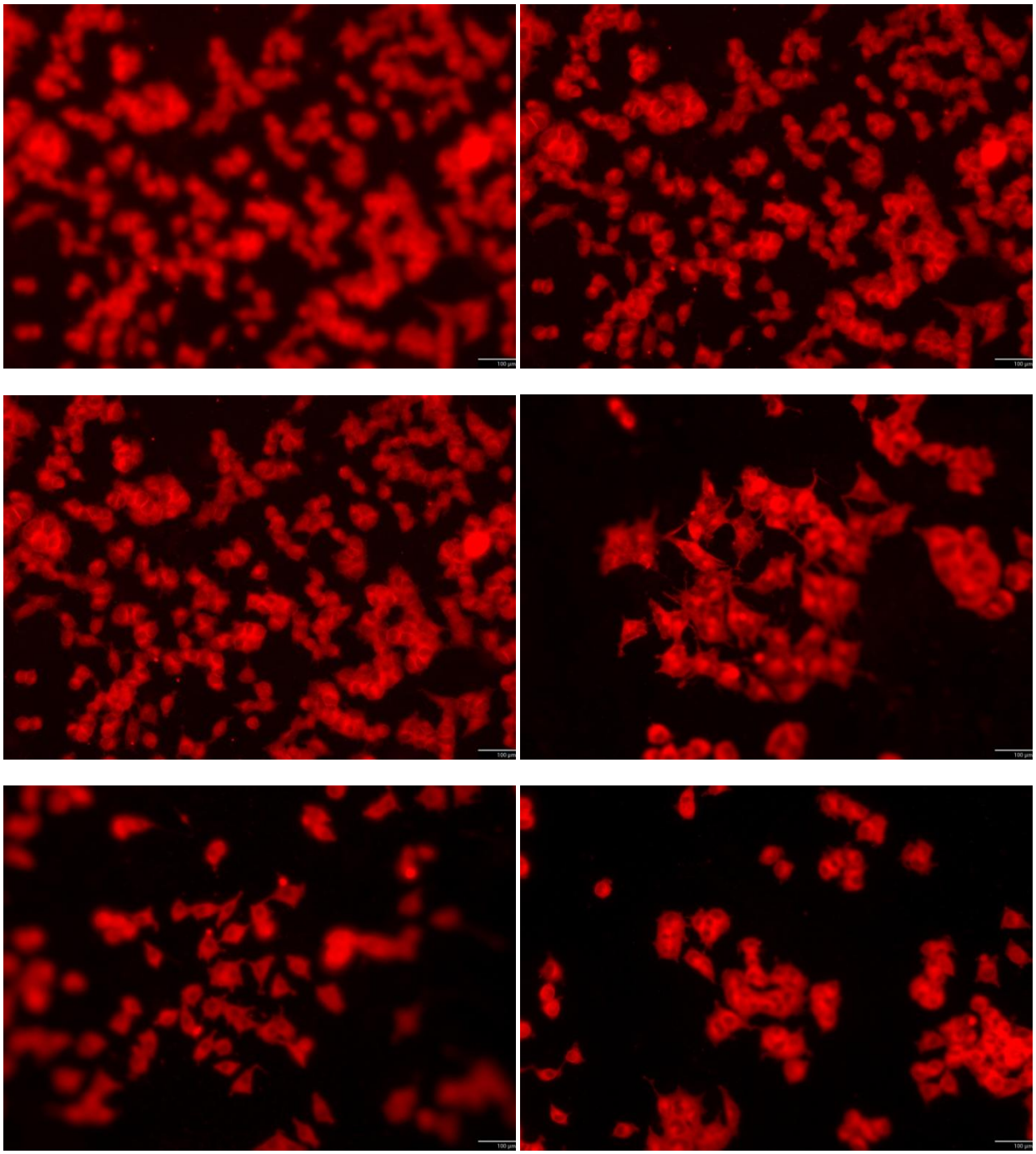

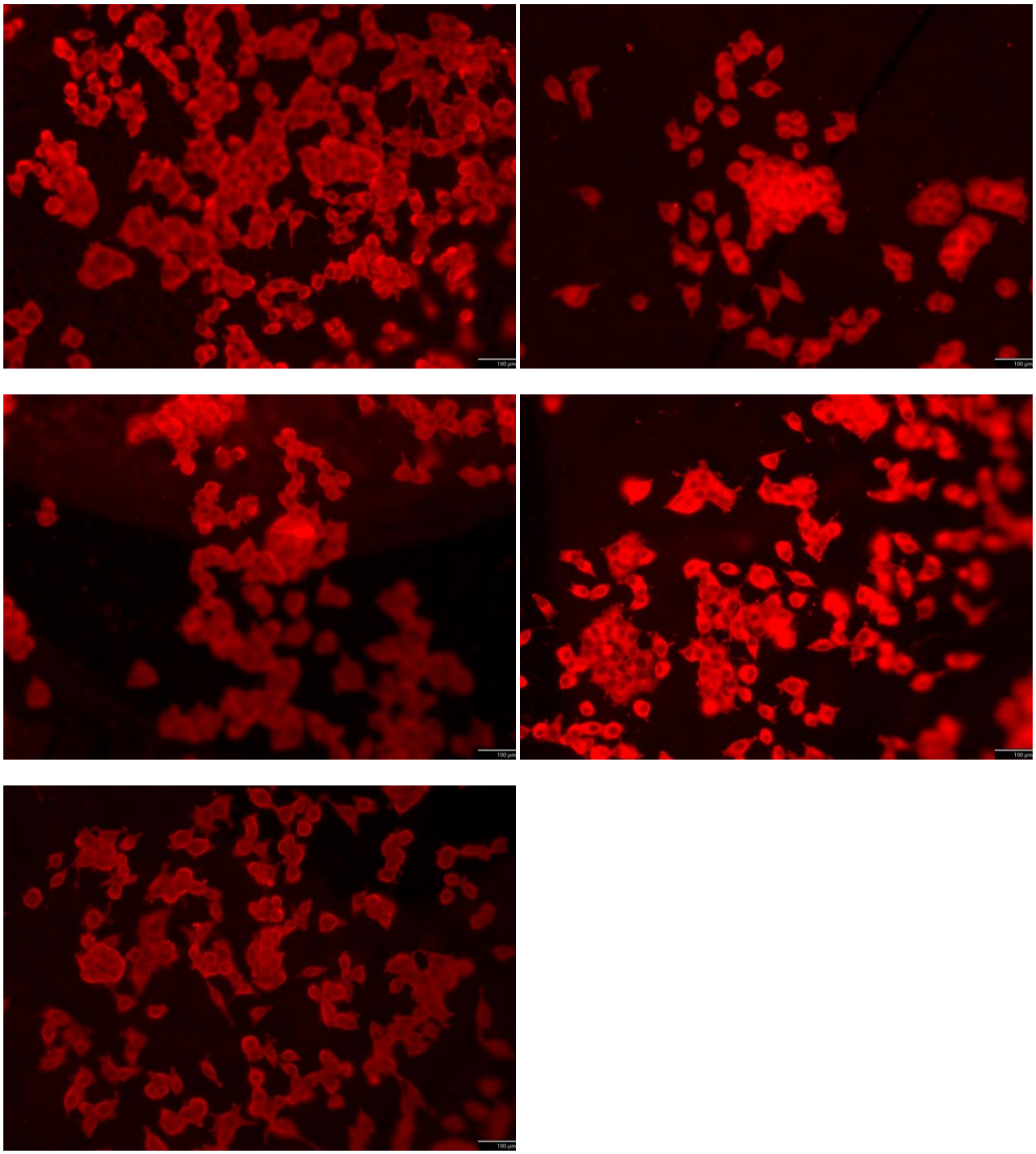

J.1.2 PL Coated Carbon

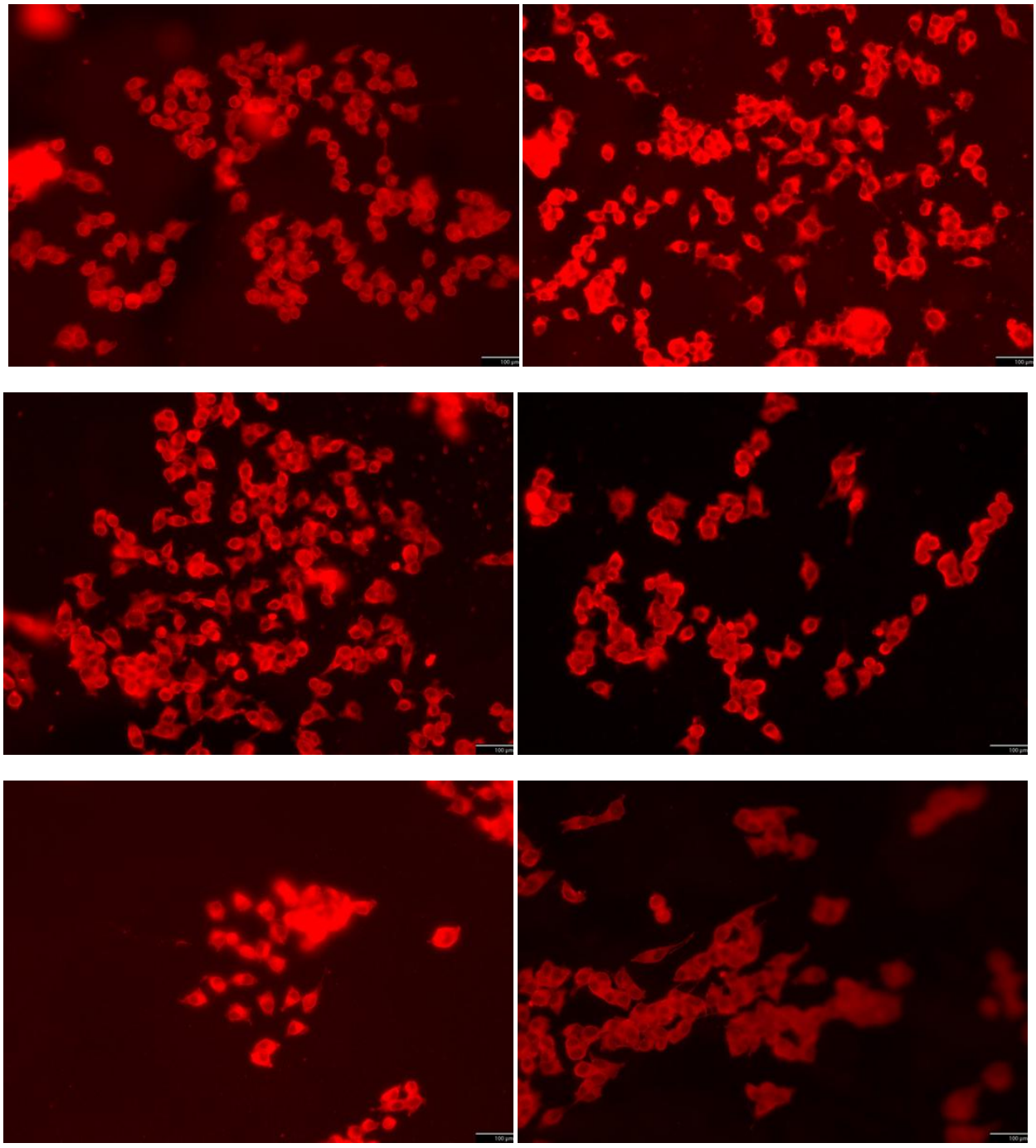

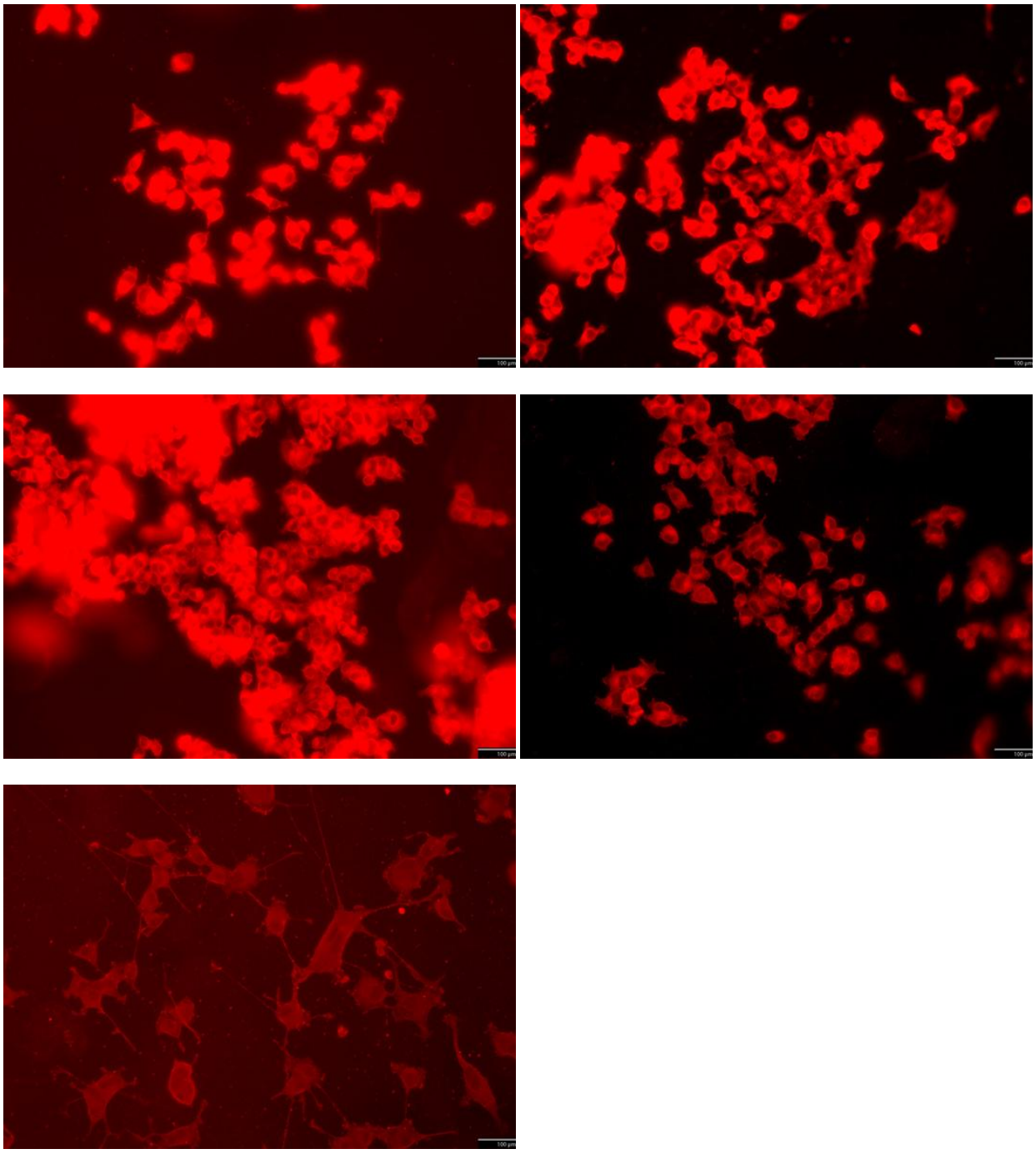

J.1.3 NGF Treated Carbon

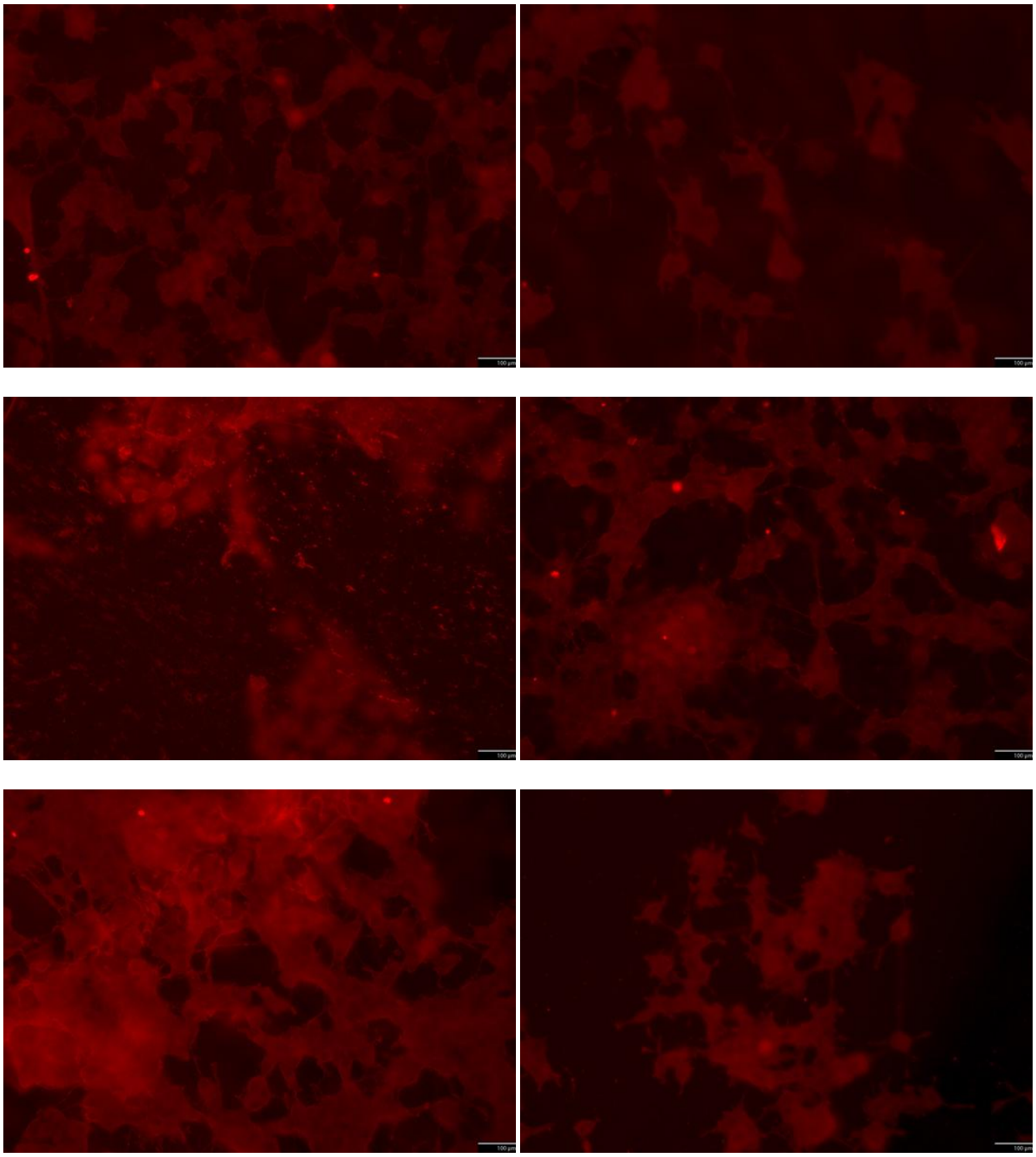

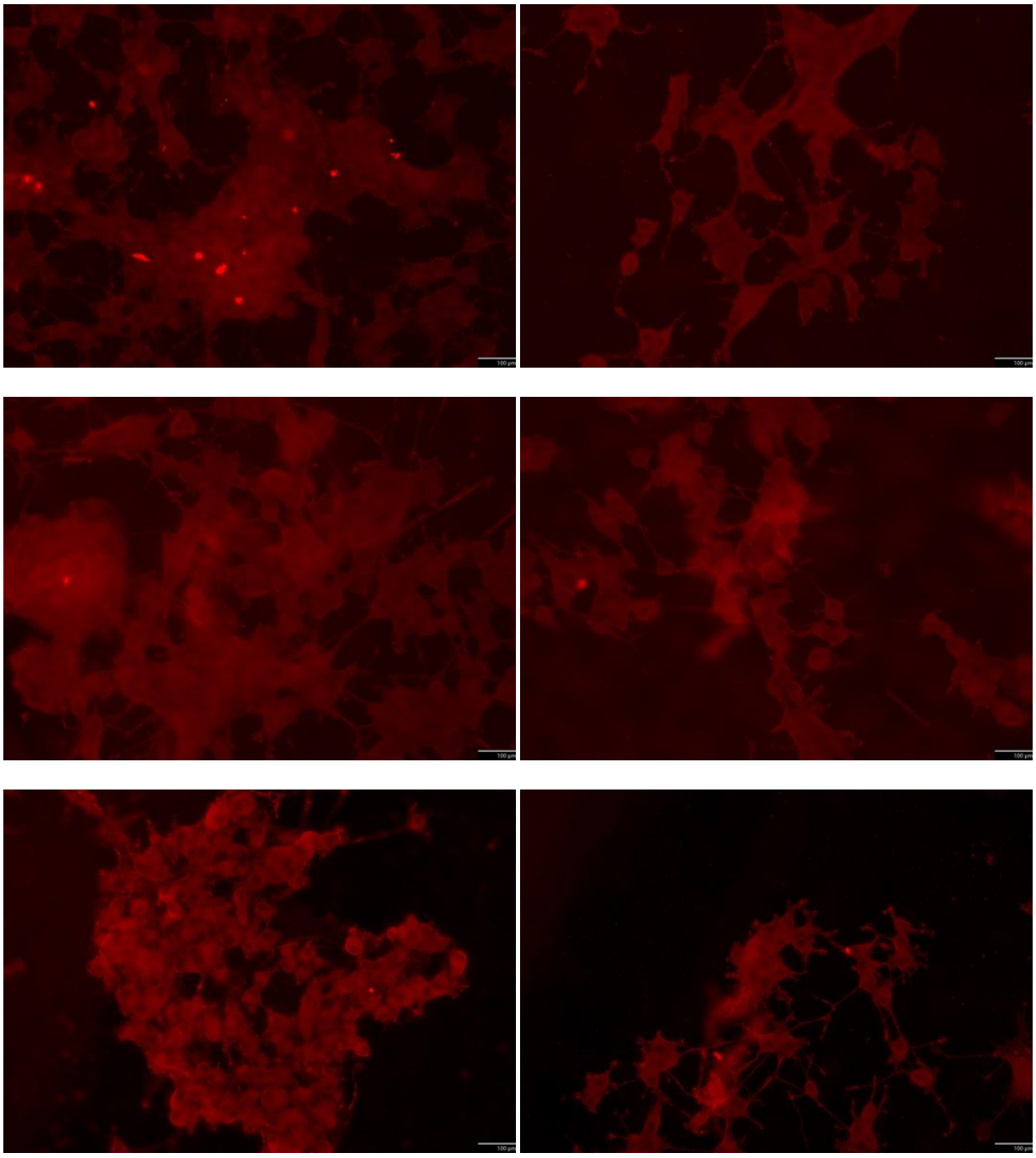

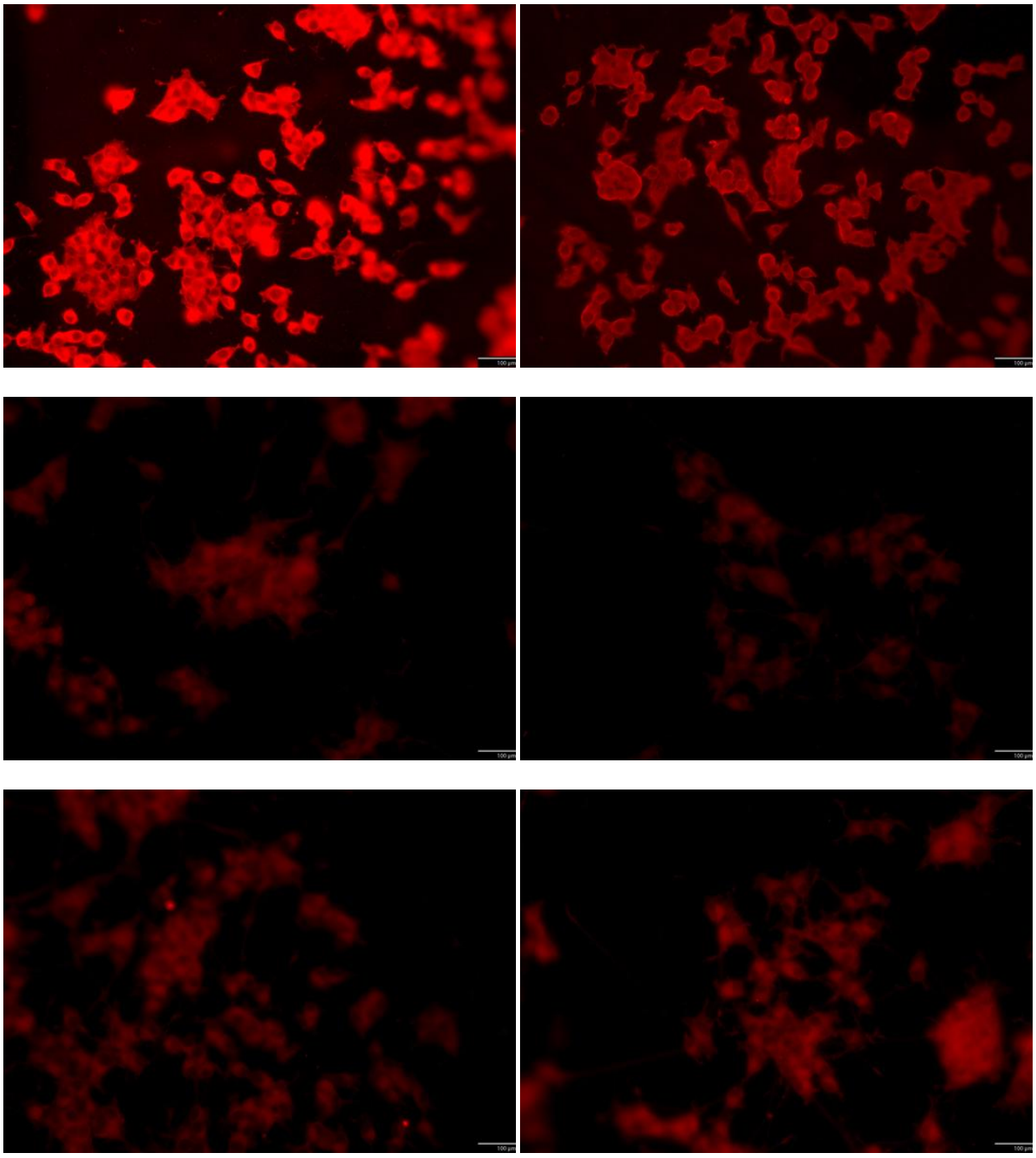

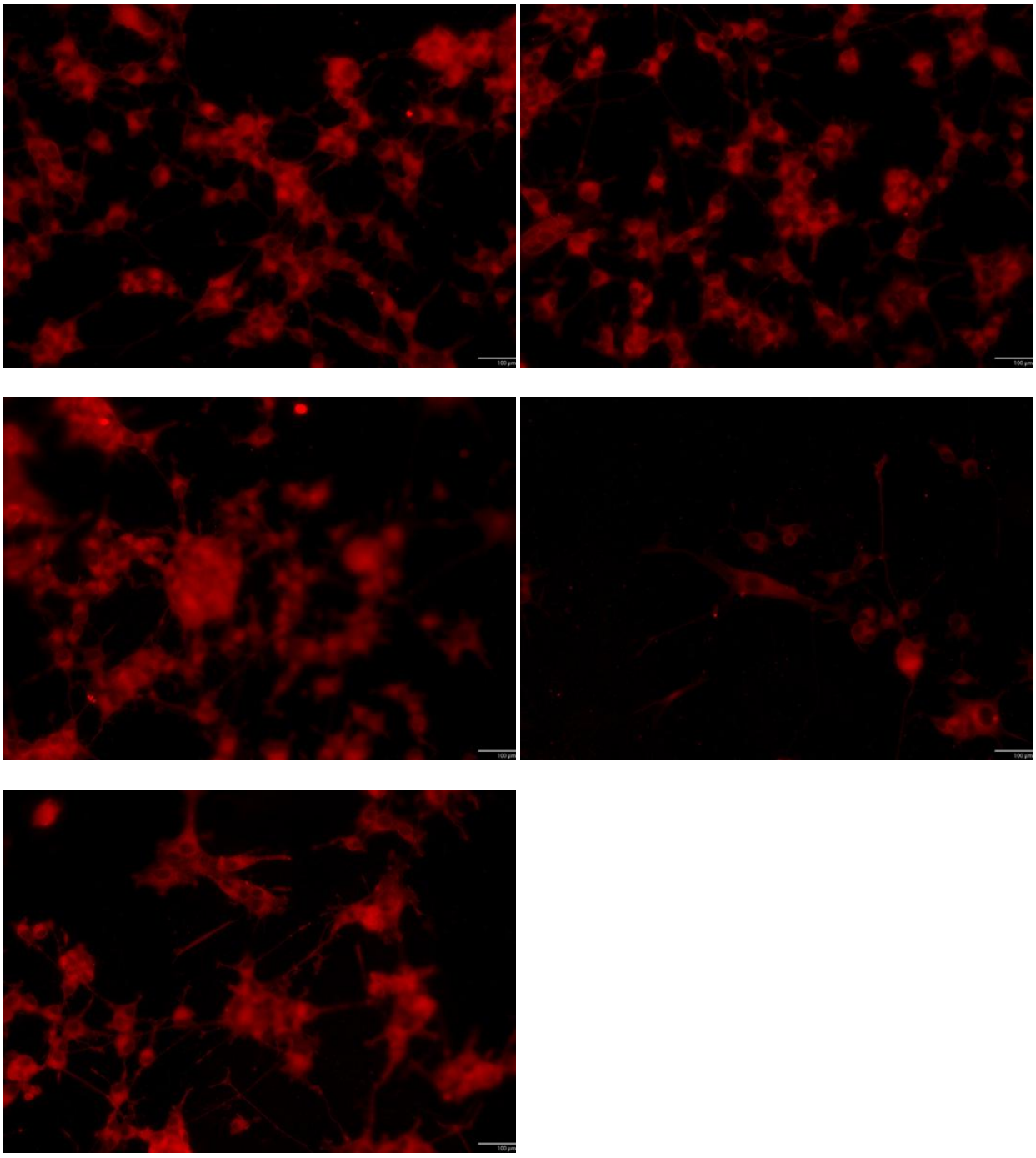

J.1.4 PL Coated and NGF Treated Carbon

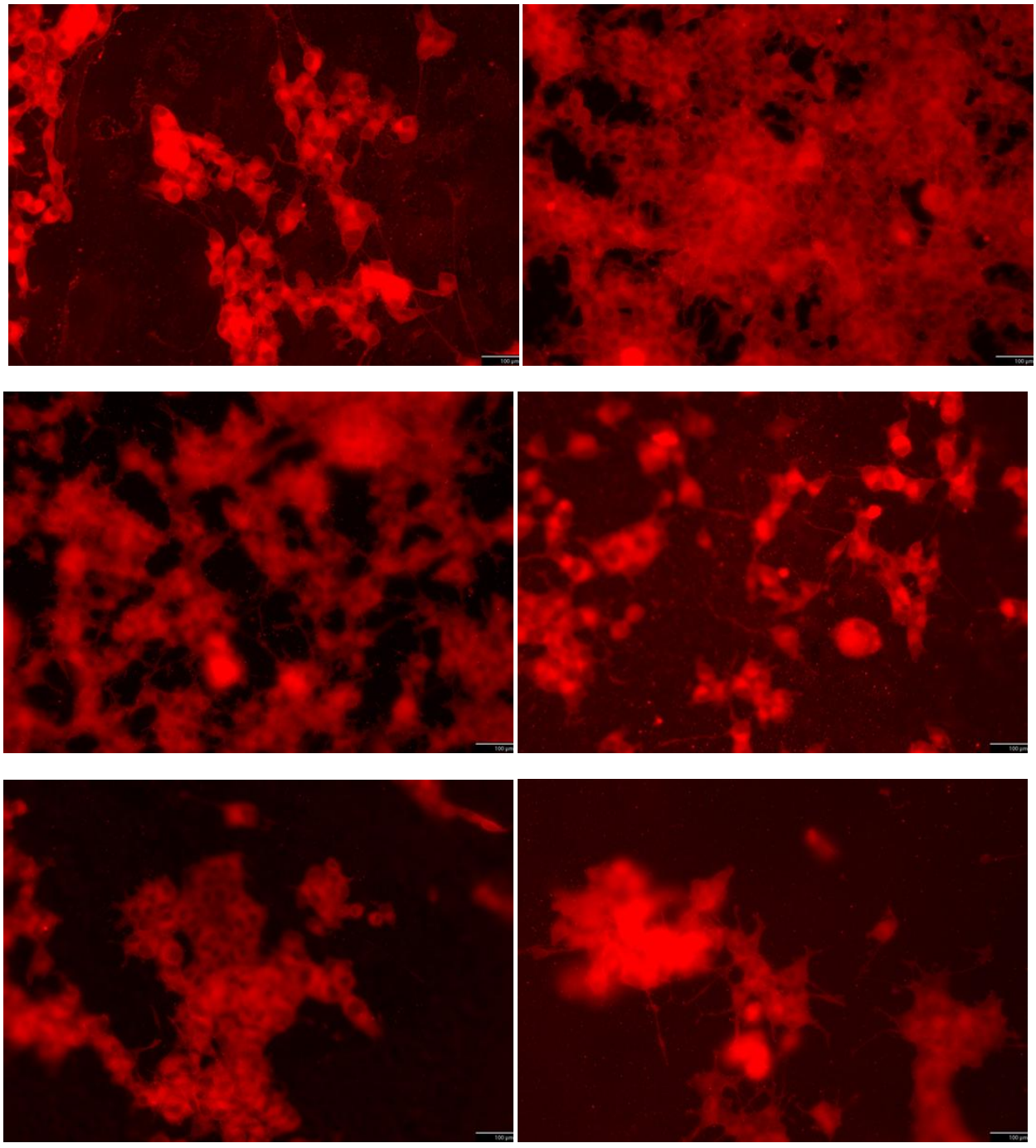

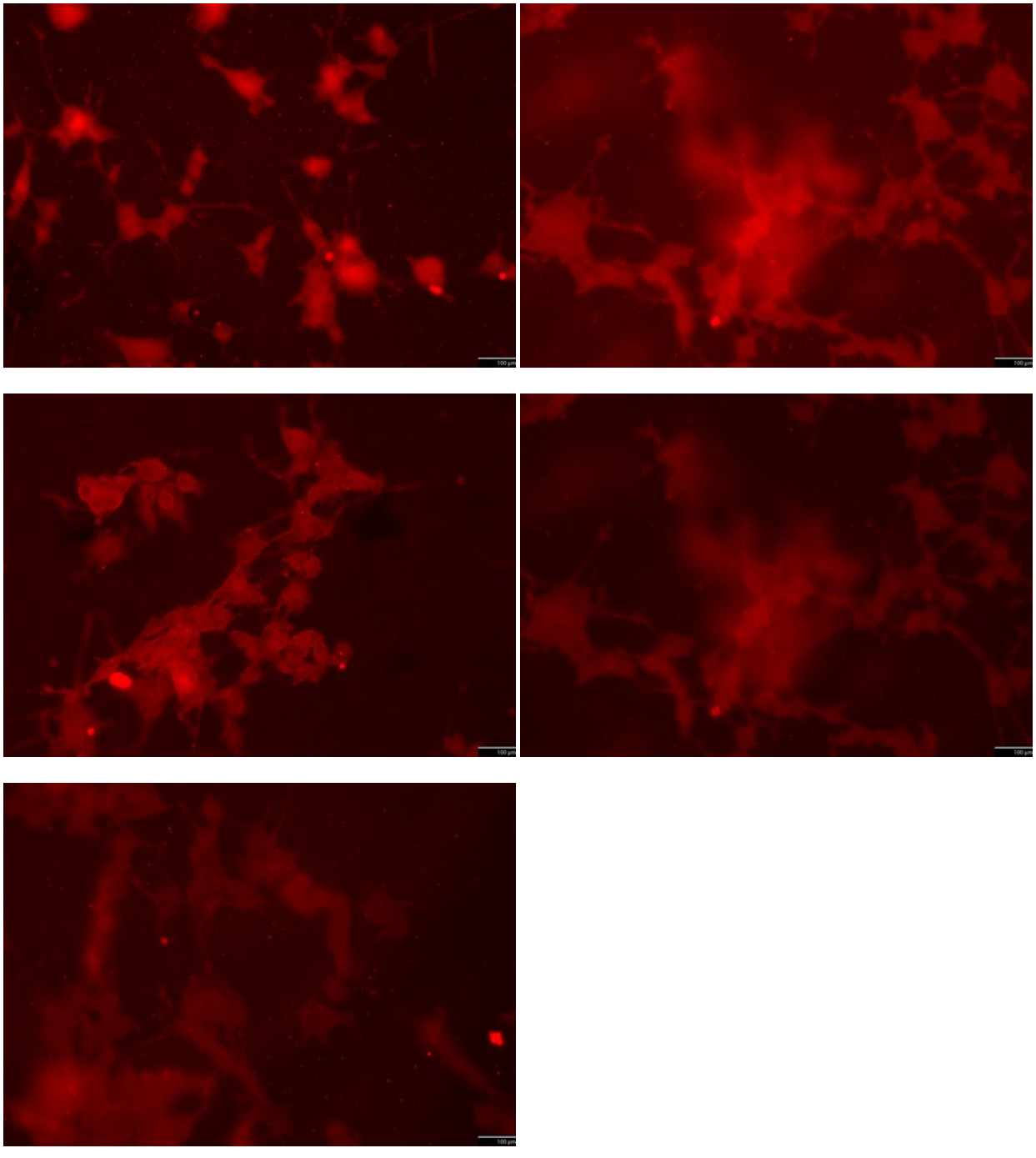

J.2 Silicon Surfaces

J.2.1 Bare Silicon

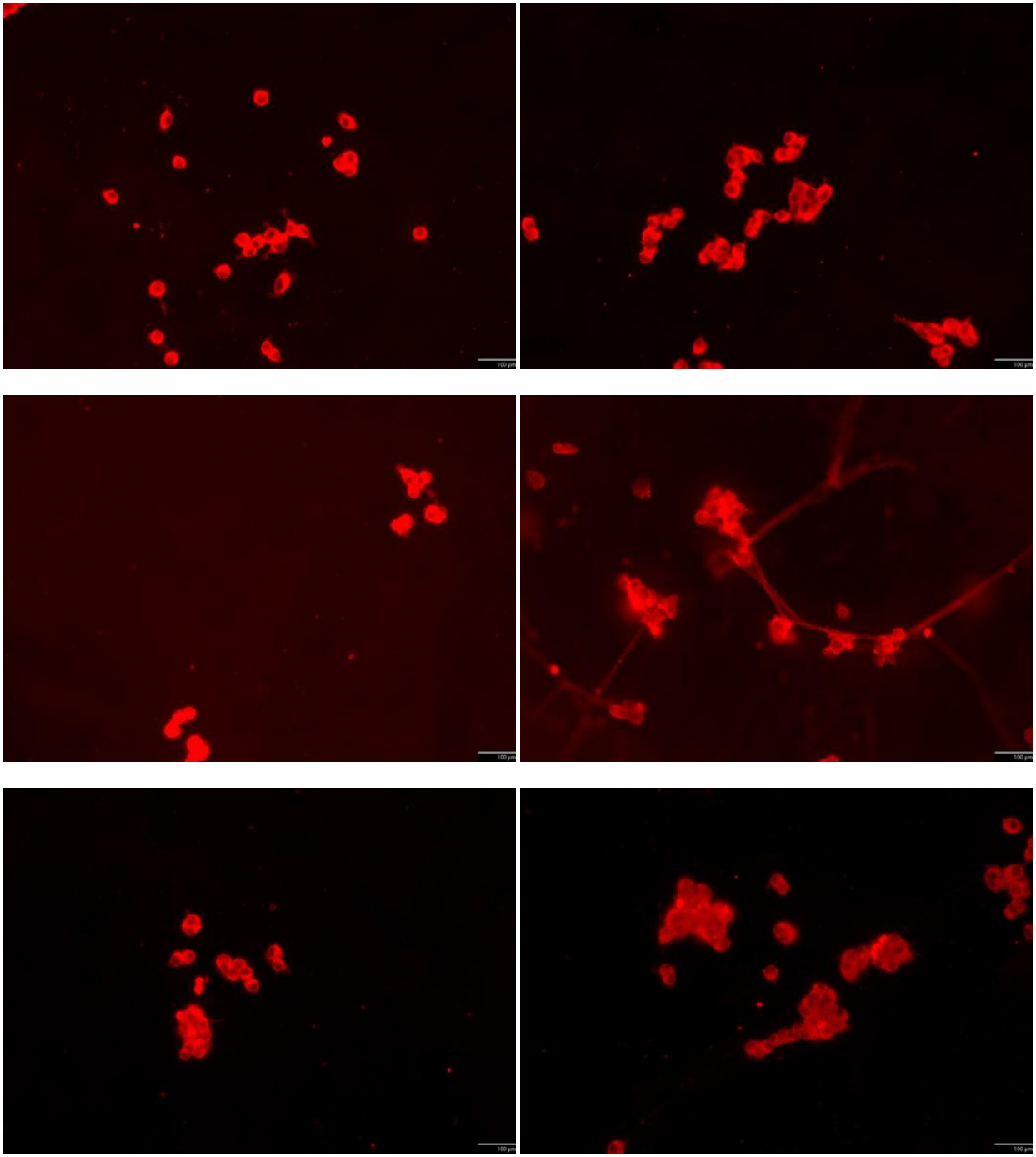

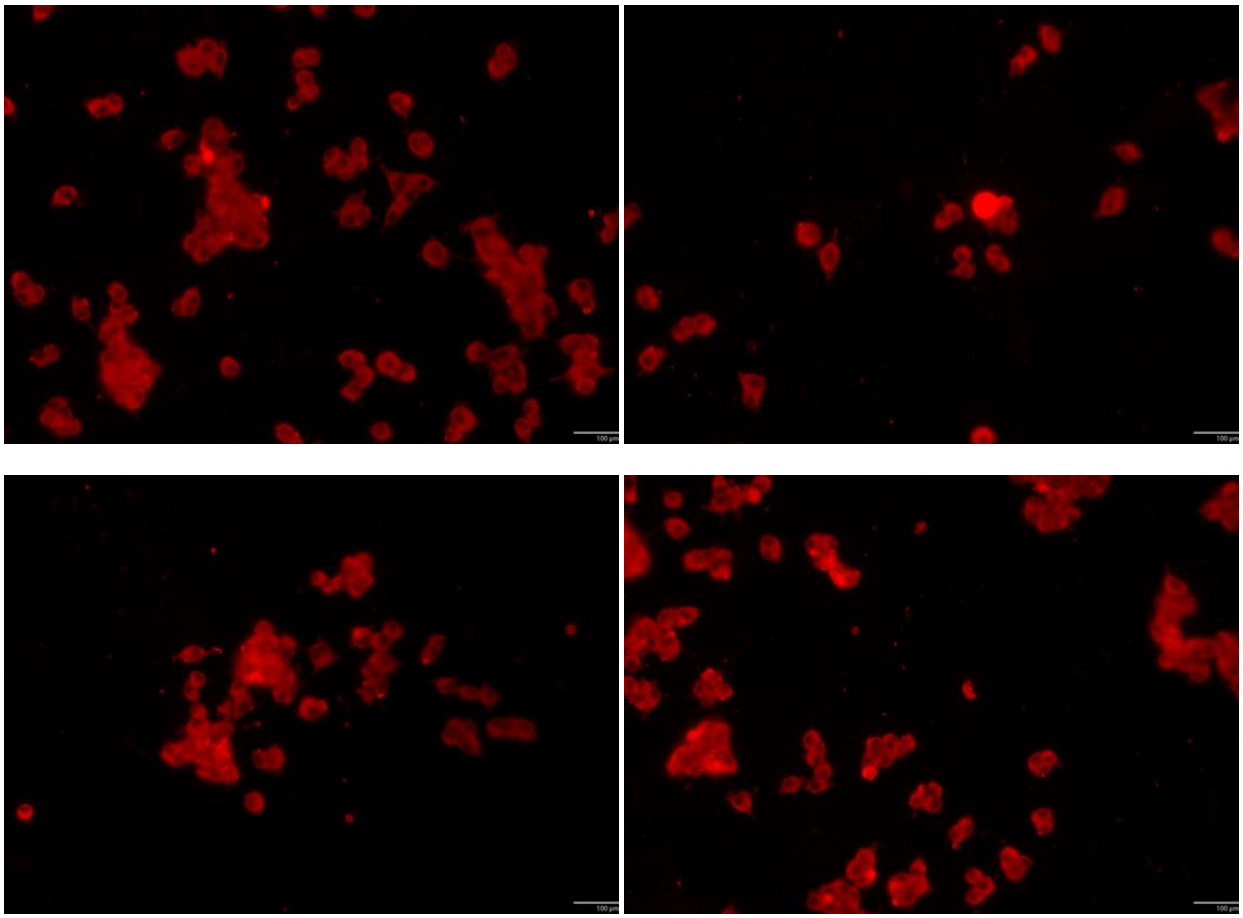

J.2.2 PL Coated Silicon

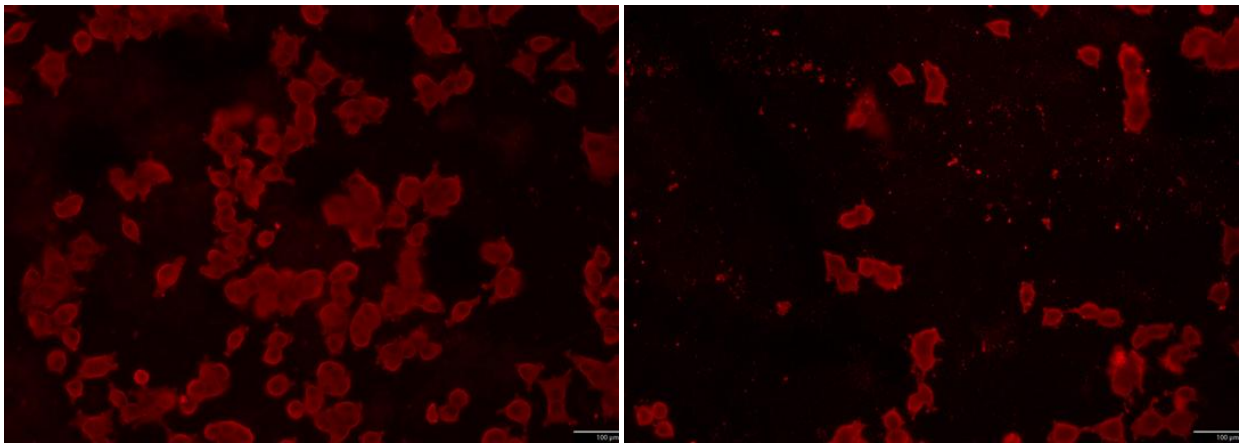

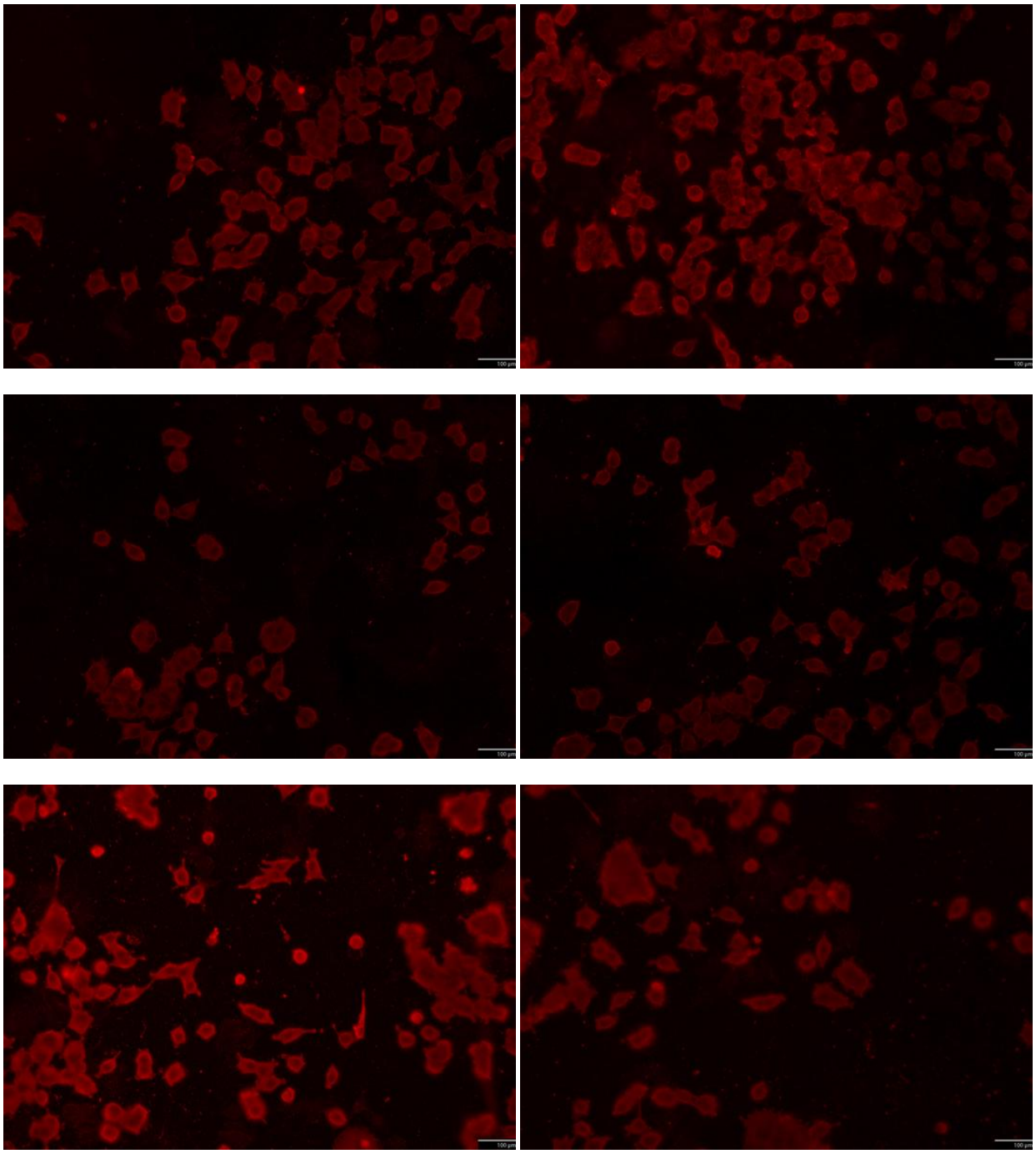

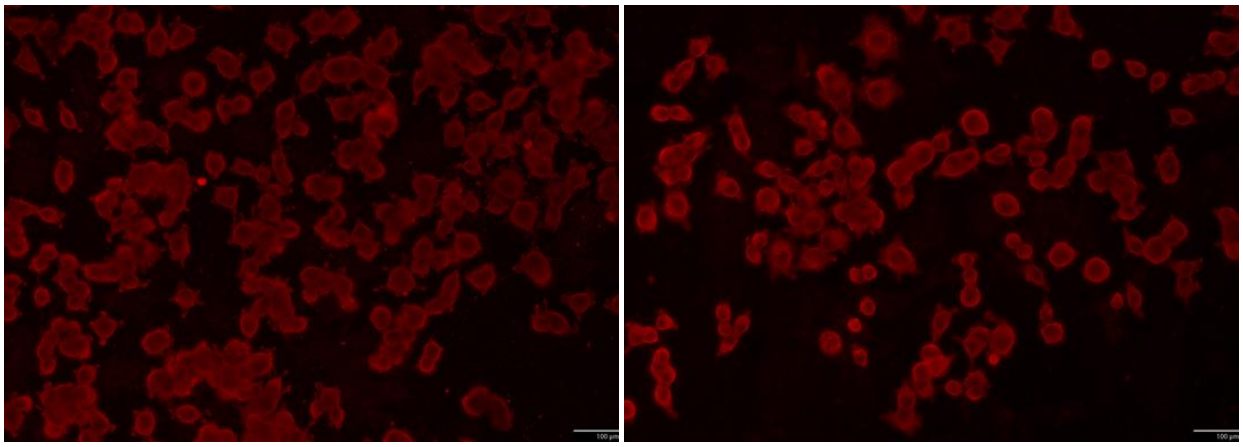

J.2.3 NGF Treated Silicon

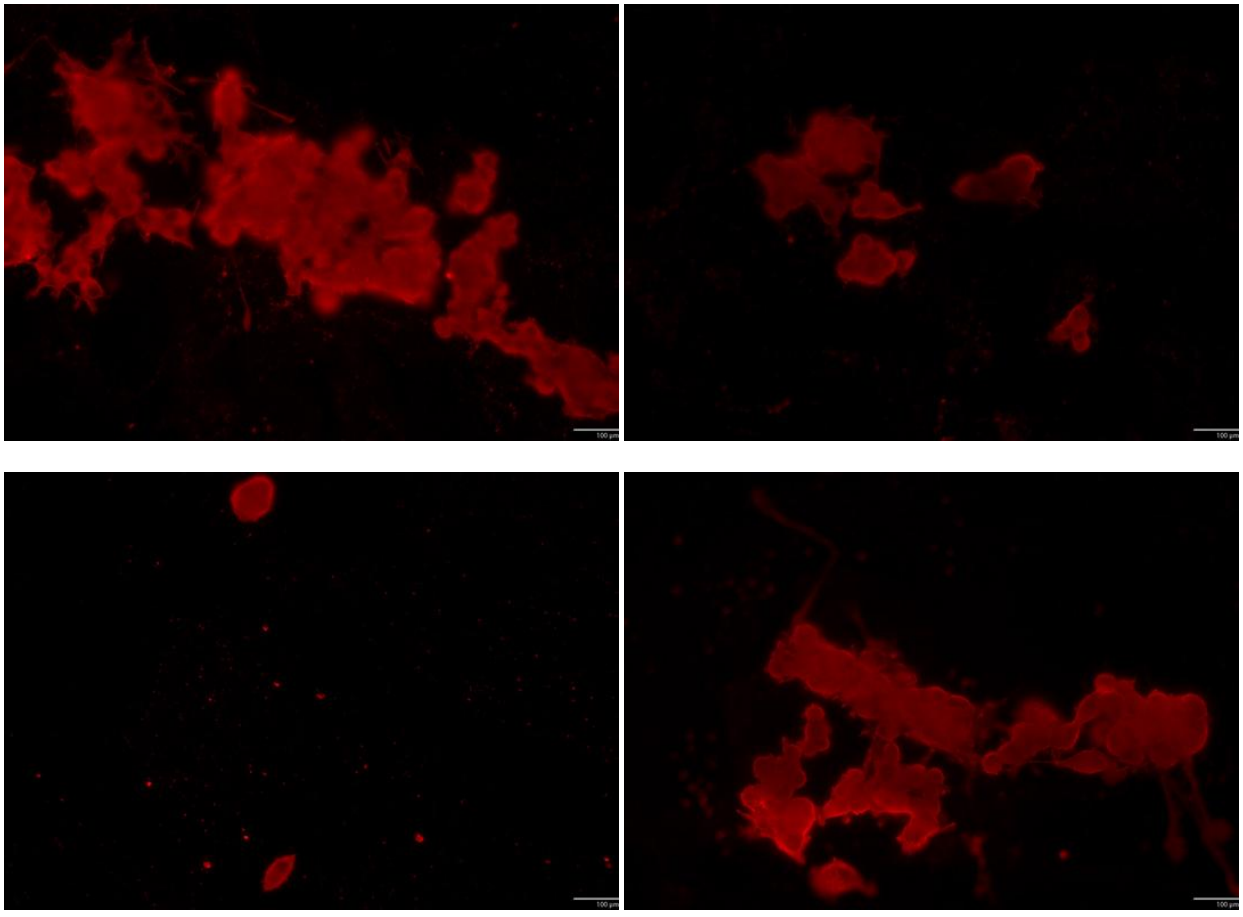

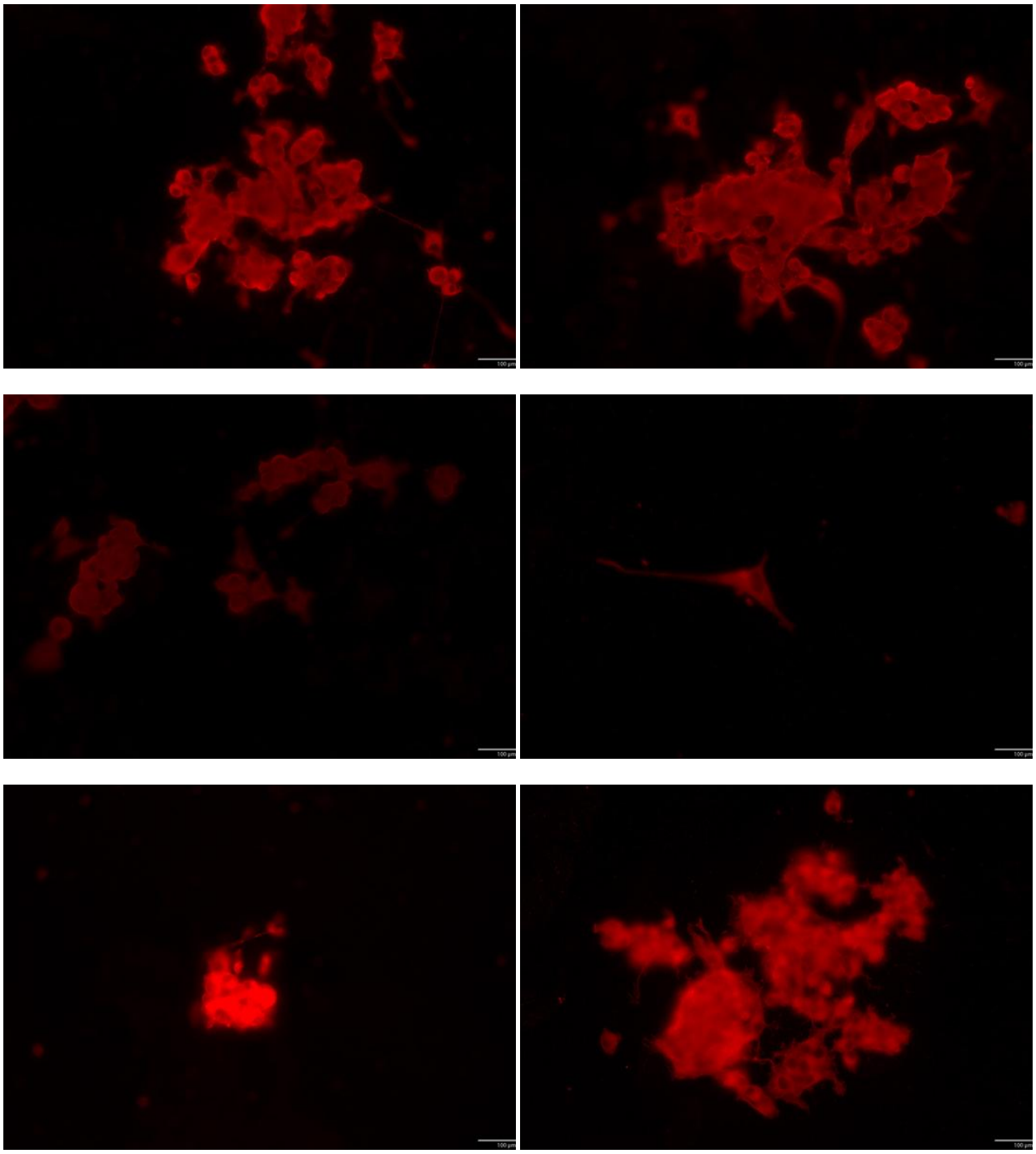

J.2.4 PL Coated and NGF Treated Silicon

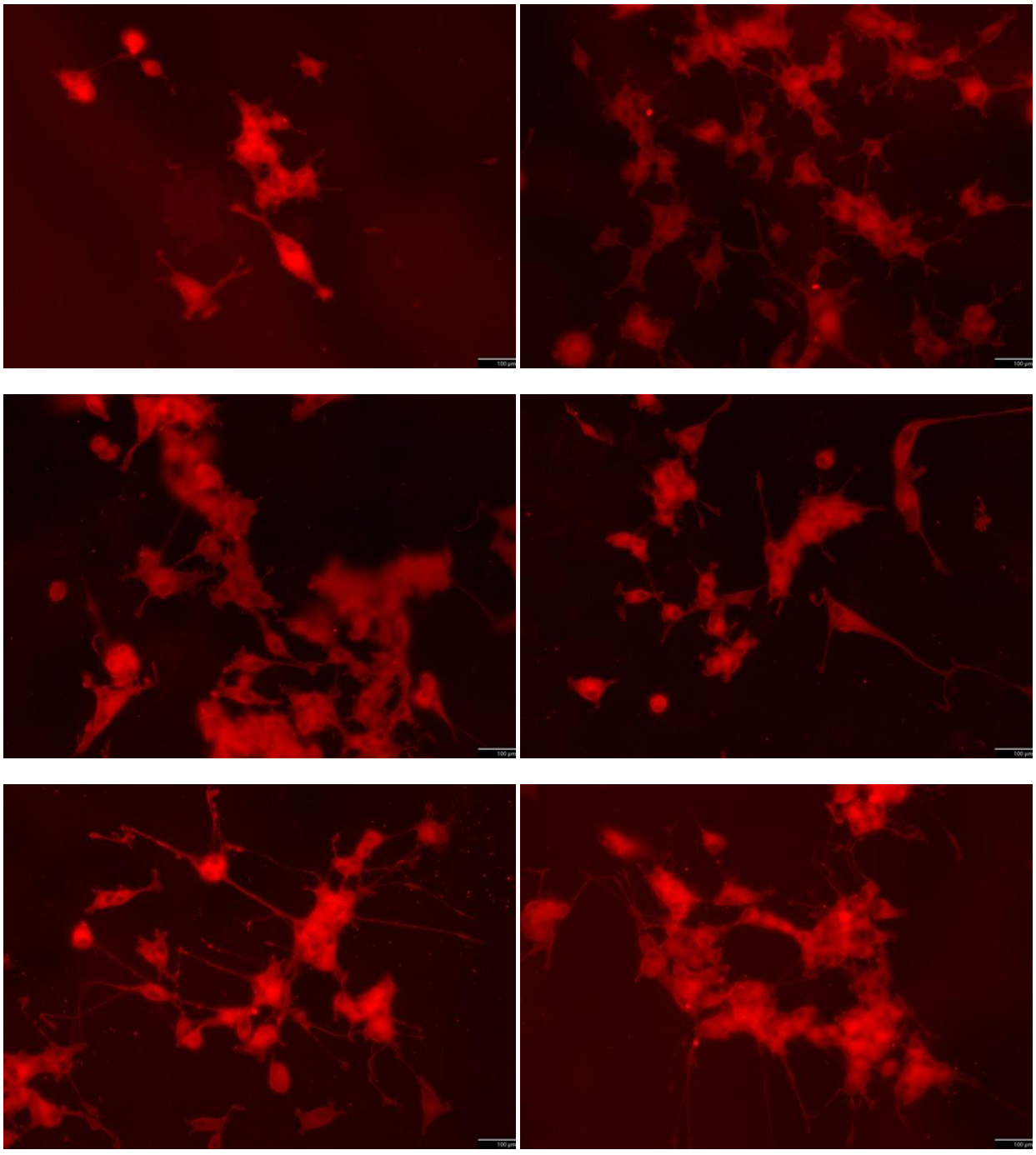

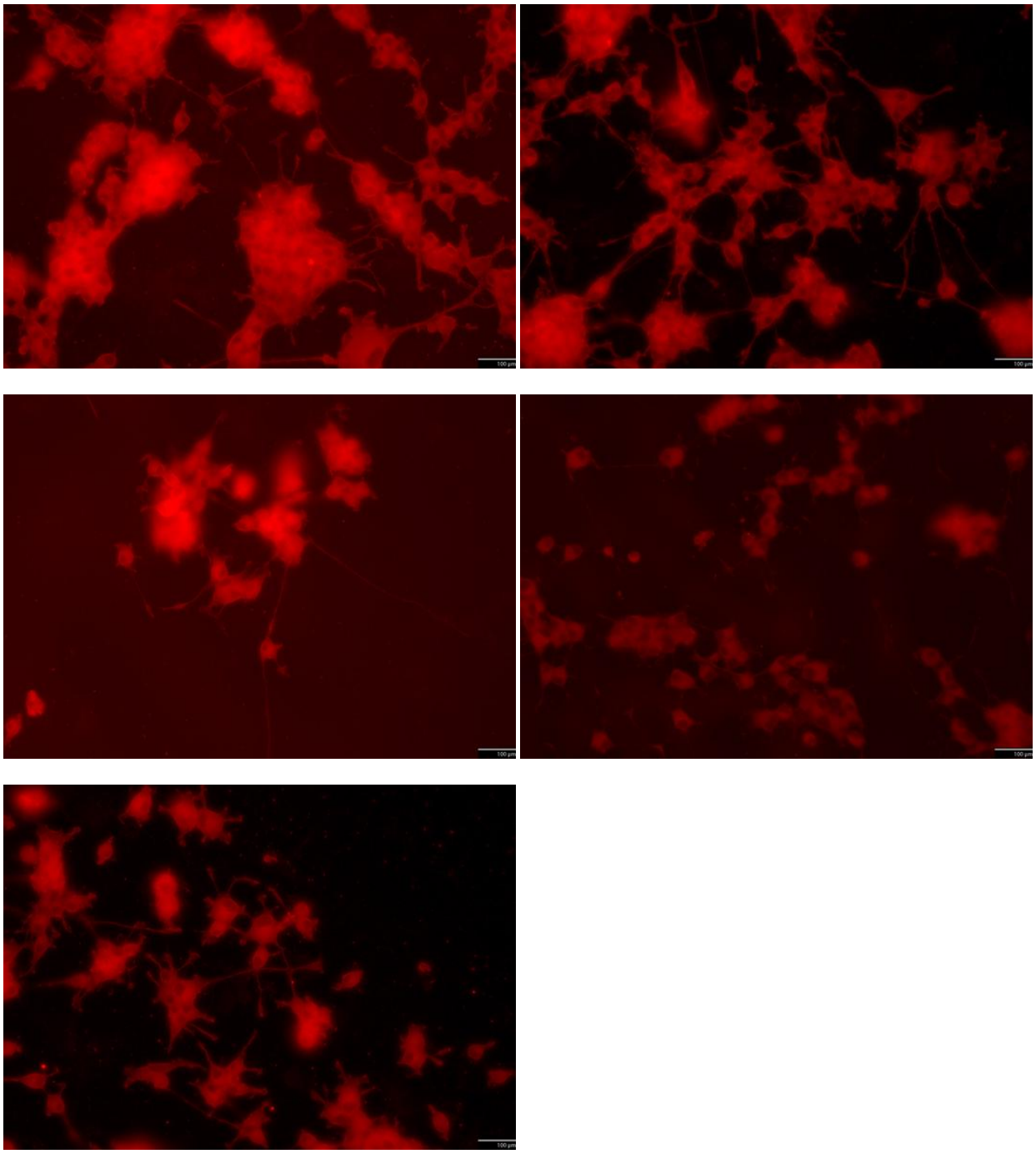

J.3 Glass Surfaces

J.3.1 Bare Glass

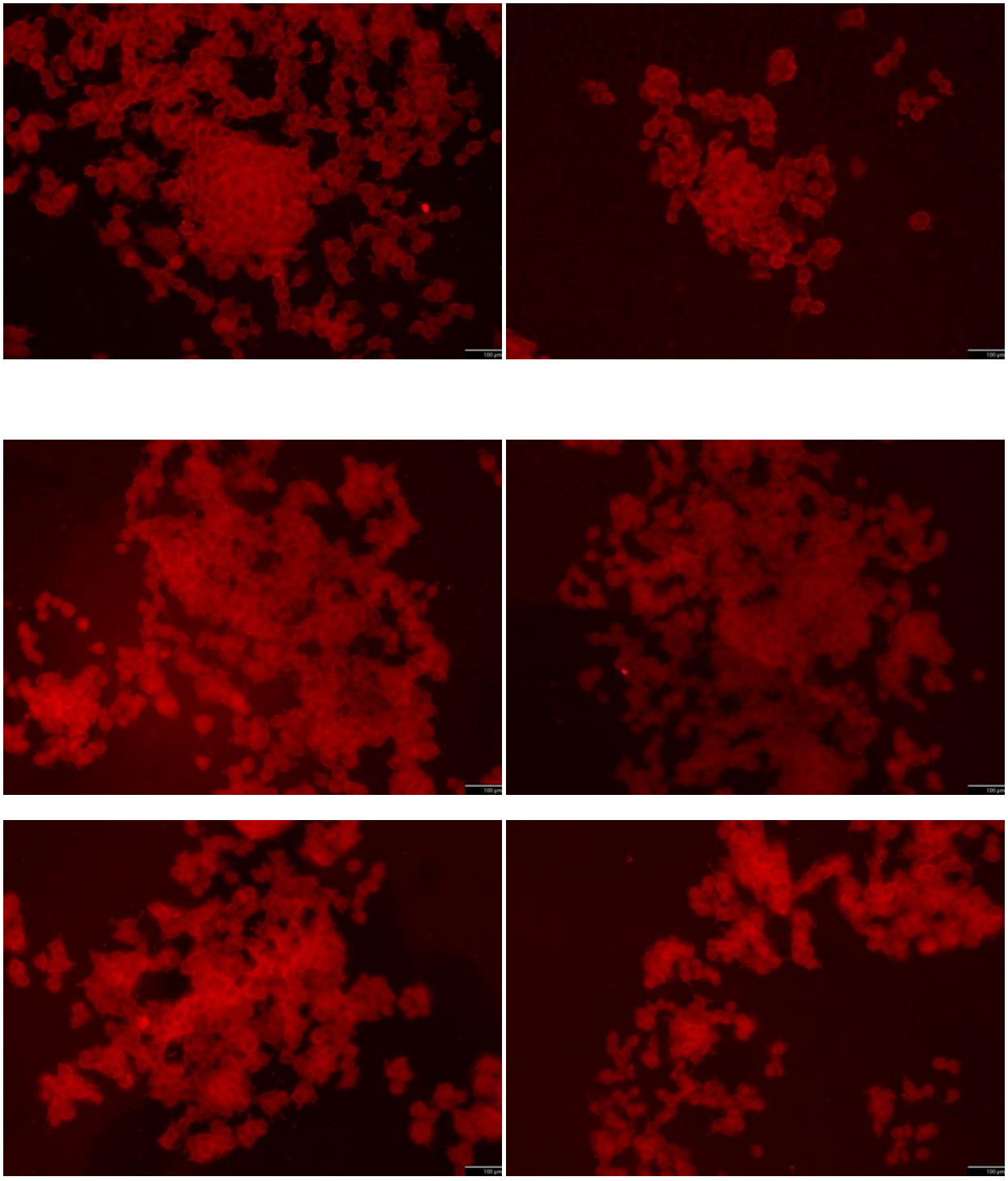

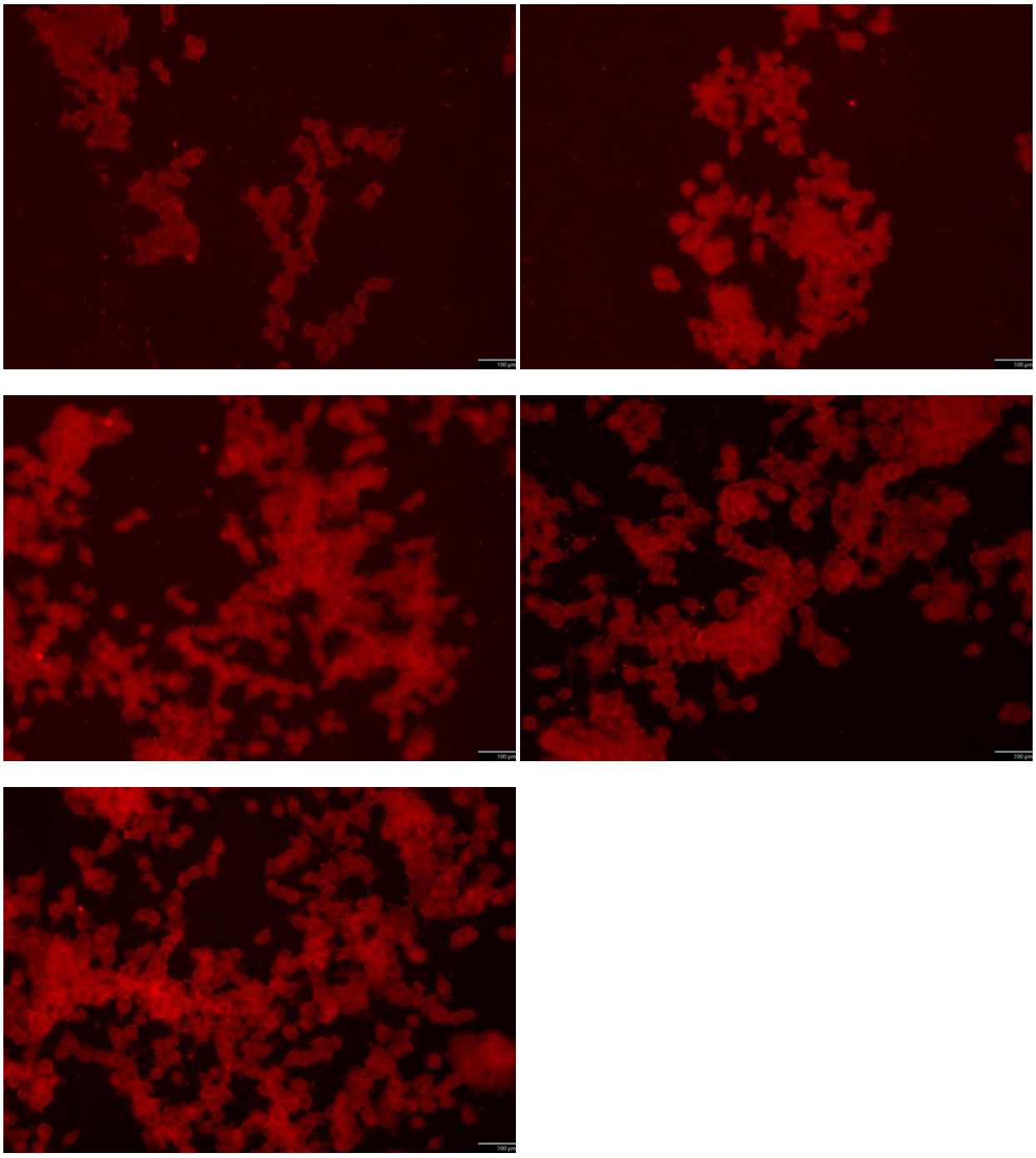

J.3.2 PL Coated Glass

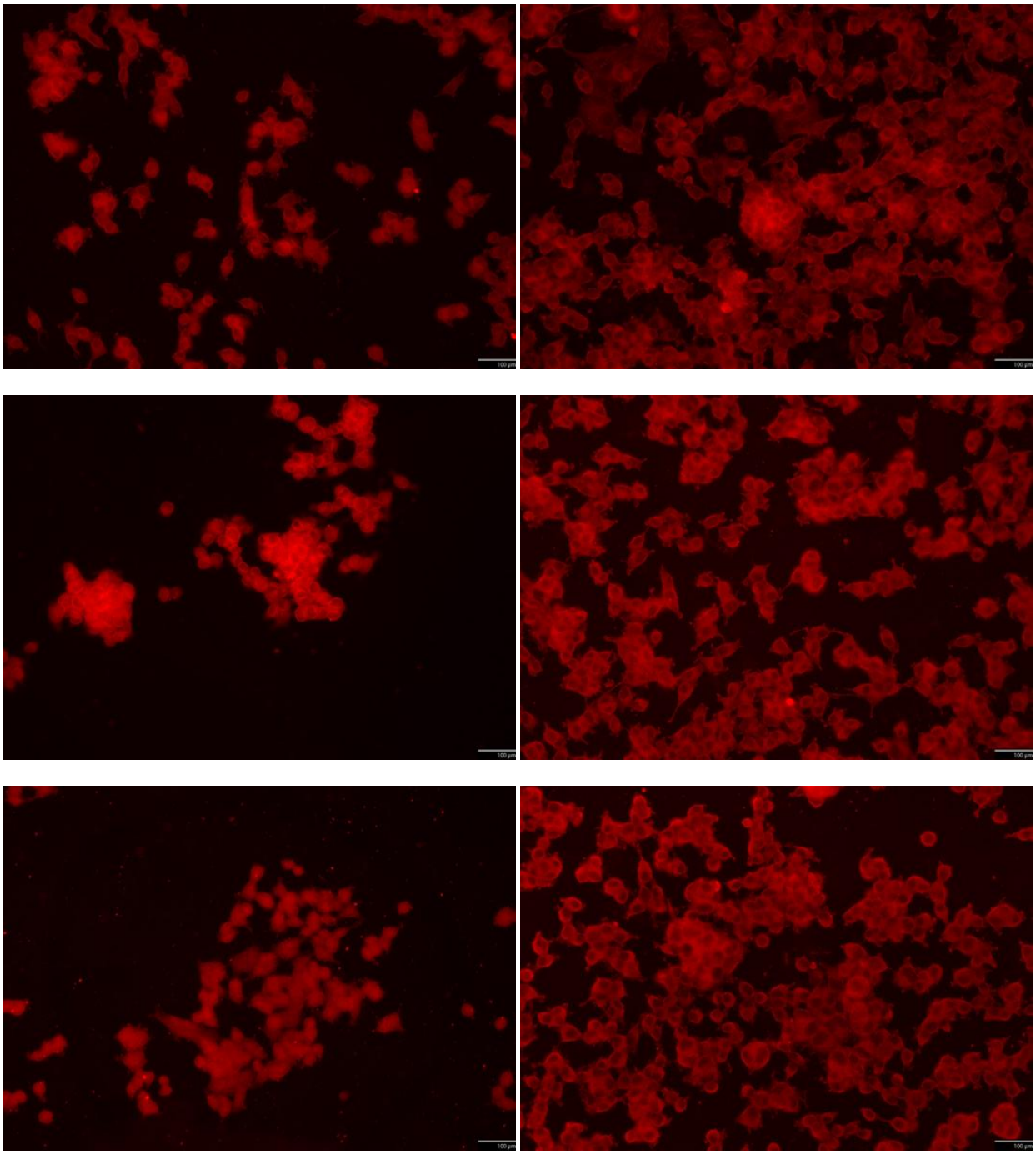

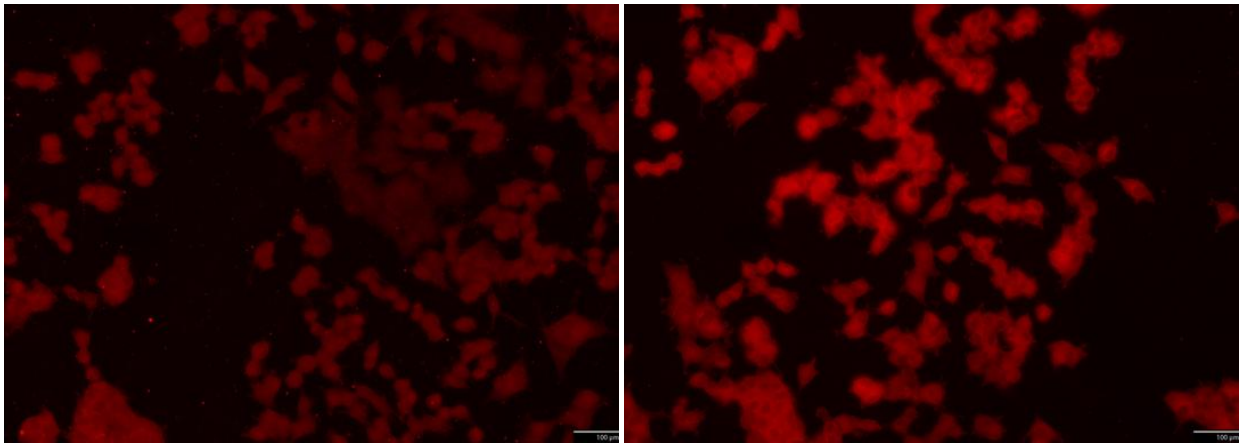

J.3.3 NGF Treated Glass

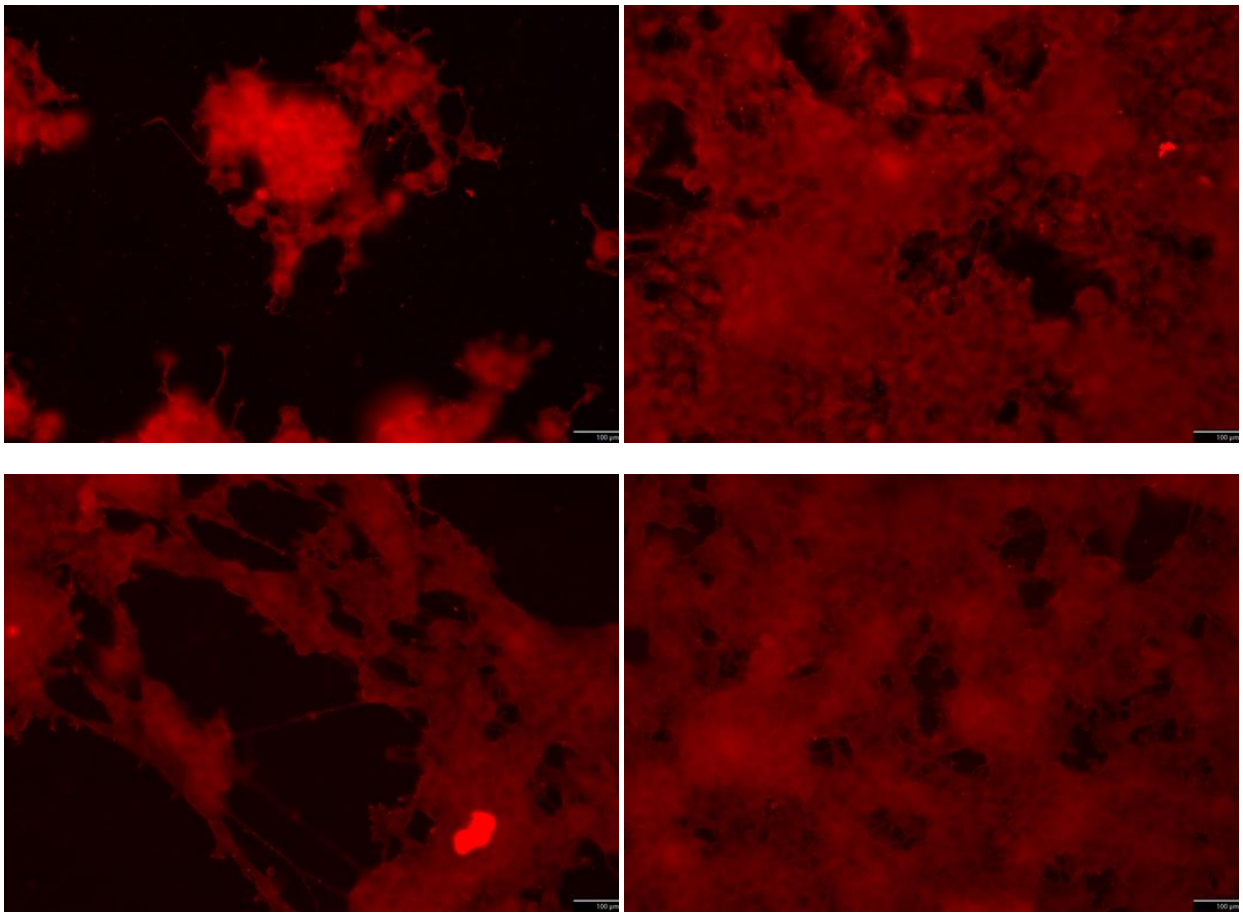

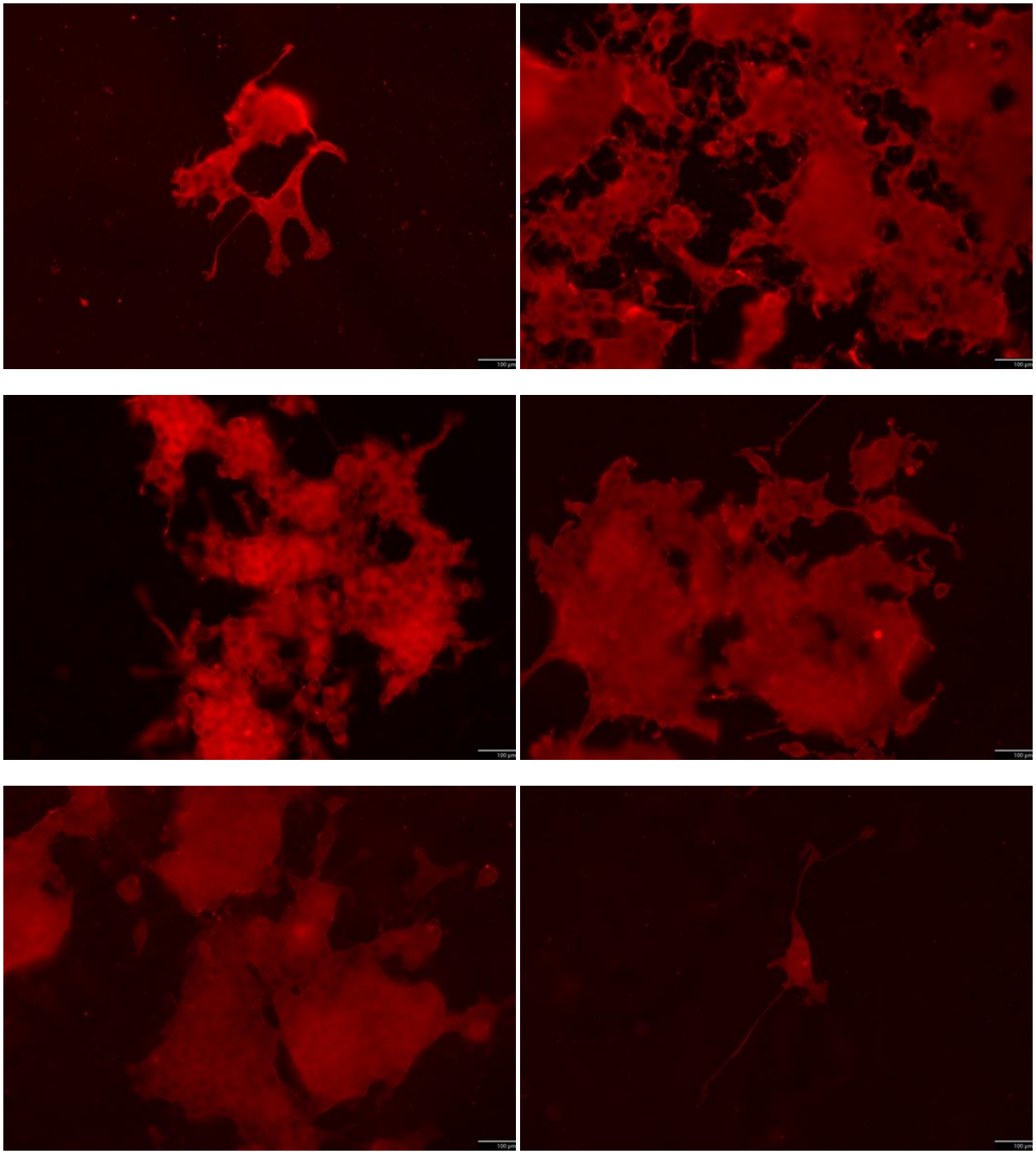

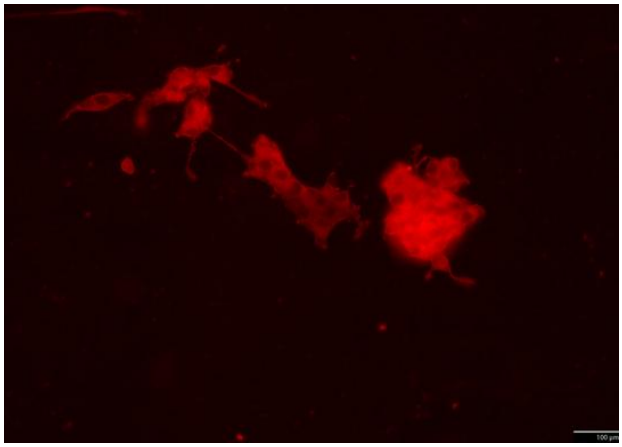

J.3.4 PL Coated and NGF Treated Glass

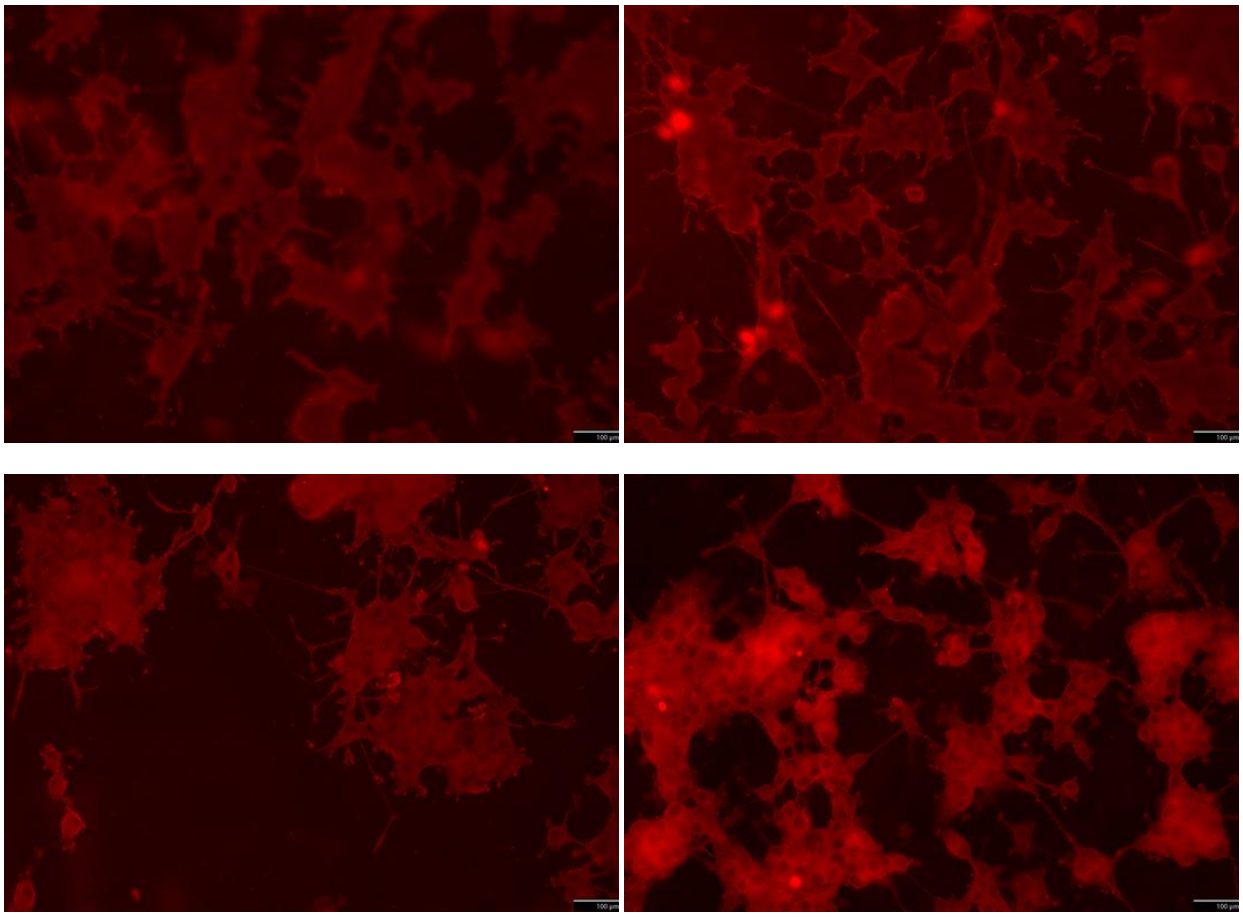

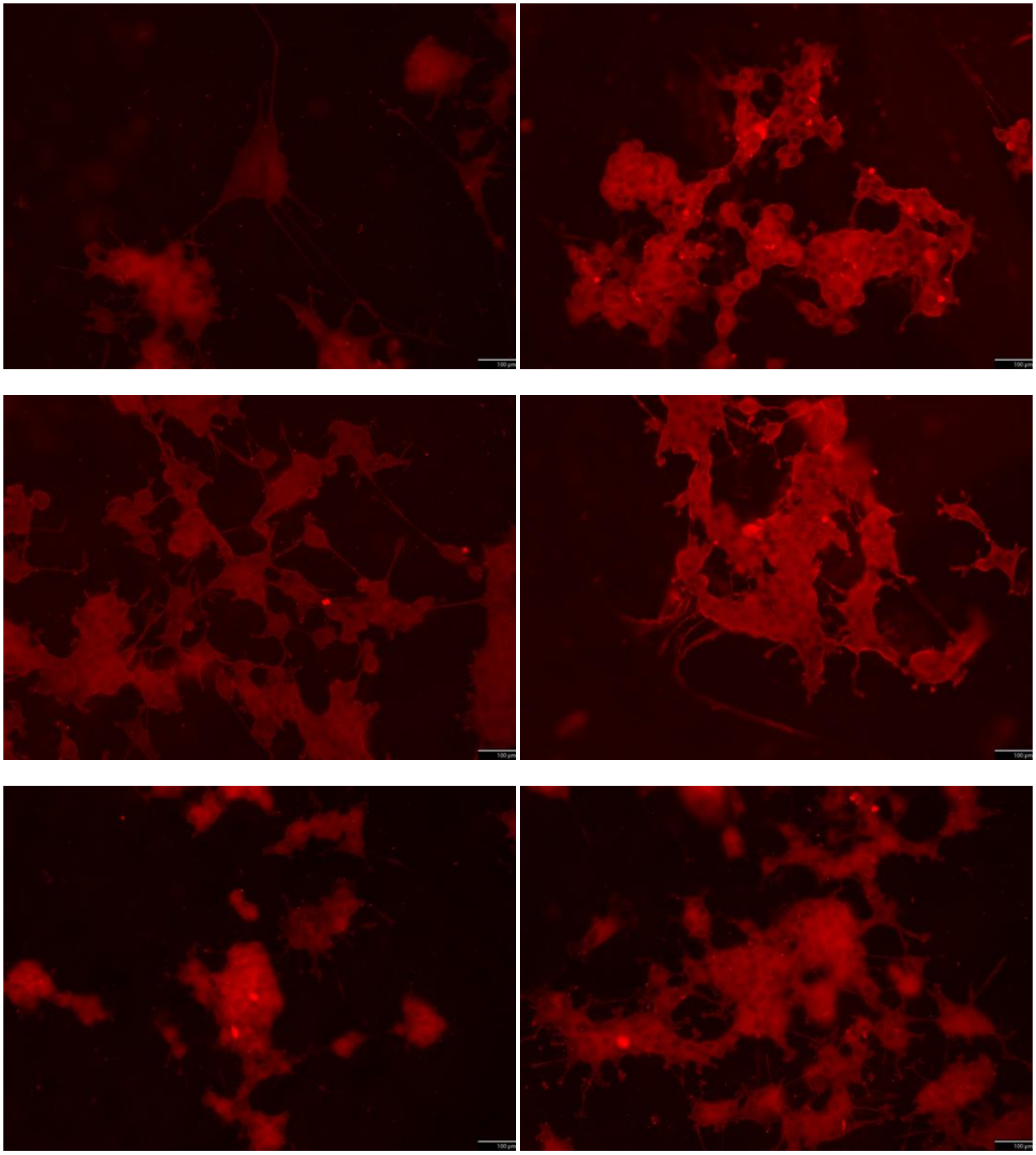

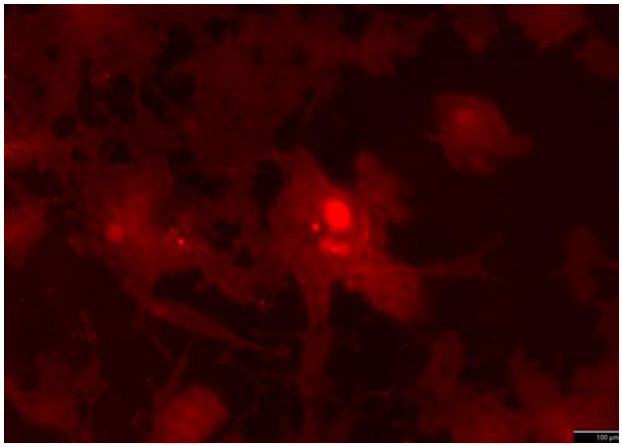

J.4 Oxygen Plasma Treated Carbon Surfaces

J.4.1 Bare Oxygen Plasma Etched Carbon

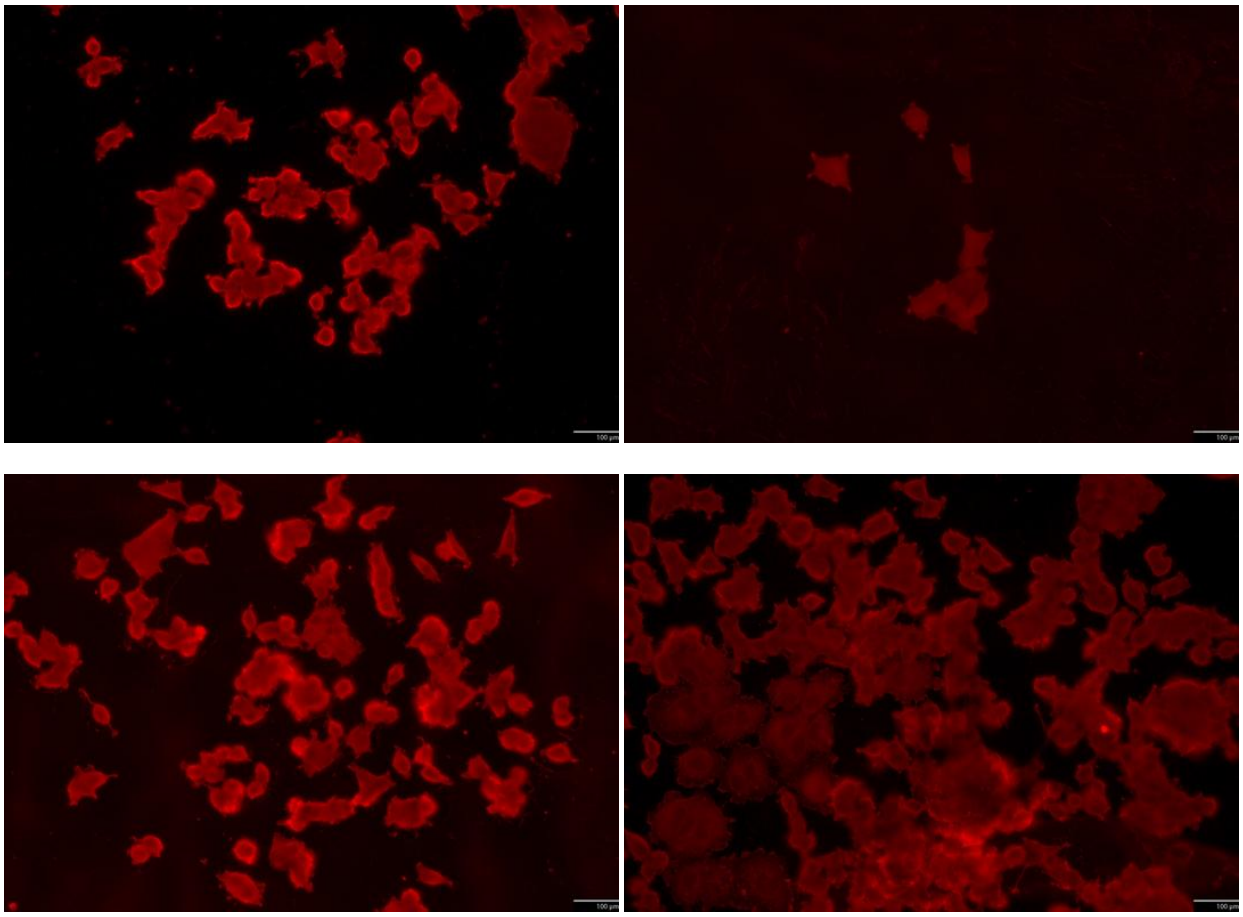

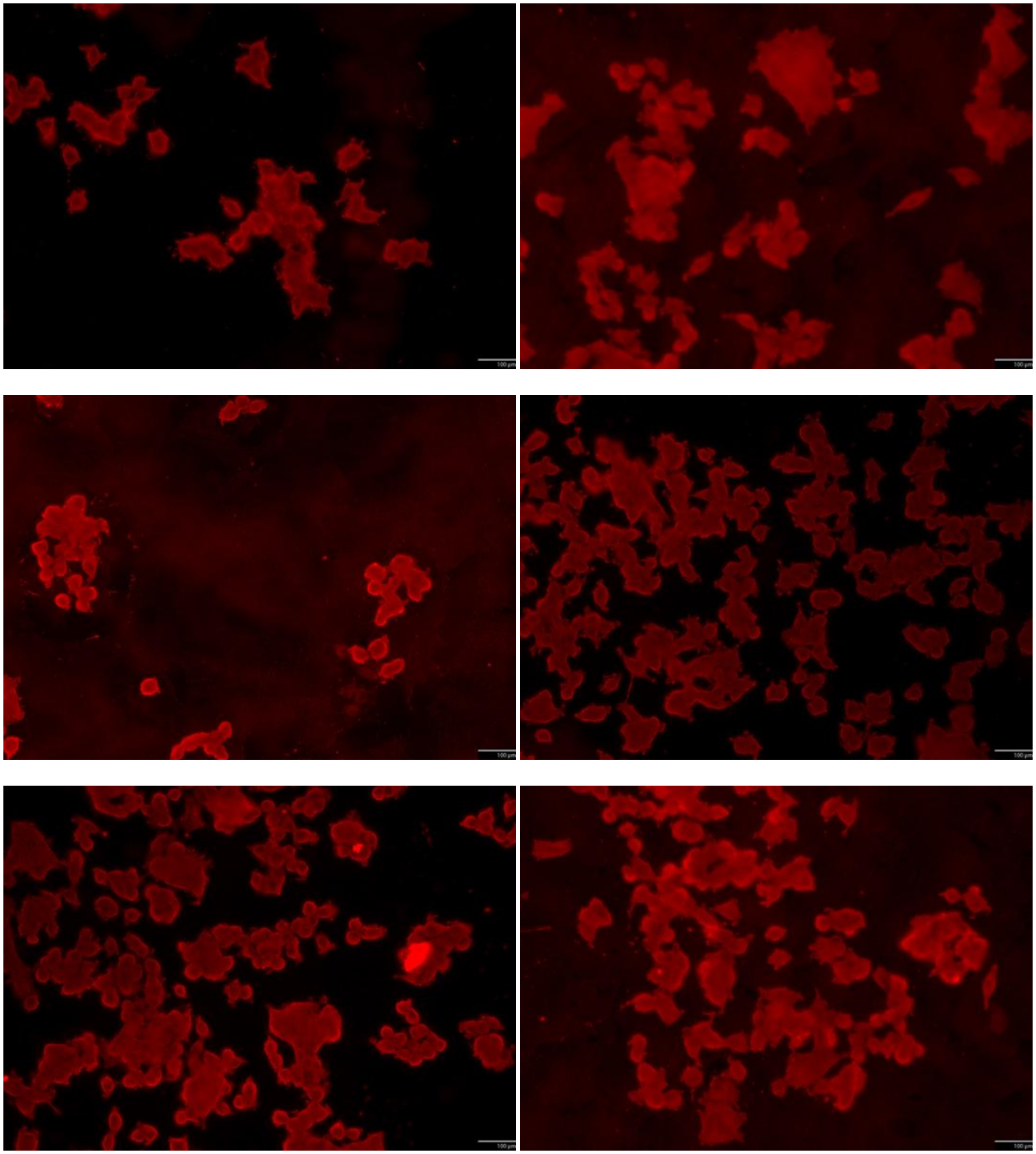

J.4.2 PL Coated Oxygen Plasma Etched Carbon

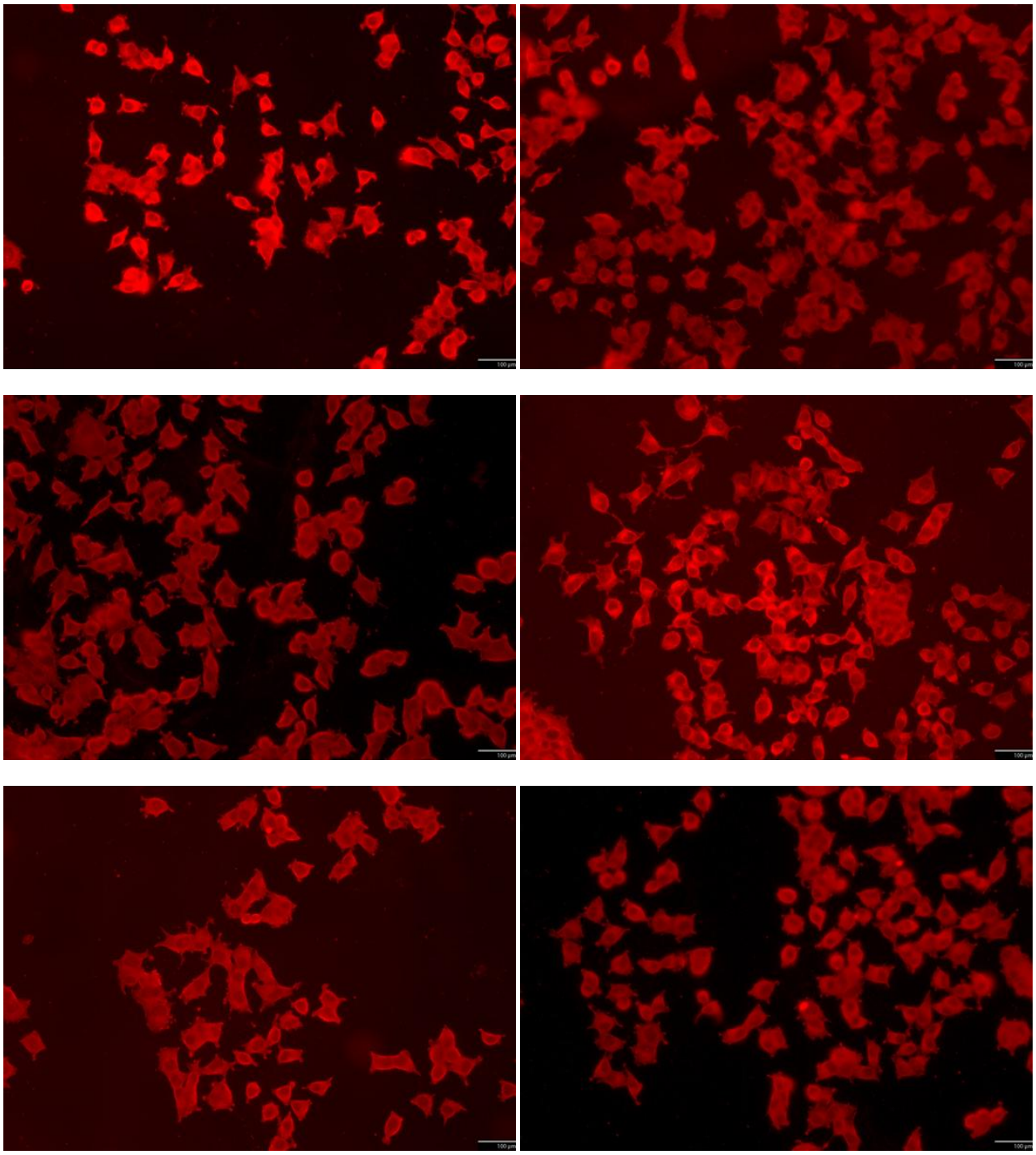

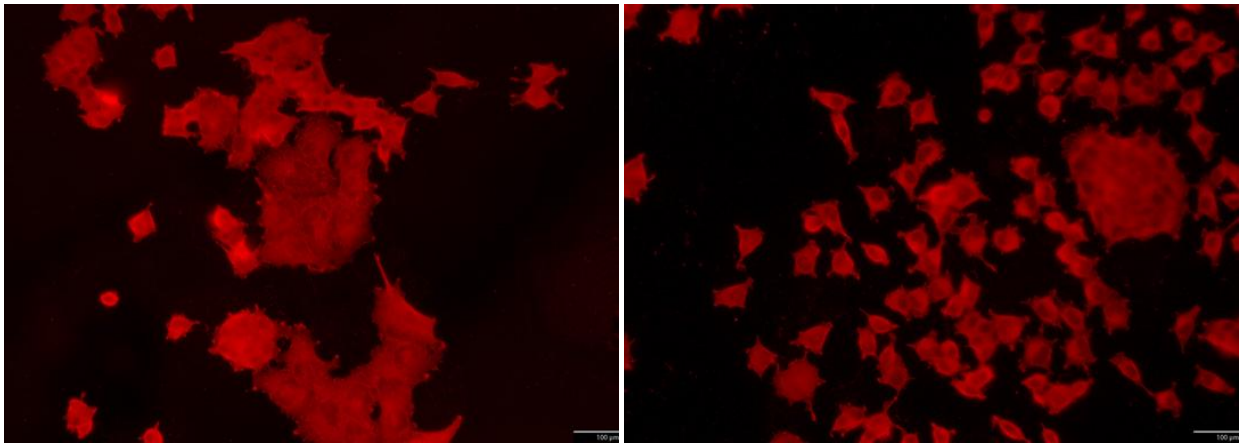

J.4.3 NGF Treated Oxygen Plasma Etched Carbon

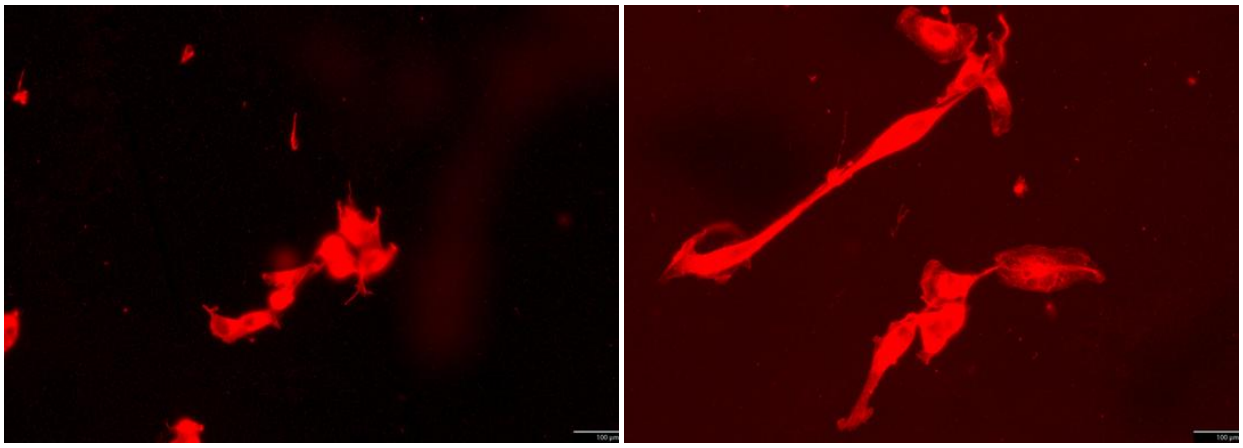

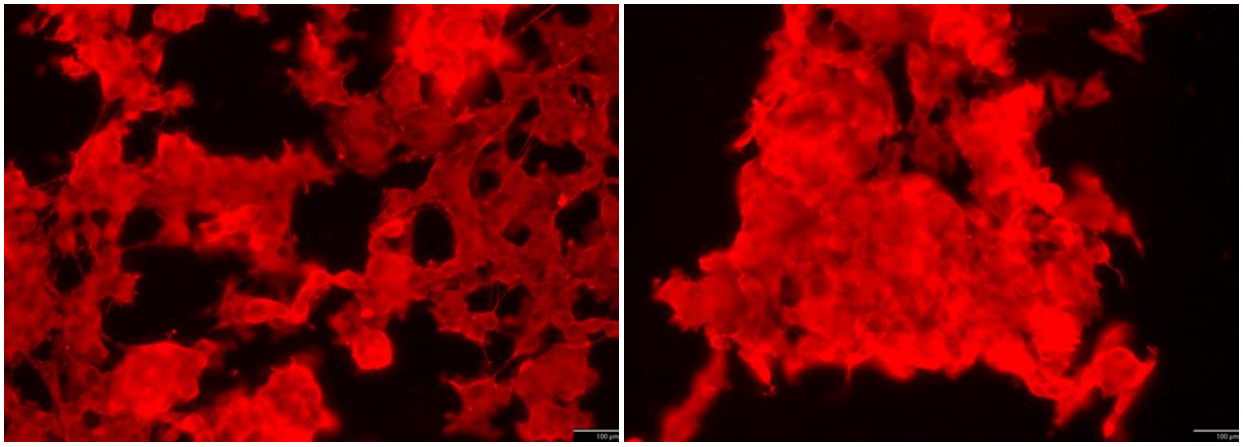

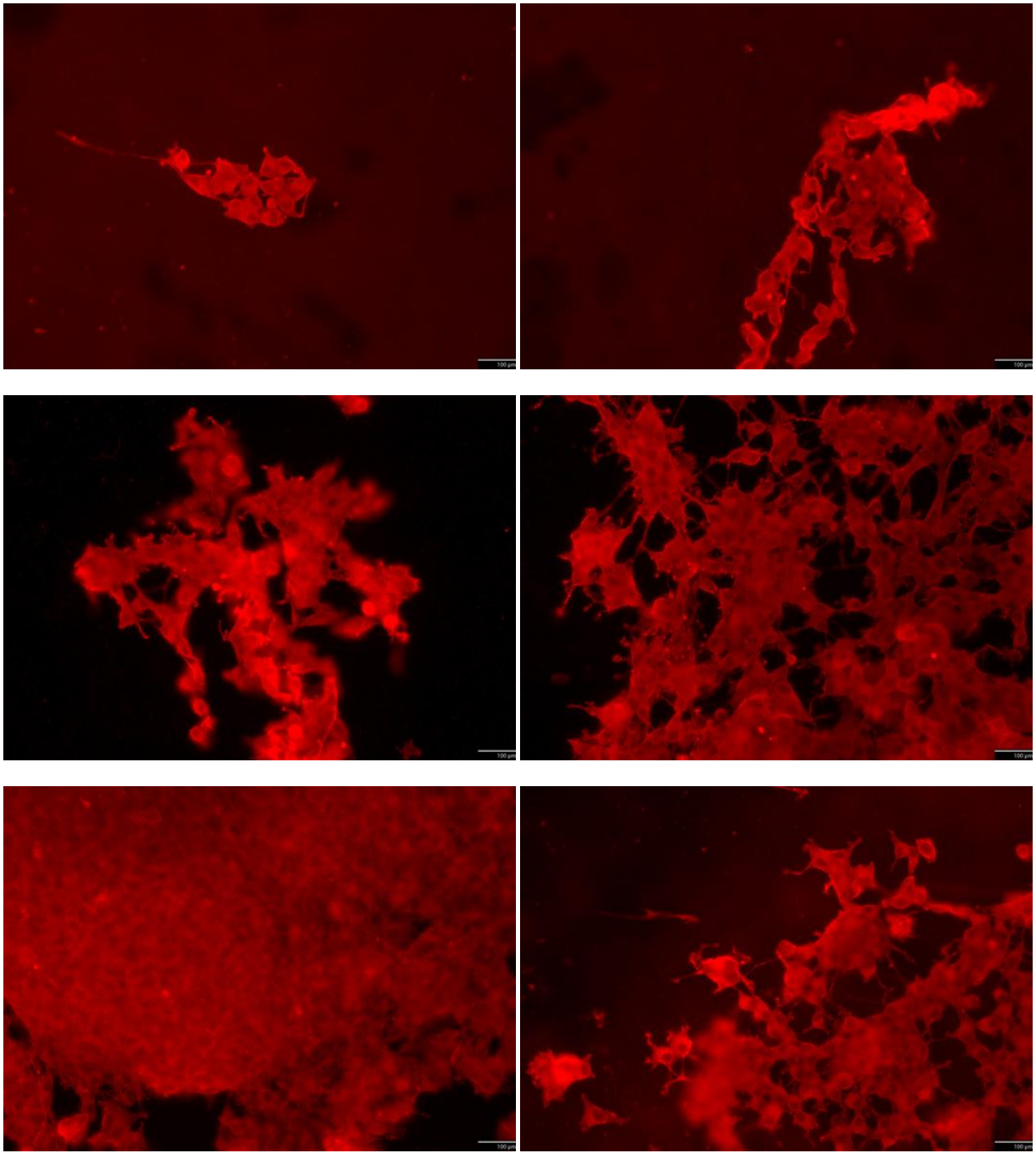

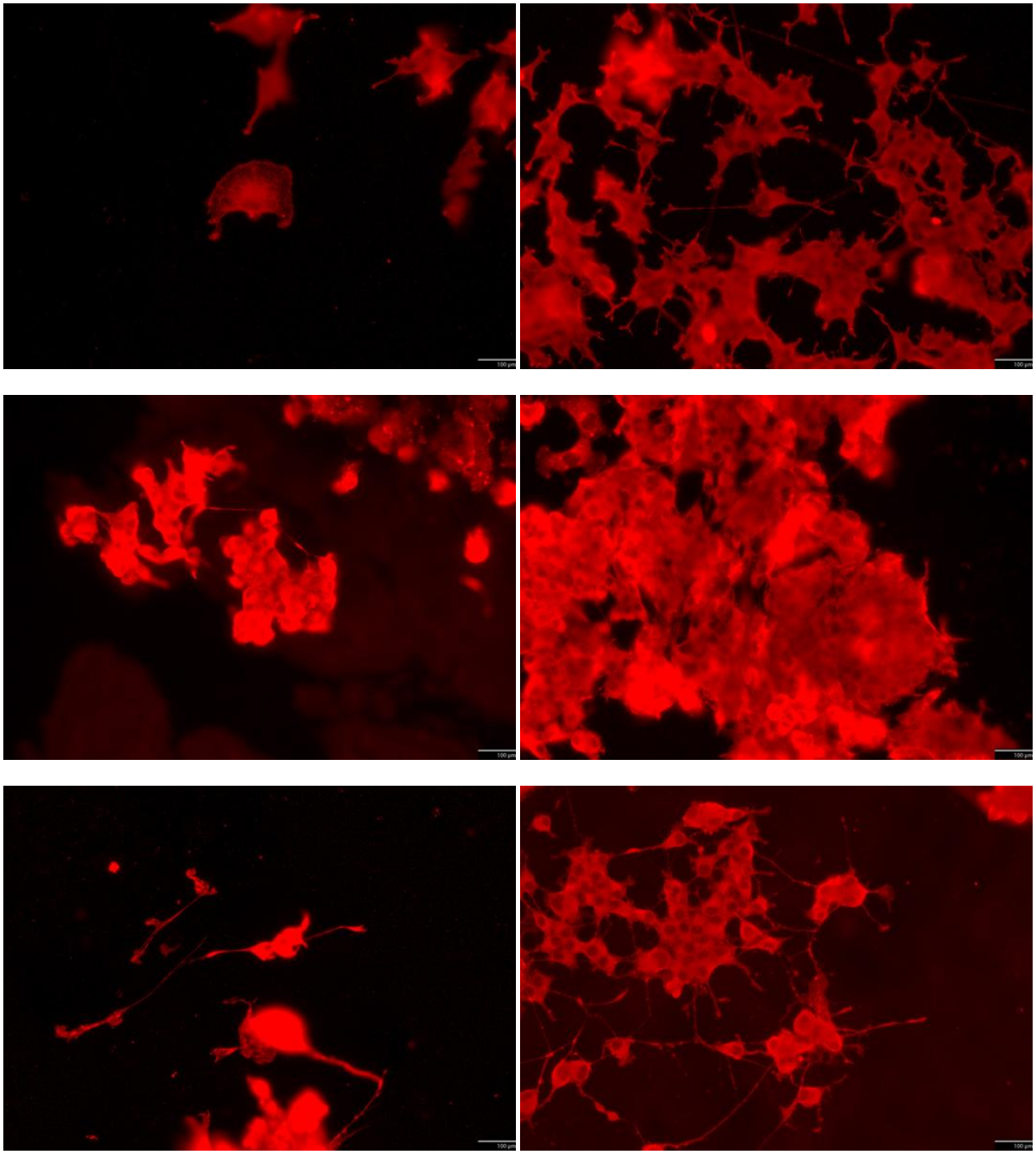

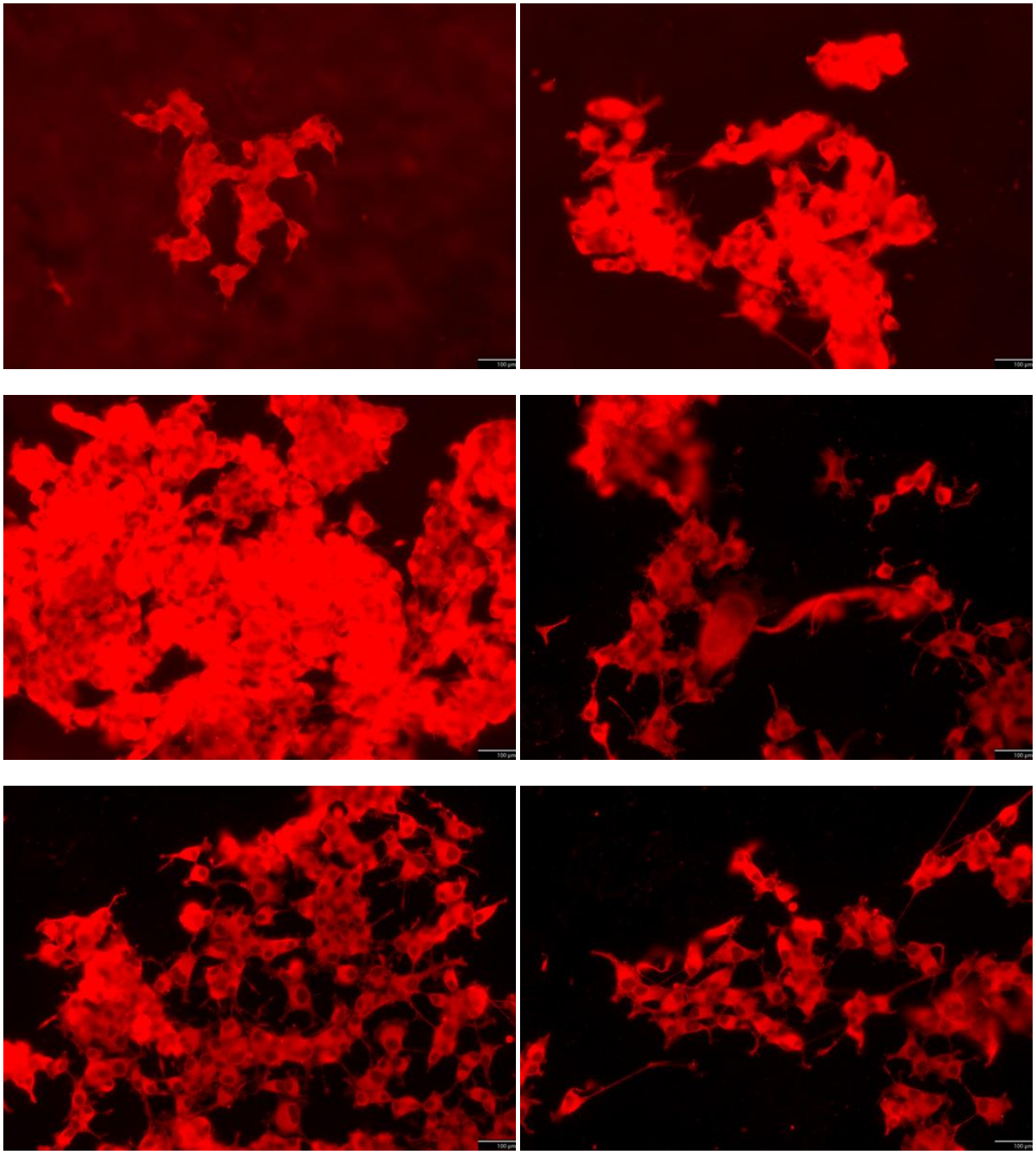

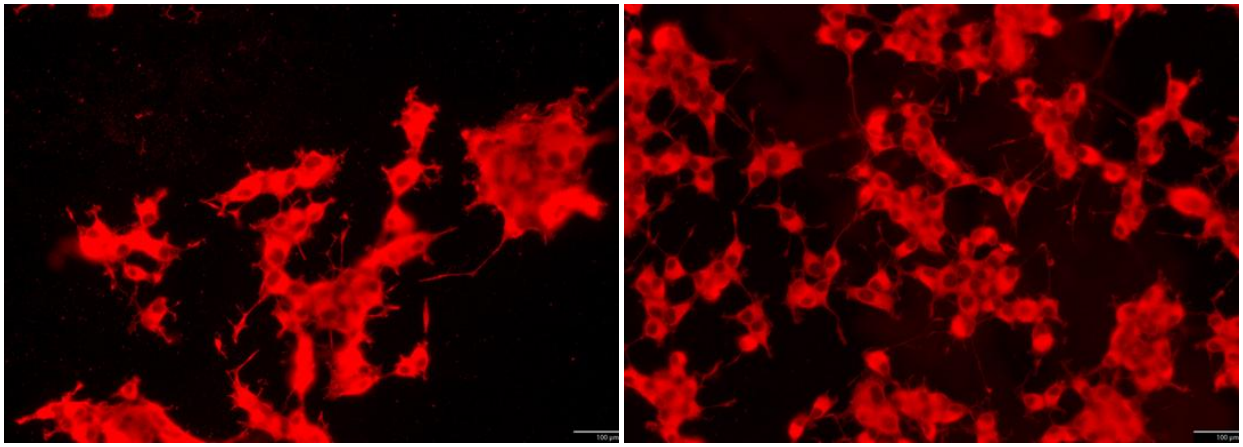

J.4.4 PL Coated and NGF Treated Oxygen Plasma Etched Carbon